Spring 2024 – Systems Biology of Reproduction
Discussion Outline (Sex Determination)
Michael K. Skinner – Biol 475/575
January 25, 2024
Week 3

Sex Determination

Primary Papers:

1. Yamauchi, et al. (2014) Science 343:69-72
2. Bhandari, et al. (2012) PLoS ONE 7:e43380
3. Okashita, et al. (2019) Scientific Reports 9:13462
4. Tsuji-Hosokawa et al. (2022) Endocrinology 1;163(1):bqab217

Discussion

Student 4: Reference #1 above
- What are the genes on the Y required?
- What was the experimental design and methods?
- What conclusions are made on the future fate of the Y?

Student 5: Reference #2 above
- What are the downstream targets of SRY?
- What was the method used to identify the targets?
- Is SOX9 the only target of SRY that is important?

Student 6: Reference #3 above
- What is Tet2 and function in DNA methylation?
- What role does DNA methylation and histone modification have in sex determination?

Reference #4 above
- What was the experimental design?
- What observations were made on sex determination and SRY?

12. L. R. Melby *et al.*, *J. Am. Chem. Soc.* **84**, 3374–3387 (1962).
13. R. A. Heintz *et al.*, *Inorg. Chem.* **38**, 144–156 (1999).
14. R. S. Potember, T. O. Poehler, D. O. Cowan, *Appl. Phys. Lett.* **34**, 405 (1979).
15. H. Miyasaka *et al.*, *J. Am. Chem. Soc.* **132**, 1532–1544 (2010).
16. B. Abeles, H. L. Pinch, J. I. Gittleman, *Phys. Rev. Lett.* **35**, 247–250 (1975).
17. A. A. Yakovenko, J. H. Reibenspies, N. Bhuvanesh, H.-C. Zhou, *J. Appl. Crystallogr.* **46**, 346–353 (2013).
18. L. H. Wee, M. R. Lohe, N. Janssens, S. Kaskel, J. A. Martens, *J. Mater. Chem.* **22**, 13742 (2012).
19. B. S. Brunschwig, C. Creutz, N. Sutin, *Chem. Soc. Rev.* **31**, 168–184 (2002).
20. S. Matsuzaki, R. Kuwata, K. Toyoda, *Solid State Commun.* **33**, 403–405 (1980).
21. J. S. Chappell *et al.*, *J. Am. Chem. Soc.* **103**, 2442–2443 (1981).
22. G. Inzelt, R. W. Day, J. F. Kinstle, J. O. Chambers, *J. Phys. Chem.* **87**, 4592–4598 (1983).

Acknowledgments: We thank S. T. Meek for organic synthesis in this work and D. Ruzmetov for help in fabrication. This work was supported by the Laboratory Directed Research and Development Program at Sandia National Laboratories and the U.S. Department of Energy (DOE) SunShot Program. Sandia is a multiprogram laboratory operated by Sandia Corporation, a Lockheed Martin company, for the U.S. DOE National Nuclear Security Administration under contract DE-AC04-94AL85000. A.A.T. was supported by the Science of Precision Multifunctional Nanostructures for Electrical Energy Storage (NEES), an Energy Frontier Research Center funded by the U.S. DOE, Office of Science, Office of Basic Energy Sciences under award DESC0001160. F.E.G. was supported by the Office of Basic Energy Sciences, Division of Materials and Engineering Sciences, U.S. DOE, under contract DE-AC04-94AL85000. A.C., R.A.K., and H.P.Y. acknowledge support under the Cooperative Research Agreement between the University of Maryland and the National Institute of Standards and Technology Center for Nanoscale Science and Technology, award 70NANB10H193, through the University of Maryland.

Supplementary Materials
www.sciencemag.org/content/343/6166/66/suppl/DC1
Materials and Methods
Figs. S1 to S8
Table S1
Movie S1
References (*23*–*39*)

2 October 2013; accepted 20 November 2013
Published online 5 December 2013;
10.1126/science.1246738

Two Y Genes Can Replace the Entire Y Chromosome for Assisted Reproduction in the Mouse

Yasuhiro Yamauchi, Jonathan M. Riel, Zoia Stoytcheva, Monika A. Ward*

The Y chromosome is thought to be important for male reproduction. We have previously shown that, with the use of assisted reproduction, live offspring can be obtained from mice lacking the entire Y chromosome long arm. Here, we demonstrate that live mouse progeny can also be generated by using germ cells from males with the Y chromosome contribution limited to only two genes, the testis determinant factor *Sry* and the spermatogonial proliferation factor *Eif2s3y*. *Sry* is believed to function primarily in sex determination during fetal life. *Eif2s3y* may be the only Y chromosome gene required to drive mouse spermatogenesis, allowing formation of haploid germ cells that are functional in assisted reproduction. Our findings are relevant, but not directly translatable, to human male infertility cases.

The mammalian Y chromosome, once thought to be a genetic wasteland (*1*), is now known to encode a battery of genes, many of which are thought to be involved in male reproduction (*2*). A substantial amount of work has been done to define which genes are important for maintaining sperm function under normal, in vivo, conditions. In the era of assisted reproduction technologies (ART), it is now possible to bypass several steps of normal human fertilization using immotile, nonviable, or even immature sperm. We have shown that infertile male mice lacking the entire Y chromosome long arm can generate live offspring when their severely morphologically abnormal sperm are delivered into oocytes via intracytoplasmic sperm injection (ICSI) (*3*). In these mice, the Y chromosome is reduced from 78 Mb to ~2 Mb and encodes only seven genes and three gene families ($XY^{*X}Sxr^{a}$ in fig. S1).

In most mammals, including humans and mice, testis determination is regulated by *Sry*, which directs developing gonads to male differentiation (*4*–*6*). Upon transgenic addition of *Sry*, mice with one X chromosome (XO*Sry*) develop testes that are populated with spermatogonia, male germ cells that have the potential to undergo differentiation and initiate spermatogenesis. In the absence of other Y chromosome genes, these spermatogonia undergo proliferation arrest, and the meiotic and postmeiotic stages of spermatogenesis are absent (*7*). Transgenic addition of individual missing Y genes led to the identification of *Eif2s3y* as the gene that restored normal spermatogonial proliferation (*7*). In XO*Sry* males transgenic for *Eif2s3y*, spermatogenesis was shown to complete meiotic prophase and the first meiotic division before the cells arrested as secondary spermatocytes, with the occasional production of spermatid-like cells (*7*, *8*). Here, we tested whether these spermatid-like cells were functional in assisted reproduction and what other components of the Y chromosome help to increase development of functional gametes.

We first examined mice with the Y gene complement limited to two transgenically derived genes, autosomally located *Sry* and X chromosome located *Eif2s3y* ($X^{E}O$*Sry* in fig. S1) (*9*). These mice had testes smaller than wild-type XY males (fig. S2) but populated with germ cells. Analysis of testicular sections confirmed that spermatogenesis was ongoing, which allowed development of germ cells with spermatid-like morphology (Fig. 1A, arrowheads), similar to those observed earlier (*7*, *10*). The occurrence of these spermatids was low, and their development was restricted to steps 5 to 7 of spermatid development, with the occasional presence of step 8 to 9 spermatids [Fig. 1A (inset) and fig. S3]. We also observed secondary changes to seminiferous tubules, with increased incidence of dying cells, multinucleate bodies, and vacuoles (Fig. 1B). These changes increased progressively as the males aged and ultimately led to Sertoli-cell-only (SCO) syndrome tubules (Fig. 1C).

We next tested the function of the spermatid-like cells from $X^{E}O$*Sry* in assisted reproduction. Round, spermatid-like cells could be found in testicular cell suspensions from all males used in ART trials, although these cells were rare and their morphology was often slightly abnormal (increased size, less pronounced nuclei, and rough rather than smooth surface) when compared with spermatids from control XY males (Fig. 1, D and E). Nevertheless, when we performed round spermatid injection (ROSI), the oocytes were successfully fertilized, as evidenced by the development of two pronuclei and extrusion of the second polar body, as well as subsequent cleavage (fig. S4). When the developed two-cell embryos were transferred into the oviducts of recipient females, live offspring were obtained (Table 1 and Fig. 1F). Three out of four males that provided spermatids for injections successfully sired offspring. The efficiency of ROSI with $X^{E}O$*Sry* males was significantly lower than with XY controls (9% versus 26%) (Table 1). All the progeny had the genotypes as expected when derived from $X^{E}O$*Sry* fathers and were healthy; those bred were fertile (Fig. 1G, fig. S5, and supplementary text).

An unpaired sex chromosome leads to meiotic arrest and apoptosis (*11*), so partial meiotic failure in $X^{E}O$*Sry* males was not unexpected. The few spermatids that could be found in the testes could be the cells that "leaked" through the meiotic arrest, i.e., finished meiosis and were haploid. Alternatively, these could be the cells that developed spermatid-like morphology without undergoing the second meiotic division (*8*, *10*).

Institute for Biogenesis Research, John A. Burns School of Medicine, University of Hawaii, 1960 East-West Road, Honolulu, HI 96822, USA.

*Corresponding author. E-mail: mward@hawaii.edu

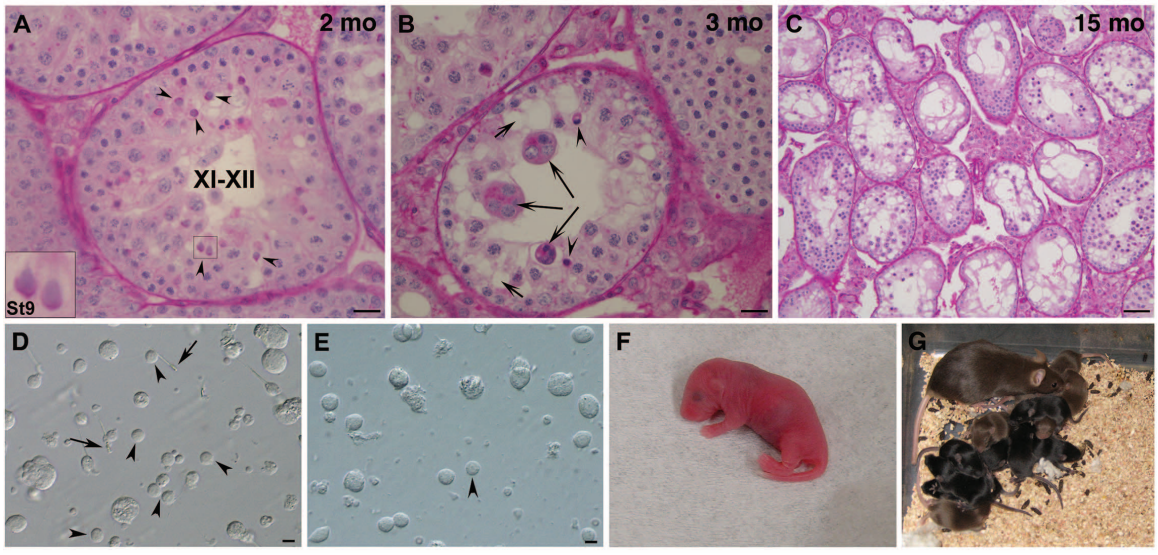

Fig. 1. Testis histology, round spermatids, and live offspring. (**A**) Males with only two Y genes, *Eif2s3y* and *Sry*, have meiotic and postmeiotic arrests that only occasionally allow formation of spermatids (arrowheads) that are frequently delayed and do not develop beyond St8/9. (**B**) Tubule degeneration with formation of "multinucleate bodies" (long arrows), vacuoles (short arrows), and dying and/or apoptotic germ cells (arrowheads) is frequently observed. (**C**) SCO syndrome–like phenotype in an old male. (**D**) Testicular suspension from wild-type males contains testicular sperm (arrows) and many round spermatids (arrowheads) with clear morphological features. (**E**) Males with two Y genes have substantially fewer germ cells in testicular cell suspension, with no sperm and very few round spermatids (arrowhead). These spermatids are functional in ROSI. (**F**) ROSI pup obtained after transfer of embryos generated with spermatids from a male with only two Y genes. (**G**) An adult female developed from the pup shown in (F) with her own litter. Roman and arabic numerals in (A) are tubule stages and steps of spermatid development (St), respectively (see fig. S3). Scale bars, 16 μm (A and B), 50 μm (C), and 10 μm (D and E); inset, ×3 magnification; mo, months of age.

Table 1. The results of round spermatid injection (ROSI) with spermatids from males with limited Y gene complement. For Y gene contribution, see fig. S1. Percentages of live offspring and implants were calculated from embryos transferred. Male ages ranged from 63 to 229 days. Statistical significance (Fisher's exact test): $^{a}P < 0.01$ and $^{b}P < 0.001$ versus XY^{RIII} control. *Sxr*^{b}: *Sry, Zfy2/1, H2al2y, Rbmy cluster* (reduced).

Male genotype	Y gene contribution	Live offspring % (no.)	Implants % (no.)
$X^{E}OSry$	*Eif2s3y* and *Sry*	9.1 (12/132)^{a}	29.5 (39/132)^{b}
$X^{E}Y^{*X}Sry$	*Eif2s3y* and *Sry*	5.7 (13/227)^{b}	27.3 (62/227)^{b}
$X^{E}Sxr^{b}O$	*Eif2s3y* and *Sxr*^{b}	20.0 (24/120)	45.8 (55/120)^{a}
$X^{E}Sxr^{b}Y^{*X}$	*Eif2s3y* and *Sxr*^{b}	16.0 (24/150)	37.3 (56/150)^{b}
XY^{RIII} control	Intact Y	26.0 (19/73)	69.9 (51/73)

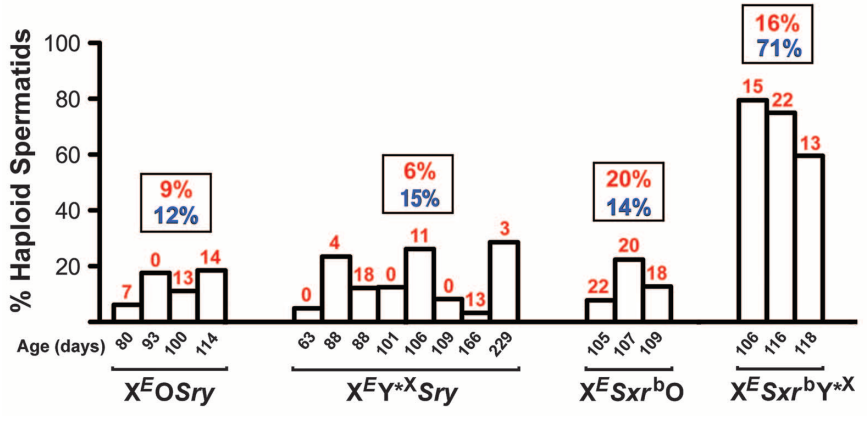

Fig. 2. Incidence of haploid spermatids. Each graph bar represents an individual male providing testicular cells for analysis; the numerals above show the percentage of pups obtained after ROSI. The data in rectangular boxes represent average percentage of haploid spermatids (blue) and ROSI offspring (red) for each genotype. Control male with intact Y chromosome had 97% (67 out of 69) of spermatids haploid. $X^{E}Sxr^{b}Y^{*X}$ males had higher average incidence of haploid spermatids than other genotypes ($P < 0.01$).

Spermatid nuclear DNA content (Fig. 2 and fig. S6) and zygotic chromosome analyses (Fig. 3) revealed that the great majority of spermatids from $X^{E}OSry$ males were diploid and yielded triploid zygotes, which would explain the poor ROSI success. In order to overcome the problem of meiotic block arising from X chromosome univalence, we used males in which a minute Y^{*X} chromosome (fig. S1) was added to provide a second pairing region (PAR) for PAR-PAR chromosome synapsis (*12*). In these $X^{E}Y^{*X}Sry$ males (fig. S1), successful pairing of Y^{*X} and X was observed in 85% of pachytene spermatocytes (fig. S8). However, the testicular phenotype did not improve (figs. S2 and S7, A to C). The proportion of live offspring obtained after injection was similarly low as with $X^{E}OSry$ males (Table 1), and only five out of eight males that provided cells for ROSI sired offspring. We therefore tested for ploidy and demonstrated that most of the $X^{E}Y^{*X}Sry$ spermatids were diploid (Fig. 2 and fig. S6) and that most zygotes after ROSI were triploid (Fig. 3). Thus, overcoming X chromosome univalence in $X^{E}Y^{*X}Sry$ males did not allow overcoming meiotic arrest and increasing ROSI success (see supplementary text).

We next asked whether other Y chromosome genes may be beneficial for spermatid function in assisted reproduction. To address this, we used males in which the *Sry* transgene driving sex determination was replaced with the sex reversal factor *Sxr*^{b} ($X^{E}Sxr^{b}O$ and $X^{E}Sxr^{b}Y^{*X}$ in fig. S1). In these males, the X chromosome carries an *Eif2s3y* transgene necessary for spermatogonial proliferation (*7*), together with the *Sxr*^{b} encoding for *Zfy2/1*, *Sry*, *H2al2y*, and the *Rbmy* gene cluster.

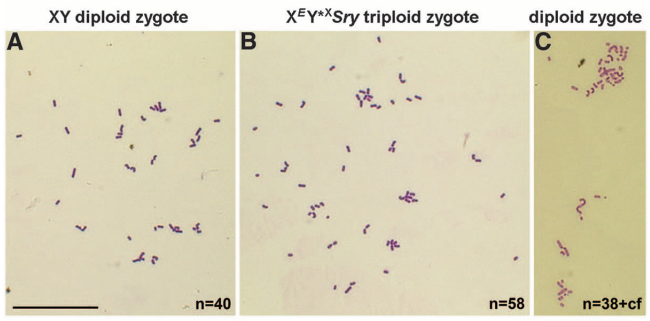

D

Genotype	Diploid zygote % (No)
$X^{E}OSry$	23 (8/35)[b]
$X^{E}Y^{*X}Sry$	25 (13/53)[b]
$X^{E}Sxr^{b}O$	71 (5/7)[a]
$X^{E}Sxr^{b}Y^{*X}$	85 (47/55)[a]
XY	100 (36/36)

Fig. 3. Zygote chromosome analysis after ROSI. (**A**) Normal diploid mouse zygote generated after ROSI with XY male contains 40 chromosomes. (**B**) Triploid zygote obtained after ROSI with spermatids from a male with two Y genes (~60 chromosomes). (**C**) Diploid zygote after ROSI with spermatids from male of the same genotype (~40 chromosomes). (**D**) Incidences of diploid zygotes generated after ROSI. cf, chromosome fragments. *n* = chromosome number. [a]$P < 0.05$, [b]$P < 0.001$ versus XY control. Scale bar, 50 μm.

The testes from $X^{E}Sxr^{b}O$ and $X^{E}Sxr^{b}Y^{*X}$ males were larger than from $X^{E}OSry$ and $X^{E}Y^{*X}Sry$ but smaller than in wild-type XY males (fig. S2). The incidence of round spermatids increased only in $X^{E}Sxr^{b}Y^{*X}$ (fig. S3). In both male types, spermatid development was more advanced, with clear elongation up to step 10, occasional presence of step 11 to 12 spermatids, and even sporadic development to mature testicular sperm (fig. S7, D and G). There were secondary changes to the seminiferous epithelium (fig. S7, E, F, H, and I), albeit in $X^{E}Sxr^{b}Y^{*X}$ males less pronounced than in the other genotypes. Zygote chromosome analysis showed that most of the zygotes after ROSI were diploid (71 to 85%) (Fig. 3), and the ROSI outcome was significantly improved, with all tested males (three per genotype) yielding live offspring with the rate now reaching 20 and 16% (Table 1). Nevertheless, the frequency of haploid spermatids in $X^{E}Sxr^{b}O$ males remained low (Fig. 2 and fig. S6). The discrepancy between the ploidy of the spermatids and zygotes raised the possibility that the second meiotic division took place in the oocytes. This suggests that Sxr^{b} encodes a gene or genes that promote the second meiotic division when all chromosomes are paired and enables overcoming of meiotic arrest of the diploid spermatid in the oocyte when an X chromosome pairing partner is missing (see supplementary text).

We have shown that only two mouse Y chromosome genes, *Sry* and *Eif2s3y*, are necessary for the development of male haploid germ cells that are sufficient for successful reproduction and yield live offspring. This minimal Y gene complement must be enough to ensure correct male-specific methylation and proper formation of any other epigenetic modifications in the paternal genome that are required for embryogenesis.

That *Sry* is one of the two genes is not surprising, as it drives testis determination (*4*–*6*). Mouse *Sry* expression and translation occur very briefly during fetal development. In adult testes, *Sry* transcripts are thought to be aberrant and not translatable (*13*, *14*), although their role as epigenetic regulator(s) cannot be excluded (*15*). Nevertheless, it is reasonable to conclude that *Sry* plays a role primarily during sex determination.

This suggests that the second Y gene, *Eif2s3y*, is the only gene necessary to drive spermatogenesis through the first meiotic division and with the occasional meiotic progression to form haploid round spermatids. *Eif2s3y* is a Y-encoded subunit 3 of the eukaryotic translation initiation factor 2. It is ubiquitously expressed and, in the testis, plays a role in spermatogonial proliferation (*7*). The *Eif2s3y* gene has been conserved on the Y chromosome during eutherian evolution, but there is no Y-linked copy of *Eif2s3* detected in any of the simian primates, including humans (*16*).

In men, spermatogonial proliferation arrest results most often from deletions of *AZFa* (azoospermia; SCO syndrome), and it has been related to a loss of *DDX3Y* (*17*–*19*). In both men and mice, the *Eif2s3* and *Ddx3* genes belong to the family of widely expressed genes encoding proteins involved in initiation of mRNA translation at the ribosome. These genes have X homologs that escape X-inactivation, and the Y and X copies are suspected to be, at least in part, interchangeable, with the Y copy conserved to provide two doses of gene product in both male and female. The loss of the mouse Y-encoded *Ddx3y* is not detrimental for spermatogenesis because of the compensation provided by an X copy retrotransposed on an autosome (*20*). Analogically, in men, the presence of a retrotransposed X copy of *EIF2S3X*, in addition to *EIF2S3X* itself, explains why the loss of the Y copy was still permissive for spermatogenesis. Although there is no human copy of *Eif2s3y*, men have a Y-encoded copy of the translation factor EIF1A (eukaryotic translation initiation factor 1A, Y-linked) (*21*), which likely acts as part of a multiprotein complex that includes EIF2S3X, as well as other EIF family members. Note that EIF1AY is found in the *AZFb* region, and its diminished expression sporadically contributes to azoospermia (*22*).

At present, our findings in mice do not translate directly to humans. ROSI is still considered experimental in human ART because of concerns regarding the safety of injecting immature germ cells and technical difficulties (*23*). In spite of this, some children have already been born (*24*, *25*), and those were healthy. As we learn more about the effects and improve technical aspects of ROSI, this method may become more acceptable. Indeed, studies on ROSI effects in mice have been encouraging (*26*). Thus, our study may bear importance for clinicians working in ART clinics by supporting the possibility that ROSI may be a viable option for overcoming infertility in men with nonobstructive azoospermia.

Considering that we have obtained live offspring using germ cells from males with only two Y chromosome genes, one could question the importance of the Y chromosome in male reproduction. We believe that the answer lies in defining the need. Human Y chromosome is not on the way to oblivion, as has been implied in the past (*27*), and its genetic information is undoubtedly important for many aspects of reproduction involving the development of mature sperm and its function in normal fertilization (*28*). Most of the mouse Y chromosome genes are involved in spermatogenesis and sperm function and, as such, are necessary for normal fertilization (*29*, *30*). However, when it comes to assisted reproduction, our mouse study proves that the Y chromosome contribution can be brought to a bare minimum consisting of *Sry* and *Eif2s3y*. Indeed, it may well be possible to eliminate mouse Y chromosome altogether if appropriate replacements are made for those two genes.

References and Notes

1. C. Stern, *Am. J. Hum. Genet.* **9**, 147–166 (1957).
2. H. Skaletsky *et al.*, *Nature* **423**, 825–837 (2003).
3. Y. Yamauchi *et al.*, *Biol. Reprod.* **81**, 353–361 (2009).
4. J. Gubbay *et al.*, *Nature* **346**, 245–250 (1990).
5. A. H. Sinclair *et al.*, *Nature* **346**, 240–244 (1990).
6. P. Koopman, J. Gubbay, N. Vivian, P. Goodfellow, R. Lovell-Badge, *Nature* **351**, 117–121 (1991).
7. S. Mazeyrat *et al.*, *Nat. Genet.* **29**, 49–53 (2001).
8. N. Vernet *et al.*, *Curr. Biol.* **21**, 787–793 (2011).
9. Materials and methods and further details are available as supplementary materials on *Science* Online.
10. N. Vernet, S. K. Mahadevaiah, P. J. Ellis, D. G. de Rooij, P. S. Burgoyne, *Reproduction* **144**, 433–445 (2012).
11. T. Odorisio, T. A. Rodriguez, E. P. Evans, A. R. Clarke, P. S. Burgoyne, *Nat. Genet.* **18**, 257–261 (1998).
12. P. S. Burgoyne, S. K. Mahadevaiah, M. J. Sutcliffe, S. J. Palmer, *Cell* **71**, 391–398 (1992).
13. B. Capel *et al.*, *Cell* **73**, 1019–1030 (1993).
14. Y. W. Jeske, J. Bowles, A. Greenfield, P. Koopman, *Nat. Genet.* **10**, 480–482 (1995).
15. T. B. Hansen *et al.*, *Nature* **495**, 384–388 (2013).
16. I. E. Ehrmann *et al.*, *Hum. Mol. Genet.* **7**, 1725–1737 (1998).
17. C. Foresta, A. Ferlin, E. Moro, *Hum. Mol. Genet.* **9**, 1161–1169 (2000).
18. C. A. Sargent *et al.*, *J. Med. Genet.* **36**, 670–677 (1999).
19. C. Sun *et al.*, *Nat. Genet.* **23**, 429–432 (1999).
20. M. J. Mitchell, *Results Probl. Cell Differ.* **28**, 233–270 (2000).

21. B. T. Lahn, D. C. Page, *Science* **278**, 675–680 (1997).
22. S. E. Kleiman *et al.*, *Hum. Reprod.* **22**, 151–158 (2007).
23. Practice Committee of American Society for Reproductive Medicine, *Fertil. Steril.* **90** (suppl.), S199–S201 (2008).
24. L. Gianaroli *et al.*, *Fertil. Steril.* **72**, 539–541 (1999).
25. A. Saremi, N. Esfandiari, N. Salehi, M. R. Saremi, *Arch. Androl.* **48**, 315–319 (2002).
26. K. L. Tamashiro, Y. Kimura, R. J. Blanchard, D. C. Blanchard, R. Yanagimachi, *J. Assist. Reprod. Genet.* **16**, 315–324 (1999).
27. J. A. Graves, *Cell* **124**, 901–914 (2006).
28. J. F. Hughes *et al.*, *Nature* **463**, 536–539 (2010).
29. J. M. Riel *et al.*, *J. Cell Sci.* **126**, 803–813 (2013).
30. Y. Yamauchi, J. M. Riel, Z. Stoytcheva, P. S. Burgoyne, M. A. Ward, *Genome Biol.* **11**, R66 (2010).

Acknowledgments: The work was supported by NIH HD072380, HD058059, and GM103457 (Project 2) and Hawaii Community Foundation 13ADVC-60314 grants to M.A.W. The authors thank P. Burgoyne for providing paternal stock mice for breeding, overall support, and insightful discussions and N. Vernet from P. Burgoyne's group for sharing protocols and expertise on histological and DNA content analyses. We are grateful to numerous students who have helped with mouse genotyping. Histological sections were prepared by John A. Burns School of Medicine Histopathology Core supported by NIH grants National Institute on Minority Health and Health Disparities, NIH. G12 MD007601 and the National Institute of General Medical Sciences, NIH, P30 GM103341.

Supplementary Materials
www.sciencemag.org/content/343/6166/69/suppl/DC1
Materials and Methods
Supplementary Text
Figs. S1 to S8
Table S1
References (*31*–*50*)

28 June 2013; accepted 28 October 2013
Published online 21 November 2013;
10.1126/science.1242544

Targeted Therapy Resistance Mediated by Dynamic Regulation of Extrachromosomal Mutant EGFR DNA

David A. Nathanson,[2] Beatrice Gini,[1]* Jack Mottahedeh,[5]* Koppany Visnyei,[5] Tomoyuki Koga,[1] German Gomez,[1] Ascia Eskin,[10] Kiwook Hwang,[3,4] Jun Wang,[3,4] Kenta Masui,[1] Andres Paucar,[2,5] Huijun Yang,[1] Minori Ohashi,[2] Shaojun Zhu,[1] Jill Wykosky,[1] Rachel Reed,[1] Stanley F. Nelson,[10] Timothy F. Cloughesy,[7,8] C. David James,[6] P. Nagesh Rao,[9] Harley I. Kornblum,[2,5,7]† James R. Heath,[3,4]† Webster K. Cavenee,[1,11]† Frank B. Furnari,[1,11]† Paul S. Mischel[1,11]†‡

Intratumoral heterogeneity contributes to cancer drug resistance, but the underlying mechanisms are not understood. Single-cell analyses of patient-derived models and clinical samples from glioblastoma patients treated with epidermal growth factor receptor (EGFR) tyrosine kinase inhibitors (TKIs) demonstrate that tumor cells reversibly up-regulate or suppress mutant EGFR expression, conferring distinct cellular phenotypes to reach an optimal equilibrium for growth. Resistance to EGFR TKIs is shown to occur by elimination of mutant *EGFR* from extrachromosomal DNA. After drug withdrawal, reemergence of clonal *EGFR* mutations on extrachromosomal DNA follows. These results indicate a highly specific, dynamic, and adaptive route by which cancers can evade therapies that target oncogenes maintained on extrachromosomal DNA.

The majority of targeted therapies have not produced substantial survival benefits for most cancer patients (*1*, *2*). A variety of resistance mechanisms have been described, including incomplete target suppression, second-site mutations, and activation of alternative kinases to maintain signal flux to downstream effector pathways (*1*–*3*). Thus, most efforts are now aimed at developing better drugs or better drug combinations to more fully suppress the target oncogenes and their downstream signals. Changes in the cellular composition of tumors, particularly in response to targeted treatment, could facilitate such a resistance mechanism and thereby dictate patient response.

In glioblastoma (GBM), the most common malignant primary brain cancer of adults, the epidermal growth factor receptor (*EGFR*) is frequently mutated, commonly giving rise to the constitutively active oncogenic variant *EGFRvIII* (*4*, *5*). EGFRvIII potently accelerates tumor growth by cell-autonomous and intercellular signaling mechanisms (*6*), but it also makes tumor cells that express it more sensitive to EGFR tyrosine kinase inhibitors (TKIs) (*7*, *8*). In clinical GBM samples, the level of EGFRvIII protein expression varies widely among cells within the tumor mass (*6*, *9*–*15*). The potential contribution of heterogeneous EGFRvIII expression to EGFR TKI resistance in GBM (*16*) is not understood.

To determine whether EGFRvIII heterogeneity contributes to EGFR TKI resistance, single-cell analyses of a patient-derived EGFRvIII-expressing xenograft model (GBM39) (*17*) were performed. GBM39 cells stably express firefly luciferase (ff-LUC), enabling definitive tumor cell identification (fig. S1A). Quantitative microfluidic image cytometry (MIC) (*18*) demonstrated detectable levels of EGFRvIII protein in 60% (±5%) of tumor cells (fig. S1B). The EGFRvIII-expressing tumor cells ($EGFRvIII^{High}$) demonstrated increased phosphatidylinositol 3-kinase–Akt–mammalian target of rapamycin (PI3K-Akt-mTOR) signaling (Fig. 1A and fig. S2), elevation in tumor cell proliferation by a factor of 4 (Fig. 1B and fig. S2), a lower basal apoptotic rate by a factor of 15 (Fig. 1C and fig. S2), and increased glucose uptake (Fig. 1D) relative to the GBM cells lacking detectable EGFRvIII protein ($EGFRvIII^{Low}$) (Fig. 1, D and E). Further, the $EGFRvIII^{High}$ tumor cells showed enhanced cell death in response to the EGFR TKI erlotinib (Fig. 1F).

To determine the effect of an EGFR TKI on EGFRvIII population dynamics, mice bearing tumors were treated daily with oral erlotinib (150 mg per kg of weight). Erlotinib treatment initially caused 80% tumor shrinkage (response) (blue line in Fig. 1G), shifting the composition of tumors from being predominantly $EGFRvIII^{High}$ to predominantly $EGFRvIII^{Low}$ tumor cells (Fig. 1H and fig. S3). This shift in the EGFRvIII population dynamics was maintained, even after tumors developed resistance to continued erlotinib treatment (resistant) [Fig. 1G (red line) and H, and fig. S3], and was also detected in another patient-derived ex vivo neurosphere culture, HK296 (fig. S4). Most important, in tumor tissue from GBM patients treated for 7 to 10 days with the EGFR/HER2 inhibitor lapatinib, the relative fraction of $EGFRvIII^{High}$ tumor cells dramatically declined relative to each patient's pretreatment sample (Fig. 1, I and J). Of note, this analysis was confined to patients whose posttreatment tumor tissue showed reduced EGFR phosphorylation relative to the pretreatment sample. We did not detect any decrease in EGFRvIII level in the two available GBMs in which no decrease in phospho-EGFR was seen after lapatinib treatment.

[1]Ludwig Institute for Cancer Research, University of California at San Diego, La Jolla, CA, USA. [2]Department of Molecular and Medical Pharmacology, David Geffen UCLA School of Medicine, Los Angeles, CA 90095, USA. [3]NanoSystems Biology Cancer Center, California Institute of Technology, Pasadena, CA, USA. [4]Division of Chemistry and Chemical Engineering, California Institute of Technology, MC 127-72, Pasadena, CA 91030, USA. [5]Neuropsychiatric Institute–Semel Institute for Neuroscience and Human Behavior and Department of Psychiatry and Biobehavioral Sciences, David Geffen UCLA School of Medicine, Los Angeles, CA 90095, USA. [6]University of California San Francisco, San Francisco, CA 94143, USA. [7]Henry Singleton Brain Tumor Program and Jonsson Comprehensive Cancer Center, David Geffen UCLA School of Medicine, Los Angeles, CA 90095, USA. [8]Department of Neurology, David Geffen UCLA School of Medicine, Los Angeles, CA 90095, USA. [9]Department of Pathology and Laboratory Medicine, David Geffen UCLA School of Medicine, Los Angeles, CA 90095, USA. [10]Department of Human Genetics, David Geffen UCLA School of Medicine, Los Angeles, CA 90095, USA. [11]UCSD School of Medicine, La Jolla, CA 92093, USA.

*These authors contributed equally to this work.
†This work is based on equal contributions from the laboratories of H.I.K, J.R.H, W.K.C, F.B.F, and P.S.M
‡Corresponding author. E-mail: pmischel@ucsd.edu

OPEN ACCESS Freely available online

PLOS ONE

Global Genome Analysis of the Downstream Binding Targets of Testis Determining Factor SRY and SOX9

Ramji K. Bhandari, Md. M. Haque, Michael K. Skinner*

Center for Reproductive Biology, School of Biological Sciences, Washington State University, Pullman, Washington, United States of America

Abstract

A major event in mammalian male sex determination is the induction of the testis determining factor *Sry* and its downstream gene *Sox9*. The current study provides one of the first genome wide analyses of the downstream gene binding targets for SRY and SOX9 to help elucidate the molecular control of Sertoli cell differentiation and testis development. A modified ChIP-Chip analysis using a comparative hybridization was used to identify 71 direct downstream binding targets for SRY and 109 binding targets for SOX9. Interestingly, only 5 gene targets overlapped between SRY and SOX9. In addition to the direct response element binding gene targets, a large number of atypical binding gene targets were identified for both SRY and SOX9. Bioinformatic analysis of the downstream binding targets identified gene networks and cellular pathways potentially involved in the induction of Sertoli cell differentiation and testis development. The specific DNA sequence binding site motifs for both SRY and SOX9 were identified. Observations provide insights into the molecular control of male gonadal sex determination.

Citation: Bhandari RK, Haque MM, Skinner MK (2012) Global Genome Analysis of the Downstream Binding Targets of Testis Determining Factor SRY and SOX9. PLoS ONE 7(9): e43380. doi:10.1371/journal.pone.0043380

Editor: Toshi Shioda, Massachusetts General Hospital, United States of America

Received March 16, 2012; **Accepted** July 23, 2012; **Published** September 12, 2012

Funding: This work was supported by a United States National Institutes of Health grant to MKS. The funders had no role in study design, data collection and analysis, decision to publish, or preparation of the manuscript.

Competing Interests: The authors have declared that no competing interests exist.

* E-mail: skinner@wsu.edu

Introduction

The process of mammalian sex determination was described by Alfred Jost in the 1940's as 1) chromosomal, 2) gonadal and 3) sexual differentiation [1,2,3]. The chromosomal composition determines the genotypic sex (XY as males and XX as females) at fertilization. Mammalian embryos are considered sexually indifferent until the transient action of a Y-linked testis determining factor (TDF) that initiates gonadal differentiation into the testis [4]. Although a number of candidate TDF genes were suggested [5,6,7], it was not until 1990 that the sex determining region of the Y-chromosome (SRY) was identified to induce Sertoli cell differentiation and testis development [8,9]. After finding *Sry* as a master male sex determining gene it was hypothesized that testis development must involve SRY interactions with other autosomal genes involved in the regulation of Sertoli cell differentiation as downstream targets of SRY [10]. Testis determination in the mouse is initiated at embryonic day E10.5 after the *Sry* is expressed in precursor Sertoli cells of the indifferent gonad. SRY up-regulates the expression of an autosomal related HMG-box gene, *Sox9*, that promotes the further differentiation of Sertoli cells [11,12]. An example of a SOX9 downstream target is Anti-Müllerian Hormone (AMH) [13,14]. The expression of *Sox9* is potentiated by actions of fibroblast growth factor (FGF9) and prostaglandin D2 in Sertoli cells [15,16,17]. SOX9 reaches a critical threshold that represses *Sry* expression via a SOX9-dependent negative feedback loop [11,18]. It is believed that at this stage SOX9 functionally replaces SRY and acts downstream to further promote the differentiation of the Sertoli cell in the fetal testis. Genetic mutational studies suggest that the loss of function of SRY and SOX9 in XY embryos results in male-to-female sex reversal [9,10]. In contrast, as the gain of function in XX embryos induces male development [10], indicating that these two genes cooperate in testis determination [19,20,21,22,23]. The current study was designed to use a genome wide analysis to identify additional downstream targets of SRY and SOX9 to further elucidate the molecular control mechanism of mammalian male sex determination.

Testis differentiation involves the actions of a genome wide network of genes initiated by SRY. In contrast, ovary differentiation has been thought to be passive and initiated in the absence of SRY expression. The complex biological process of either testis or ovary development requires active networks of factors that tip the balance of phenotypic sexes. For example, SOX9, FGF9, PDGS, DMRT1 promote testis differentiation, while factors such as WNT4, FOXL2, RSPO1 repress male genes to promote ovary development [22]. These mutually antagonistic forces lead to the development of opposite gonadal sex. However, in a systems biology perspective it is likely that genome wide networks of the genes that regulate this critical biological process will be required and not a few selected genes.

Currently it is widely believed that the primary function of SRY is to trigger molecular events underlying fetal testis differentiation through the induction of *Sox9* expression. At the time of Sertoli cell differentiation and testis development, SRY and steroidogenic factor 1 (SF1) synergistically act on testis-specific enhancer region of the *Sox9* promoter to induce testis-specific expression of *Sox9*. Therefore, *Sox9* has been found to be one of the direct downstream targets of the protein encoding SRY [24]. In 2009, cerebillin precursor 4 (*Cbln4*) gene was found to be one of the downstream

targets of SRY and SOX9 [25]. Cbln4 encodes a transmembrane protein and is expressed in a male-specific manner, but the function of Cbln4 product in testicular development is not known. Recently, we have shown in the rat that the basic helix-loop-helix transcription factor *Tcf21* and the growth factor neurotrophin 3 (*Ntf3*) are direct downstream targets of SRY [26,27]. TCF21 and NTF3 have previously been reported to have roles in formation of testis cords [28,29]. Therefore, the majority of SRY downstream genes remain to be elucidated.

Following the expression of *Sry* in precursor Sertoli cells of the bipotential gonad a myriad of genes are thought to act in networks to initiate the differentiation of precursor cells into Sertoli cells. In the absence of SRY, testis differentiation derails and leads to the development of an ovary. Mutually exclusive and equally powerful molecular forces are acting to ensure the differentiation of the bipotential gonad into proper gonadal structures [19]. Interestingly, even in the presence of SRY the conditional deletion of Sox9 in precursor Sertoli cells causes a distinct male-to-female sex reversal with a multitude of molecular changes, suggesting that SRY and SOX9 have common functions but specific molecular targets [30]. Studies over the past two decades have expanded our understanding of the importance of SRY and SOX9 in testis differentiation, however, the information on how these two determinants are acting downstream to promote testis differentiation is not known. The current study took an *in vivo* genome wide systems level approach to pull down downstream binding targets from rat embryonic gonads that were undergoing male sex differentiation. Observations identify the direct downstream binding targets of SRY and SOX9. Global gene networks of binding targets of these two critical sex determination factors provides insight and opportunities for future investigation of the molecular control of Sertoli cell differentiation and testis development.

Results

Downstream Binding Targets of SRY

Since the discovery of SRY as a male sex determination and testis determining factor [8,9], only a few genes have been identified as *in vivo* direct downstream targets. Currently, only *Sox9, Tcf21, Ntf3* and *Cbln4* are reported as downstream targets of SRY. The existence of other downstream targets has been debated [21,22,23]. One of the limitations for not having any significant progress in finding downstream targets is the classic *in vivo* chromatin immunoprecipitation (ChIP) method that requires a large amount of chromatin for performing a ChIP assay and detection of low affinity binding sites. To perform a conventional cross-linked ChIP assay at least 5 million cells are required. During gonadal sex determination the gonads are small and precursor Sertoli cells that express *Sry* are low in number. In order to collect 5 million *Sry* expressing cells hundreds of embryos are required. To overcome this issue we established a native (not involving cross-linking) ChIP assay that utilizes twenty to thirty embryonic testis and carrier cell chromatin of fly origin. The native ChIP identifies the high affinity binding sites and reduces lower affinity sites compared to the conventional ChIP. The protocol developed involved the use of genome wide promoter tiling arrays to perform a ChIP-Chip assay using a competitive hybridization with non-immune IgG to eliminate false positives. The cell purity of the samples is irrelevant since the only site of SRY and SOX9 is the Sertoli cell in the gonad. The SRY or SOX9 Chip will only pull-down the Sertoli cell targets. The method dramatically increased sensitivity and specificity of the analysis.

Initially this ChIP approach was used to identify *Tcf21* and *Ntf3* as direct downstream SRY target genes [26,27]. In order to pull-down all the downstream targets three independent ChIP assays with a specific SRY antibody on chromatin from E13 rat testis (13–18 tail somite stage embryos) were performed. A comparative hybridization of SRY-ChIP DNA with non-immune IgG-ChIP DNA to a rat promoter tiling array (Nimblegen) containing at least 4–5 kb for each of 15,287 proximal-promoter regions in the rat genome was performed. To identify genes bound by SRY and SOX9 a sliding window of 600 bp (the majority of our ChIP DNA fragments ranged approximately 400–600 bp) was used to detect SRY- specific enrichment present in proximal-promoter regions. This required the detection of at least three consecutive probes in all three replicates at a statistical significance level less than $p<0.001$. A total of 1773 promoters were represented. To select the target promoters from this analysis a cut-off of $p<1\times10^{-7}$ was used that identified 71 genes as direct downstream binding targets with distinct SRY binding sites (response elements, [T/A]AACAA[T/A] & [T/A]TTGTT[A/T]) (Table 1). Atypical binding targets without any SRY binding site identified 159 additional promoters (Supplementary Table S1). A representative example of downstream direct targets is shown in Figure 1. PCR confirmation of each representative SRY site for the downstream binding target is shown next to the ChIP-Chip hybridization plot.

The three examples of SRY downstream direct targets shown are *Tcf21, Atn1*, and *Higd29*. The positive hybridization is specific to SRY-ChIP DNA hybridization and negative hybridization is specific to the non-immune IgG-ChIP-DNA, Figure 1(A–C). The localization of the SRY response element motif is indicated for each promoter. The other SRY downstream direct binding target ChIP-Chip hybridization profiles are shown in Supplemental Figure S1. Although *Sox9* is a direct downstream target of SRY, it was not detected by the ChIP-Chip assay. *Sox9* could not be found because hybridization probe sets contained only 4K base of the promoter regions and SRY binding to the *Sox9* promoter occurs at an upstream −7K base region of the promoter [24]. Therefore, the SRY-ChIP DNA was used to test the presence of *Sox9* by PCR in all three of the SRY-ChIP biological replicates, Figure 2. As expected, the SOX9 TESCO [23] binding site was detected in the SRY-ChIP DNA samples. Therefore, the two previously identified SRY targets SOX9 and TCF21 were detected in the SRY ChIP-Chip analysis helping validate the protocol. However, a limitation of the current study is that SRY binding sites outside of 4K base of the promoter would not be detected. This suggests the downstream binding targets detected will be a subset of a potentially larger set of SRY direct binding gene targets.

As a negative control, a non-immune IgG was used for each replicate of the ChIP assay. A comparative hybridization in the ChIP-Chip assay was then used to assess non-specific IgG binding. Hybridization results show that IgG also pulls down a significant number of gene promoter sites. In order to reduce the inclusion of false positives or false negatives in the list, manual screening of both SRY-bound and IgG-bound promoters at $p<1\times10^{-7}$ significance was performed. From 213 total IgG binding sites detected, 32 were found to be SRY binding positives, but their peaks were masked by adjacent larger peaks of IgG binding (Supplemental Figure S2, Supplemental Table S2). These binding target gene promoters were termed questionable positives and several were tested with PCR and found to be positive with SRY ChIP-PCR.

In addition to the direct SRY gene targets that contain an SRY response element motif, 159 atypical binding targets were identified that did not contain an SRY binding motif, Supple-

Table 1. Direct downstream binding targets of SRY during male sex determination.

Gene Symbol and Category	GenBank/Reference Sequence	Binding Site Chromosomal Location	p-value	# of SRY Motifs	Gene Title
Apoptosis					
Higd2a	NM_001106102	chr17:16083944-16084731	2.16E-21	1	HIG1 hypoxia inducible domain family, member 2A
Pdcd6ip	NM_001029910	chr8:118351413-118352013	1.59E-21	1	Programmed cell death 6 interacting protein
Cell Cycle					
RGD1560888	NM_001109061	chr8:40571831-40572431	5.07E-08	1	Similar to Cell division protein kinase 8
Development					
Atn1	NM_017228	chr4:160887462-160888360	1.28E-12	1	Atrophin 1
Crygb	NM_001109875	chr9:63736296-63737096	2.92E-11	1	Crystallin, gamma B
Lrrc68	NM_001107482	chr1:78888269-78888869	1.59E-08	2	Leucine rich repeat containing 68
Lcn11	NM_001135809	chr3:3888687-3889792	8.46E-09	1	Lipocalin 11
RGD1565947	NM_001106780	chr7:30717183-30717983	2.25E-09	3	Similar to netrin 4
Sar1b	NM_001009622	chr10:37281198-37281897	4.60E-10	3	SAR1 homolog B (S. cerevisiae)
Tex10	NM_001106653	chr5:65166327-65167127	4.78E-09	1	Testis expressed 10
Electron Transport					
Pdcl3	NM_001025709	chr9:38002255-38002855	8.65E-09	3	Phosducin-like 3
Immune Response					
Cd24	NM_012752	chr20:47499009-47499609	2.95E-20	2	CD24 molecule
Sec1	NM_001135584	chr1:96149778-96150598	4.18E-08	1	Secretory blood group 1
Metabolism & Transport					
Afg3l2	NM_001134864	chr18:63975093-63975767	6.73E-16	2	AFG3(ATPase family gene 3)-like 2
Exoc4	NM_053875	chr4:60405518-60406118	8.64E-09	1	Exocyst complex component 4
Gltp	NM_001134413	chr12:43194112-43195012	8.14E-32	1	Glycolipid transfer protein
Hpgds	NM_031644	chr4:94639300-94639900	2.34E-09	1	hematopoietic prostaglandin D synthase
Hyal1	NM_207616	chr8:112828762-112829362	4.39E-14	1	Hyaluronoglucosaminidase 1
Hyal3	NM_207599	chr8:112828762-112829362	4.39E-14	1	Hyaluronoglucosaminidase 3
Sdha	NM_130428	chr1:29738109-29738709	1.53E-10	1	Succinate dehydrogenase complex, A
Sdhd	NM_198788	chr8:53967070-53967670	4.44E-08	1	Succinate dehydrogenase complex, subunit D
Sec24a	NM_001105780	chr10:37281198-37281897	4.60E-10	3	SEC24 family, member A (S. cerevisiae)
Timm8b	NM_022541	chr8:53967070-53967670	4.44E-08	1	Translocase of inner mitochondrial membrane 8
Tmed4	NM_001107238	chr14:87002671-87003360	5.63E-08	1	Transmembrane emp24 protein transport 4
Tpi1	NM_022922	chr4:160936834-160937434	4.38E-11	1	Triosephosphate isomerase 1
Proteolysis					
Cpa2	NM_001013083	chr4:57449368-57449968	6.76E-08	1	Carboxypeptidase A2 (pancreatic)
Cul2	NM_001108417	chr17:62742775-62743470	1.46E-08	2	Cullin 2
LOC689226	BC167074	chr7:18614322-18614922	9.65E-11	2	Similar to ubiquitin-conjugating enzyme E2R 2
Tmprss6	NM_001130556	chr7:116422114-116422899	2.30E-12	1	Transmembrane protease, serine 6
Receptors & Binding Proteins					
Grm2	NM_001105711	chr8:111851299-111852092	5.01E-09	2	Glutamate receptor, metabotropic 2
Il1rapl1	NM_177935	chrX:74472070-74472768	2.96E-14	4	interleukin 1 receptor accessory protein-like 1
Olr122	NM_001000156	chr1:161468724-161469324	4.12E-08	3	Olfactory receptor 122
Olr1553	NM_001000051	chr11:42266451-42267051	1.33E-10	1	Olfactory receptor 553
Olr1657	NM_001000536	chr17:50544822-50545500	2.98E-08	1	Olfactory receptor 1657
Olr463	NM_001000934	chr3:69098160-69098859	5.02E-08	1	Olfactory receptor 463
Olr669	NM_001000349	chr3:73187159-73187759	1.57E-08	2	Olfactory receptor 669
Olr770	NM_001000372	chr3:97220204-97221208	2.48E-09	1	Olfactory receptor 770
Olr853	NM_001000398	chr5:70398861-70399461	9.49E-08	1	Olfactory receptor 853
Vom1r59	AY510282	chr1:73592390-73592990	1.52E-10	1	vomeronasal 1 receptor, 59

Table 1. Cont.

Gene Symbol and Category	GenBank/Reference Sequence	Binding Site Chromosomal Location	p-value	# of SRY Motifs	Gene Title
Vom2r11	NM_001099470	chr1:57382648-57383341	7.39E-08	2	Vomeronasal 2 receptor 11
Vom2r8	NM_001099464	chr1:49588680-49589280	1.60E-08	2	Vomeronasal 21 receptor 8
Signaling					
Jkamp	NM_001106738	chr6:94284244-94284963	1.46E-23	1	JNK1/MAPK8-associated membrane protein
RGD1562638	NM_001100944	chr16:68750676-68751465	6.94E-22	1	MAP/microtubule affinity-regulating kinase 3
Transcription					
Armc7	BC166454	chr10:105554314-105555129	5.38E-08	3	armadillo repeat containing 7
Btbd4	NM_001107808	chr3:170570362-170570962	3.04E-09	1	Zinc finger and BTB domain containing 46
Ccdc127	NM_198766	chr1:29738109-29738709	1.53E-10	1	Coiled-coil domain containing 127
Gata1	NM_012764	chrX:26564683-26565464	7.55E-08	1	GATA binding protein 1
Maff	NM_001130573	chr7:117329082-117329787	3.55E-08	1	V-maf musculoaponeurotic fibrosarcoma F
Meis1	NM_001134702	chr14:99835529-99836129	4.65E-15	2	Meis homeobox 1
Nop16	NM_001047095	chr17:16083944-16084731	2.16E-21	1	NOP16 nucleolar protein homolog (yeast)
Nsfl1c	NM_031981	chr3:141798504-141799104	2.81E-08	2	NSFL1 (p97) cofactor (p47)
Phox2a	NM_053869	chr1:159272192-159273082	4.67E-14	1	Paired-like homeobox 2a
Rag1	NM_053468	chr3:86795336-86796015	1.34E-11	2	Recombination activating gene 1
Rai14	NM_001011947	chr2:60062344-60063029	1.37E-09	1	Retinoic acid induced 14
Zfp354a	NM_052798	chr10:36652409-36653009	1.28E-08	1	Zinc finger protein 354A
Znf507	NM_001106248	chr1:88364838-88365940	3.47E-12	4	Zinc finger protein 507
Ddx46	NM_139098	chr17:15030355-15030955	1.78E-13	3	DEAD (Asp-Glu-Ala-Asp) box polypeptide 46
Tcf21	NM_001032397	chr1:23209070-23210356	1.76E-10	3	Transcription factor 21/Pod1/Capsulin/ Epicardin
Translation & Protein Modification					
Tsen2	NM_001014057	chr4:151669335-151669935	4.91E-08	1	tRNA splicing endonuclease 2 homolog
Arfgef2	NM_181083	chr3:157964936-157965536	1.30E-10	1	ADP-ribosylation factor guanine factor 2
Mrpl51	NM_001106621	chr4:161309657-161310257	4.88E-09	2	Mitochondrial ribosomal protein L51
Rpl24	NM_022515	chr11:45636727-45637615	1.07E-10	1	Ribosomal protein L24
Rtf1	NM_001108958	chr3:106189897-106190688	4.05E-09	1	Rtf1, Paf1/RNA polymerase II complex
Miscellaneous & Unknown					
Cytsa	NM_001039455	chr20:13946693-13947489	1.35E-09	1	Cytospin A
Dcaf7	NM_001107057	chr10:95425513-95426318	6.60E-12	1	DDB1 and CUL4 associated factor 7
Fam12b	NM_178103	chr15:27107548-27108246	1.48E-11	1	Epididymal protein 3B
LOC308990	NM_001025001	chr1:186339810-186340908	7.02E-10	3	Hypothetical protein LOC308990
RGD1303127	NM_001004244	chr7:137280915-137281694	3.89E-12	1	Similar to hypothetical protein FLJ20436
RGD1562533	BC127538	chr12:7302557-7303157	1.79E-08	1	Similar to mKIAA0774 protein
ESTs					
RGD1305721	NM_001108031	chr6:94284244-94284963	1.46E-23	1	Similar to RIKEN cDNA 2810055F11
LOC298139	NM_001013930	chr5:91664056-91664656	1.57E-09	1	Similar to RIKEN cDNA 2310003M01
RGD1307325	BC082052	chr16:49407004-49407724	6.84E-08	1	Similar to RIKEN cDNA 4933411K20

doi:10.1371/journal.pone.0043380.t001

mental Table S1, but were identified in the ChIP-Chip assay. This suggests SRY associates with transcription factor complexes independent of DNA binding. Therefore, a large number of SRY binding sites are atypical downstream targets not involving DNA binding. An example of such an SRY indirect target was *Cbln4* that was previously shown to be downstream of SRY [25], but does not have an SRY binding sequence motif in the 4K base proximal promoter. The functional significance and mechanism of SRY regulation of these regions in the absence of SRY DNA sequence binding remains to be investigated.

Downstream Binding Targets of SOX9

Downstream binding targets of SOX9 were analyzed using the same strategy as for SRY with an antibody specific for rat SOX9 [27]. Two *in vitro* confirmed distinct binding motifs [17,31] were found for SOX9 binding: [T/C]TTG[T/A]G and [T/A]AACAA[T/A]. At a statistical significance of $p<1\times10^{-7}$, a total of 109 promoters were found to be direct binding targets of SOX9, Table 2. From these, 86 promoters have a SOX9 specific DNA sequence binding motif and 72 have an SRY HMG box DNA sequence binding motif. Combined there were 49 promoter

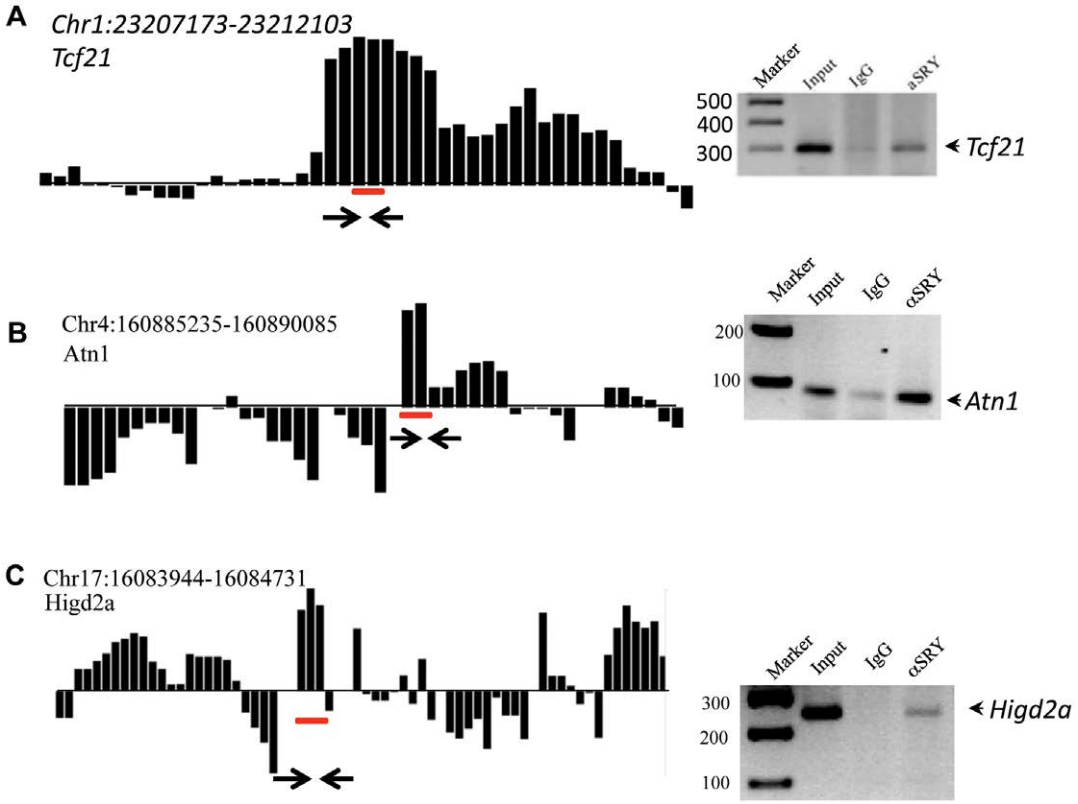

Figure 1. Representative examples SRY downstream direct binding target gene promoters for (A) *Tcf21*, (B) *Atn1*, and (C) *Higd2a*. The positive hybridization is specific to SRY ChIP-DNA signal and negative hybridization to the non-immune IgG ChIP-DNA signal. Hybridization signals are the average of three biological replicates of ChIP assays. Hybridization signals below the statistical significance of $p<1\times10^{-7}$ was not considered. The localization of SRY response element motif is indicated for each promoter as a horizontal line under the bar. PCR primers were designed from the position indicated by two arrows. The PCR gel identifies PCR product size with (Markers), genomic DNA (Input), IgG ChIP (IgG) and SRY ChIP (aSRY). Data represent ChIP-PCR assays from three different experiments and biological replicates.
doi:10.1371/journal.pone.0043380.g001

regions with both SOX9 specific and HMG box binding motifs (Table 2). There were 24 promoter regions without a SOX9 binding motif (Supplemental Table S3) and 39 regions (Supplemental Table S4) with adjacent IgG negative peaks (termed here as questionable positives). Representative examples of downstream direct binding targets are shown in Figure 3 and PCR confirmation of each representative is shown next to the ChIP-Chip hybridization plot. Interestingly, the number of direct SRY binding targets of 71 and atypical binding targets of 159 when compared to the 109 direct SOX9 binding targets and 24 atypical binding targets suggests SRY has a much larger role in binding indirectly to transcription factor complexes compared to SOX9 that predominately has direct binding targets.

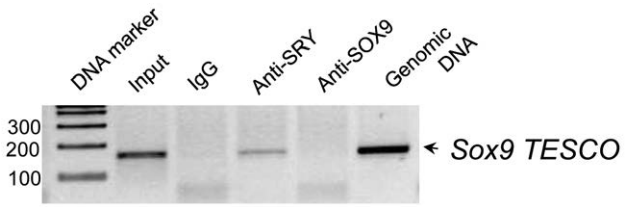

Figure 2. ChIP-PCR confirmation of *Sox9* as a downstream direct target of SRY. *Sox9* hybridization signals were not detected as the binding of SRY to Sox9 promoter is shown to occur at the TESCO region located at −7K upstream of the transcription start site. Non immune IgG was used as a negative control for each assay. ChIP DNA from IgG represented negative control throughout the experiment. PCR was conducted on 200 ng DNA amplified by whole genome amplification kit (Sigma). Data represent ChIP-PCR assay from three different experiments and biological replicates.
doi:10.1371/journal.pone.0043380.g002

Overlap between SRY and SOX9 Binding Targets

Considering the 71 direct downstream binding targets of SRY identified and 109 direct binding targets for SOX9, and including questionable positives, only five promoters were common between SRY and SOX9 targets. These common targets are Higd2a, Nop16, Orl770, Rtf1, and Vom2r11. A comparison of atypical binding targets (those without binding motifs) identified only one promoter in common at $p<1\times10^{-7}$. Using a less stringent statistical cut off ($p<1\times10^{-5}$), we found 175 in SRY ChIP and 259 in SOX9 as direct binding targets. Of these less stringent binding targets, only 13 overlapped. An analysis of the overlap between direct and atypical binding targets was performed. Between direct binding targets of SRY and atypical binding targets of SOX9, there were none at both $p<1\times10^{-5}$ and $p<1\times10^{-7}$ cut-offs, whereas between SRY atypical and SOX9 direct binding targets there were 15 promoters in common, Table 2. Therefore, some atypical binding targets of SRY may be the direct binding targets for SOX9. Interestingly, combined observations demonstrate minimal (<10%) overlap between SRY and SOX9 targets suggesting the two factors are functionally

Table 2. Direct downstream binding targets of SOX9 during male sex determination.

Gene Symbol and Category	GenBank/Reference Sequence	Binding Site Chromosomal Location	p-value	# of motifs		Gene Title
				Sox9	SRY	
Apoptosis						
Higd2a	NM_001106102	chr17:16084544-16085239	1.38E-13	1	0	HIG1 hypoxia inducible 2A
Cytoskeleton-ECM						
Cntn4	NM_053879	chr4:141196887-141197487	3.01E-13	0	1	Contactin 4
Dnah1	NM_001033655	chr16:6759427-6760027	1.94E-08	1	1	Dynein, axonemal, heavy chain 1
Enam	NM_001106001	chr14:21163829-21164930	1.11E-11	3	1	Enamelin
Fxc1	NM_053371	chr1:163372155-163373134	3.76E-13	3	1	Fractured callus expressed transcript 1
LOC689770	NM_001142304	chr4:165929907-165930589	1.75E-12	3	0	Similar to osteoclast inhibitory lectin
Pcdhb9	NM_001109390	chr18:30207966-30208648	2.85E-20	0	2	Protocadherin beta 9
Spast	NM_001108702	chr6:21051125-21051725	1.98E-10	2	0	Spastin
Development						
Ang1	NM_001006992	chr15:27080104-27080796	5.75E-30	0	1	Angiogenin, ribonuclease A family, member 1
Dscr3	NM_001108316	chr3:15864716-15865316	1.88E-10	2	1	Down syndrome critical region gene 3
Gsg1	NM_001013166	chr4:172210431-172211196	3.79E-08	1	0	Germ cell associated 1
Lmln	NM_001108843	chr11:69550989-69551670	3.81E-08	0	2	Leishmanolysin-like
Neurod6	NM_001109237	chr4:84479894-84480494	5.46E-08	1	0	Neurogenic differentiation 6
Per3	NM_023978	chr5:168190800-168191622	2.83E-12	3	1	Period homolog 3 (Drosophila)
Pcp4l1	NM_001126093	chr13:87085586-87086186	2.70E-08	1	0	Purkinje cell protein 4-like 1
Sv2b	NM_057207	chr1:130887128-130887728	8.05E-19	1	0	Synaptic vesicle glycoprotein 2b
Electron Transport						
Cyp11a1	NM_017286	chr8:61792218-61792818	2.97E-17	0	1	Cytochrome P450, family 11, a1
Epigenetics						
Wbscr22	NM_001135743	chr12:22726326-22726926	4.69E-10	3	1	Williams Beuren syndrome chromosome region 22
Growth Factors						
Ngfrap1	NM_053401	chrX:123585655-123586255	1.78E-10	1	0	Nerve growth factor receptor associated protein 1
Immune Response						
Hrg	NM_133428	chr11:80264162-80264838	1.74E-12	2	0	Hhistidine-rich glycoprotein
Metabolism & Transport						
Aox3l1	NM_001008522	chr9:56944915-56945610	5.72E-10	1	0	Aldehyde oxidase 3-like 1
Ehhadh	NM_133606	chr11:81472220-81472820	1.32E-14	1	1	Hydratase/3-hydroxyacyl CoA dehydrogenase
Exosc4	NM_001134860	chr7:114375307-114376102	1.22E-09	1	4	Exosome component 4
Gnpnat1	NM_001134756	chr15:21287426-21288103	2.56E-16	0	1	Glucosamine-phosphate N-acetyltransferase 1
Gsk3b	NM_032080	chr11:64429588-64430188	7.30E-08	1	0	Glycogen synthase kinase 3 beta
Hsd3b	M38179	chr2:193507626-193508226	4.87E-09	1	2	3 beta-hydroxysteroid dehydrogenase
Hsd3b1	NM_001007719	chr2:193507626-193508226	4.87E-09	1	2	hydroxy-delta-5-steroid dehydrogenase, 3 beta- and steroid delta-isomerase 1
LOC311352	NM_001014047	chr3:107941134-107941734	1.61E-08	2	0	Similar to Adenosine deaminase CG11994-PA
LOC500959	NM_001033072	chr8:24855879-24856479	3.90E-09	0	1	Similar to triosephosphate isomerase
Lypla1	NM_013006	chr5:14912620-14913220	1.85E-12	1	0	Lysophospholipase 1
Mblac2	NM_001108934	chr2:9807293-9807893	5.07E-30	2	6	Metallo-beta-lactamase domain containing 2
Ndufa10	NM_199495	chr6:62282076-62283066	4.34E-10	0	1	NADH dehydrogenase 1 alpha subcomplex 10
Pop1	NM_001130550	chr7:69940911-69941511	2.41E-23	2	0	processing of precursor 1

Table 2. Cont.

Gene Symbol and Category	GenBank/Reference Sequence	Binding Site Chromosomal Location	p-value	# of motifs		Gene Title
				Sox9	SRY	
Slc22a7	NM_053537	chr9:9932589-9933384	5.04E-11	1	0	Solute carrier family 22, member 7
Ugt1a6	BC107931	chr9:87035929-87036629	8.29E-11	3	3	UDP glucuronosyltransferase 1 A6
Ugt1a7c	AF461738	chr9:87029719-87030319	9.85E-12	0	1	UDP glucuronosyltransferase 1 A7C
Proteolysis						
P22k15	NM_199266	chr3:138338313-138338913	1.71E-12	0	1	Cystatin related protein 2
Ube2s	NM_001106224	chr1:67742581-67743181	1.66E-11	1	2	Ubiquitin-conjugating enzyme E2S
Receptors & Binding Proteins						
Grm3	NM_001105712	chr4:20745927-20746648	1.17E-08	2	1	Glutamate receptor, metabotropic 3
Hspbp1	NM_139261	chr1:67879661-67880261	9.96E-19	1	0	HSPA (heat shock 70kDa) binding protein, cytoplasmic cochaperone 1
Ly49s3	AY747628	chr4:168209700-168210300	1.16E-17	1	1	Ly-49 stimulatory receptor 3
Olr1006	NM_001000075	chr7:6593954-6595067	1.12E-10	0	7	Olfactory receptor 1006
Olr1057	NM_001000072	chr7:7914900-7915500	9.52E-10	3	1	Olfactory receptor 1057
Olr1162	NM_001000870	chr8:18233917-18234517	4.36E-10	0	1	Olfactory receptor 1162
Olr1339	NM_001000481	chr8:43021887-43022487	5.95E-10	2	0	Olfactory receptor 1339
Olr1370	NM_001000979	chr10:12391699-12392299	2.70E-08	0	3	Olfactory receptor1370
Olr1496	NM_001000716	chr10:60966886-60967486	4.45E-08	1	3	Olfactory receptor 1496
Olr1533	NM_001000496	chr11:41855848-41856448	5.37E-12	0	1	Olfactory receptor 1533
Olr1546	NM_001001106	chr11:42154682-42155282	9.41E-08	2	2	Olfactory receptor 1546
Olr1622	NM_001000838	chr15:26338868-26339468	1.12E-11	1	1	Olfactory receptor 1622
Olr1737	NM_001001422	chr20:1384704-1385401	2.59E-08	4	2	Olfactory receptor 1737
Olr1738	NM_001006599	chr20:1384704-1385401	2.59E-08	4	2	Olfactory receptor 1738
Olr1742	NM_001001424	chr20:1436423-1437023	1.45E-08	2	1	Olfactory receptor 1742
Olr1766	NM_001000490	chrX:136392211-136392811	4.00E-10	0	1	Olfactory receptor 1766
Olr185	NM_001000183	chr1:162806198-162806895	6.91E-12	3	0	Olfactory Receptor 185
Olr186	NM_001001031	chr1:162806198-162806895	6.91E-12	3	0	Olfactory receptor 186
Olr331	NM_001000760	chr1:215223740-215224437	1.07E-13	2	2	Olfactory receptor 331
Olr340	NM_001000253	chr1:216001183-216001783	4.16E-10	1	0	Olfactory receptor 340
Olr522	NM_001000562	chr3:70113851-70114451	4.46E-08	0	2	Olfactory receptor 522
Olr557	NM_001000669	chr3:70965140-70965837	9.09E-08	0	2	Olfactory receptor 557
Olr621	NM_001000652	chr3:72132250-72133033	4.98E-23	3	3	Olfactory receptor 621
Olr664	NM_001000347	chr3:73090449-73091049	6.82E-09	2	4	Olfactory receptor 664
Olr734	NM_001000617	chr3:74546184-74546962	4.49E-08	2	3	Olfactory receptor 734
Olr770	NM_001000372	chr3:97220509-97221208	3.73E-16	2	1	Olfactory receptor 770
Olr795	NM_001000601	chr3:97991622-97992349	1.66E-08	1	0	Olfactory receptor 795
Olr81	NM_001001271	chr1:160920906-160921506	1.44E-21	0	3	Olfactory receptor 81
Olr821	NM_001000842	chr4:70985769-70986369	3.28E-11	1	1	Olfactory receptor 821
Trip13	NM_001011930	chr1:30162343-30163033	4.06E-08	1	0	Thyroid hormone receptor interactor 13
Vom1r29	AY510346	chr1:63196521-63197705	3.75E-18	2	3	vomeronasal 1 receptor, 29
Vom1r3	AY510342	chr1:57221331-57221931	3.17E-13	1	5	vomeronasal 1 receptor 3
Vom1r56	AY510280	chr1:73406816-73407416	3.38E-10	1	1	vomeronasal 1 receptor, 56
Vom1r84	AY510312	chr4:86887717-86888419	2.05E-13	0	2	vomeronasal 1 receptor, 84
Vom1r86	AY510308	chr4:86950403-86951088	3.40E-11	1	2	vomeronasal 1 receptor, 86
Vom1r87	AY510311	chr4:87006096-87006786	1.93E-08	1	1	Vomeronasal 1 receptor 87
Vom1r93	U36896	chr4:123911382-123911982	3.12E-09	3	1	vomeronasal 1 receptor, 93
Vom2r11	NM_001099470	chr1:57382648-57383341	2.68E-08	2	2	Vomeronasal 2 receptor 11
Vom2r36	NM_001099483	chr1:73188300-73188900	4.39E-11	2	1	Vomeronasal 2 receptor 36
Vom2r60	NM_001099480	chr12:1140789-1141389	7.98E-08	2	2	Vomeronasal 2 receptor 60

Table 2. Cont.

Gene Symbol and Category	GenBank/Reference Sequence	Binding Site Chromosomal Location	p-value	# of motifs		Gene Title
				Sox9	SRY	
Signaling						
Brsk1	NM_001127337	chr1:67879661-67880261	9.96E-19	1	0	BR serine/threonine kinase 1
Defa9	AY623753	chr16:75272675-75273275	6.03E-10	1	0	Defensin alpha 9
Eepd1	NM_001014088	chr8:25170198-25170876	3.27E-14	1	3	Endo-/exonuclease/phosphatase family domain 1
Frmpd4	NM_001106960	chrX:47679803-47680403	2.02E-10	2	0	FERM and PDZ domain containing 4
Gpaa1	NM_001004240	chr7:114375307-114376102	1.22E-09	1	4	Glycosylphosphatidylinositol anchor attachment 1
Hrsp12	NM_031714	chr7:69940911-69941511	2.41E-23	2	0	Heat-responsive protein 12
Iqcg	NM_001014230	chr11:69550989-69551670	3.81E-08	0	2	IQ motif containing G
Plekhg2	BC169013	chr1:83483036-83483636	1.96E-08	4	0	Pleckstrin family G member 2
Pik3c3	NM_022958	chr18:22494497-22495193	2.29E-13	3	3	Phosphoinositide-3-kinase, class 3
Sel1l2	NM_001014049	chr3:128562470-128563250	1.06E-10	0	1	Sel-1 suppressor of lin-12-like 2
Transcription						
Ccdc7	NM_001011561	chr19_r:835125-835824	1.66E-20	4	0	coiled-coil domain containing 7
Ciz1	NM_001106568	chr3:11486246-11486846	6.90E-43	2	2	CDKN1A interacting zinc finger protein 1
Dnajc30	NM_001109024	chr12:22726326-22726926	4.69E-10	3	1	DnaJ (Hsp40) homolog, subfamily C, member 30
Fbxo15	NM_001108436	chr18:81502980-81503580	5.97E-11	2	1	F-box protein 15
Mina	NM_153309	chr11:41651274-41651977	5.97E-08	1	0	Myc induced nuclear antigen
Nfyb	NM_031553	chr7:23187814-23188499	1.38E-57	3	0	Nuclear transcription factor-Y beta
Nop16	NM_001047095	chr17:16084544-16085239	1.38E-13	1	0	NOP16 nucleolar protein homolog
Polr3g	NM_001109468	chr2:9807293-9807893	5.07E-30	2	6	Polymerase (RNA) III polypeptide G
Reck	NM_001107954	chr5:60339205-60339805	6.79E-08	1	0	Reversion-inducing-cysteine-rich kazal motifs
Snapc4	NM_001108574	chr3:4555001-4555601	1.08E-10	1	0	Small nuclear RNA activating complex, 4
Translation & Protein Modification						
Arfip2	NM_001004222	chr1:163372155-163373134	3.76E-13	3	1	ADP-ribosylation factor interacting protein 2
Rpl31	NM_022506	chr9:38437621-38438221	1.97E-08	2	0	Ribosomal protein L31
Rpl35a	NM_021264	chr11:69550989-69551670	3.81E-08	0	2	Ribosomal protein L35a-like
Rtf1	NM_001108958	chr3:106189897-106191081	7.77E-09	1	1	Paf1/RNA polymerase II complex component
Taf9b	NM_133615	chrX:94353049-94354039	1.88E-10	0	1	TATA box binding protein (TBP) 9b
Miscellaneous & Unknown						
Brd9	NM_001107453	chr1:30162343-30163033	4.06E-08	1	0	Bromodomain containing 9
RGD1359529	NM_001014193	chr5:153696495-153697095	9.47E-08	3	0	Similar to chromosome 1 open reading frame 63
Sdccag3	NM_001013135	chr3:4555001-4555601	1.08E-10	1	0	Serologically defined colon cancer antigen 3
ESTs						
RGD1305537	NM_001108822	chr16:13555220-13555820	4.93E-08	1	1	Similar to RIKEN cDNA 3110001I22

doi:10.1371/journal.pone.0043380.t002

distinct in the induction and progression of Sertoli cell differentiation and testis development.

SRY and SOX9 Binding Motifs

The DNA sequence binding motifs or response elements have been previously described using a limited number of binding sites to investigate the SRY binding motif as [T/A]AACAA[T/C] and [T/A]TTGTT[A/T] and the SOX9 binding motif as [T/C]TTG[T/A]G and [T/A]AACAA[T/A] [22,31]. Using all the SRY and SOX9 direct binding targets a computerized bioinformatics procedure (Meme Suite) previously described [32] identified the consensus DNA sequence binding motifs. The SRY binding motif is shown in Figure 4A and presents the various nucleotides at each base pair associated with the SRY binding site.

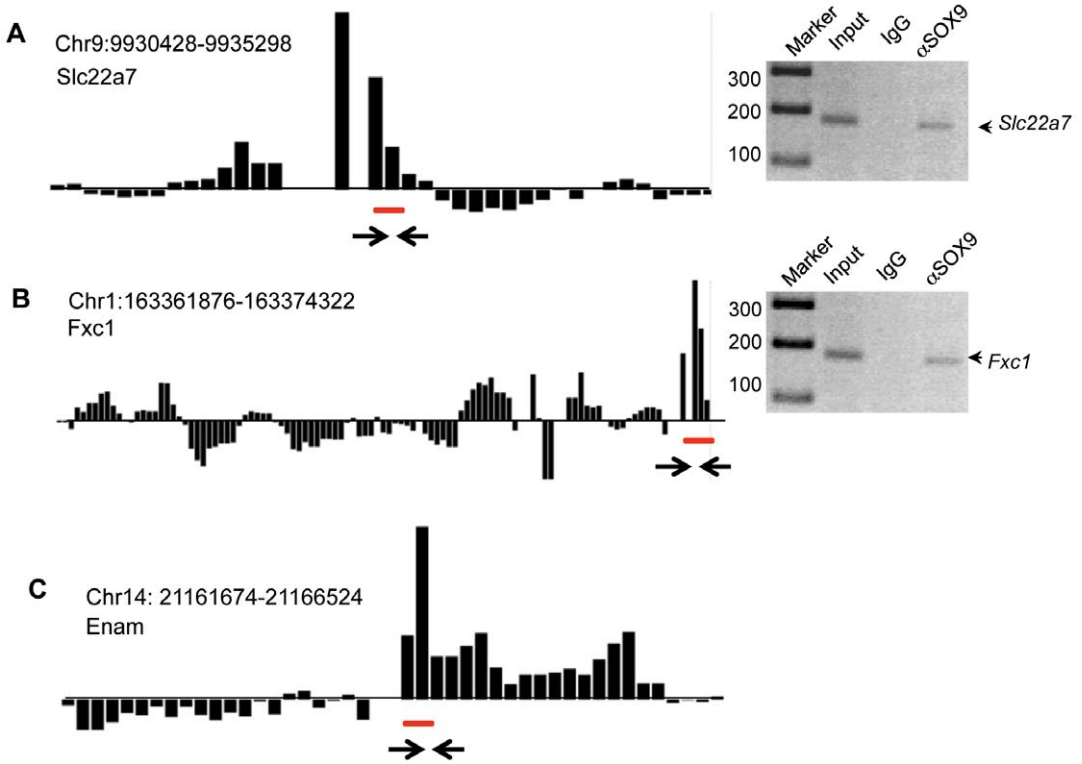

Figure 3. Representative examples of SOX9 binding to the target promoter. (A) *Slc22a7*, (B) *Fxc1*, and (C) *Enam*. The positive hybridization is specific to SOX9 ChIP-DNA signal (bar above the horizontal line) and negative hybridization (bar below the horizontal line) to the non-immune IgG ChIP-DNA signal. Hybridization signals are the average of three biological replicates of ChIP assays. Hybridization signals below the statistical significance of $p<1\times10^{-7}$ was not considered. The localization of SRY response element motif is indicated for each promoter as a horizontal line under the bar. PCR Primers were designed from the position indicated by two arrows. The PCR gel identifies PCR product size with (Markers), genomic DNA (Input), IgG ChIP (IgG) and SRY ChIP (aSRY). Data represent ChIP-PCR assays for three different experiments and biological replicates.
doi:10.1371/journal.pone.0043380.g003

The most common nucleotides were similar to the previously described SRY site and gave alternate nucleotides to consider. The SOX9 binding motif is shown in Figure 4B and shows similarity with the most common nucleotides and the previously described SOX9 site [22,31]. This current analysis has extended previous studies and presents a potentially more accurate consensus SRY and SOX9 binding motifs described due to the use of all major direct downstream binding targets identified. However, further investigation with mutagenesis and in vitro binding analysis is needed to confirm the consensus motifs identified.

Gene Expression of SRY and SOX9 Binding Target Genes

Previously the developmental expression pattern of genes in rat and mouse testis at various periods during gonadal sex determination was investigated [33,34]. Expression patterns of genes that had a statistically significant change in gene expression ($p<0.05$) from the previous rat microarray analysis were plotted (Figure 5). Expression data indicate that among the genes from the SRY binding target list that eight had a statistically significant ($p<0.05$) change during male sex determination: Loc689226, Tmed4. Znf507, Rtf3, Cpa2, Jkamp, Timm8b and Ndufs4. Similarly eight from the SOX9 list were changed: Cyp11a1, 3beta HSD1, Tpi1, Mcm7, Wbscr22, Spast, Eepd1, and Cyrl1. Observations do not identify general trends in altered gene express for either SRY or SOX9 response genes. A limitation to this analysis is that the microarray analysis used whole testis, such that Sertoli cell specific expression and regulation could not be assessed.

The current study was designed to identify the binding targets and not assess transcriptional regulation of the binding targets by SRY or SOX9. Since both stimulatory and repressive roles for SRY and SOX9 have been demonstrated, not all binding targets are anticipated to be directly regulated at the developmental time point examined. A preliminary analysis used a previous report involving an E13 gonadal cell culture and a transient transfection of an SRY expression construct to over-express SRY and then assess effects on gene expression with a microarray analysis [27]. From the list of genes with a statistically significant ($p<0.05$) alteration in gene expression after SRY over-expression 13 were found to overlap with the SRY binding targets identified. The direct binding targets that were induced were Ragl, Rpl24, Fam12b, and Phox2a. The direct binding targets that we suppressed were Exoc4 and RGD1303127. The atypical binding targets that were induced were Thap1, Cd7 and RGD1306839. The atypical binding targets that were suppressed were Chrna3, Id2, F2rl2 and Rspo3. Observations suggest approximately 10% of the SRY direct binding targets are transiently regulated in the E13 gonadal cell culture by SRY. Future studies will need to be directed at the transcriptional regulation of the downstream targets identified.

Functional Gene Categories, Pathways and Network Analysis

Analysis of specific functional gene categories combined both the SRY and SOX9 direct downstream binding target genes. As shown in Tables 1 and 2, all the genes were presented in specific

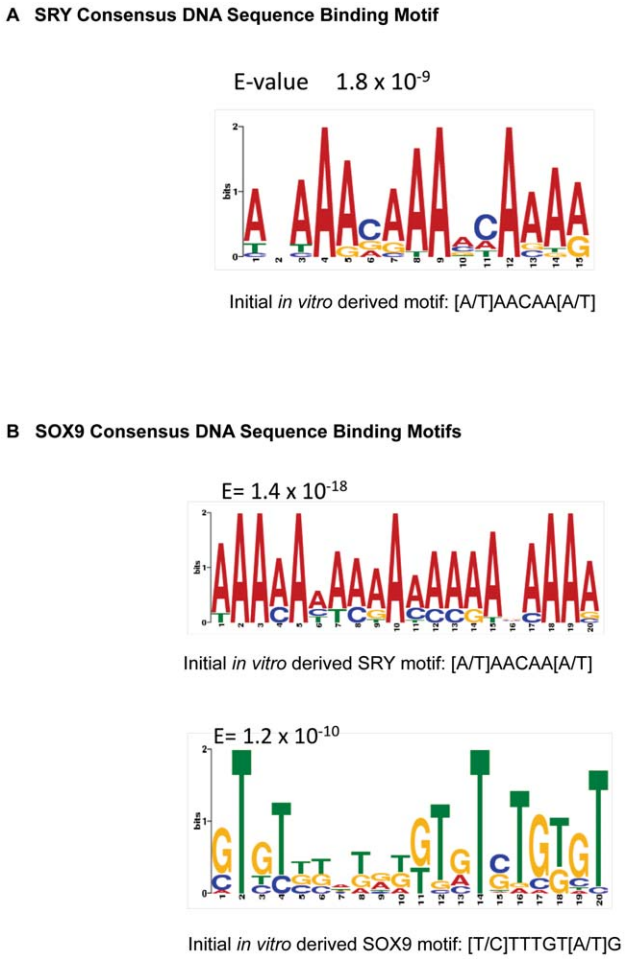

Figure 4. SRY (A) and SOX9 (B) DNA sequence binding motifs. The y-axis indicates the base and size performance for binding, and x-axis the base pair sequence for the motif.
doi:10.1371/journal.pone.0043380.g004

functional categories. The general functional categories for both the SRY and SOX9 gene sets are summarized in Figure 6. The cellular receptors and binding proteins, metabolism and transport and transcription were the most abundant categories for both SRY and SOX9 targets. In order to understand whether SRY and SOX9 direct binding targets are enriched for specific cellular signaling pathways the SRY and SOX9 target genes were analyzed with a KEGG pathway analysis as described in the Methods. The analysis identified significant enrichment for several signaling pathways including: olfactory transduction, RNA processing, metabolic pathways, steroid hormone biosynthesis, protein processing in endoplasmic reticulum, oxidative phosphorylation, and several disease pathways (Table 3). Olfactory transduction was the most highly enriched pathway for both SRY and SOX9 targets. This was due to the large number of olfactory receptors identified, Supplemental Figure S3.

A gene network analysis of SRY and SOX9 direct binding target genes identified specific gene networks. No significant direct interaction (connection) gene networks were identified for either SRY or SOX9. In contrast, indirect connection gene networks with associations with various cellular processes were identified. The SRY target genes that have indirect associations showed connections with cell proliferation, apoptosis, cell differentiation, cell death, cell cycle, chromatin remodeling and immune response, Figure 7. SOX9 binding target genes had more complex associations with cell differentiation, cell proliferation, embryonic development, cell cycle, DNA processing, spermatogenesis, cell growth, chromatin remodeling, cell survival, cell migration, and DNA damage, Figure 8. Although indirect connection gene networks were identified, no specific pathways or cellular processes were predominant. The SOX9 direct binding targets had a much larger number of associated cellular processes than the SRY binding targets.

Comparison of Literature-based SRY Target Genes

Although SRY has been shown to have multiple functions, only a handful of downstream targets have been previously identified. Comparison of the complete SRY and SOX9 direct target lists with the published literature identified five genes from Bradford et al. 2009 [25] that were found to overlap with the complete target gene list. Among those overlapped, Adam23 was the one that is a direct target of SRY and the other four (*Cbln4*, *Nr5a1*, *Flrt2*, and *Tmem95*) were atypical binding targets. The genes that are known to participate in Sertoli cell differentiation such as *Fgf9*, *Gata4*, *Amh* were not found using the statistical $p<1\times10^{-7}$ cut-off. These genes are part of the testis differentiation gene network, but may not be directly regulated by SRY. Interestingly, hematopoetic prostaglandin D synthase (*Pdgs*) gene was found to be the direct binding target of SRY at the significant level of $p<1\times10^{-9}$. Prostaglandin has been previously found to be regulated by SOX9 [17] and to promote Sertoli cell differentiation.

Discussion

Jost's sex determination theory [1] states that the sex of an individual will be determined and expressed as 1) chromosomal sex (genetic) in presence or absence of Y chromosome, 2) gonadal sex which is controlled by presence or absence of testis determining factor (TDF), and 3) phenotypic sex which is determined by the hormonal products produced by the gonads. In 1970s and 1980s, several potential TDF in male sex determination were considered including H-Y antigen and ZFY, which was suggested based on mutations in the Y chromosome that led to sex reversal in humans and mice [4,5,6,7]. In 1990, SRY was discovered as the TDF that initiates mammalian testis differentiation from a bipotential gonad [8,9,10]. Studies then identified the SRY downstream target SOX9 as facilitating Sertoli cell differentiation and male gonadal sex determination [11,12]. The *in vivo* downstream targets of these two master regulators of male sex determination have eluded scientists for decades. The current study was designed to identify the *in vivo* downstream binding targets of both SRY and SOX9 using a genome-wide ChIP-Chip comparative hybridization procedure. These two key factors were found to interact with distinct developmental gene networks during testis differentiation.

A chromatin immunoprecipitation (ChIP) with antibodies specific for SRY or SOX9 was performed as previously described [27]. Due to the potential of non-specific binding of IgG to chromatin, we performed a comparative hybridization of SRY or SOX9 antibody ChIP DNA with a non-immune IgG ChIP DNA to eliminate the potential of detecting false positive SRY or SOX9 targets. As discussed, the negative ChIP-Chip peaks identified demonstrate a relatively high degree of non-immune IgG binding that needs to be considered in assessing ChIP-Chip data. The questionable binding targets identified were those that had a positive peak in the ChIP-Chip adjacent to a negative IgG peak. Therefore, the current procedure of a ChIP-Chip comparative hybridization with a non-immune IgG control reduces the false

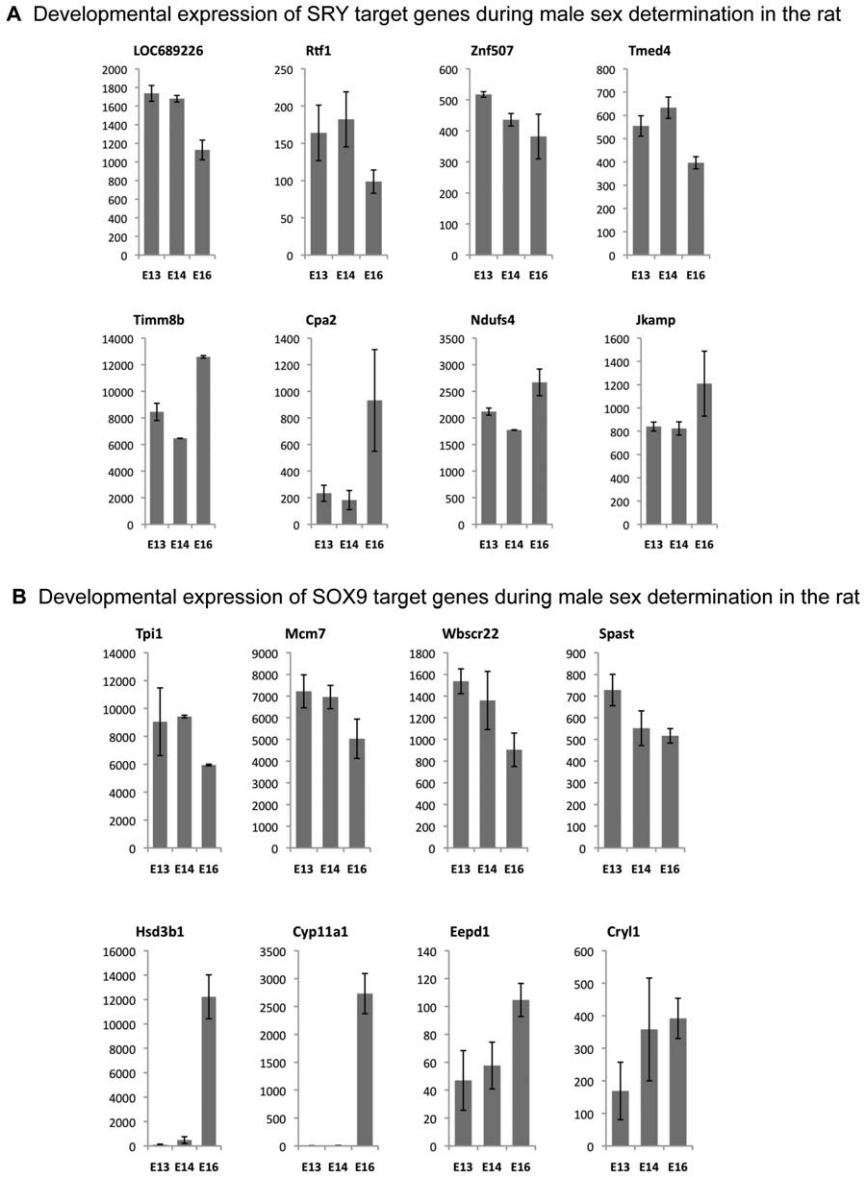

Figure 5. SRY (A) and SOX9 (B) direct binding target gene expression profiles for genes with a statistically ($p<0.05$) significance change in expression between the developmental periods. Microarray analysis of embryonic day E13, E14 and E16 testis data previously described [26] was used to construct the expression profiles of the selected genes.
doi:10.1371/journal.pone.0043380.g005

positive in the analysis. However, the potential that an IgG non-specific peak may mask a true positive ChIP-Chip peak is a limitation of this approach. The downstream candidates identified are likely a subset of a number of downstream binding targets that remain to be identified. Therefore, some anticipated targets may not be present due to this technical limitation.

SRY has been proposed to have several functions including the repression of testis repressors [35], chromatin remodeling [36], pre-RNA splicing [37], and transcriptional activation [38], suggesting that there might be a number of different target genes for SRY. The first functional *in vivo* target gene that was identified and studied is SOX9. SOX9 does regulate several downstream pathways underlying differentiation of embryonic testicular somatic cells [22] and inhibition of meiosis in the germ cells [39,40,41]. Interestingly, the current study did not detect SRY ChIP hybridization signals for SOX9 because only approximately 5000 base pairs of the promoter regions were present on the promoter tiling array. The testis specific enhancer of *Sox9* for SRY binding is located at 7 Kb upstream of the transcription start site so could not be detected. Therefore, the presence of *Sox9* enrichment in the SRY ChIP was confirmed and validated by *Sox9* TESCO PCR, Figure 2. The TESCO sequence in the mouse and rat *Sox9* promoters is highly conserved [24] and the PCR data confirmed *Sox9* is a direct downstream target of SRY. This observation with *Sox9* suggests SRY targets outside the 5 Kb promoter region will not be detected, such that the current SRY downstream target list is a subset of a potentially larger list that remains to be determined. An additional validation of the SRY ChIP-Chip analysis used two recently identified direct targets for SRY. The ChIP-Chip arrays identified the presence of *Tcf21* in the SRY ChIP [27], Figure 1. Our previous studies have also found *Ntf3* a direct downstream target of SRY in the rat [26]. Both

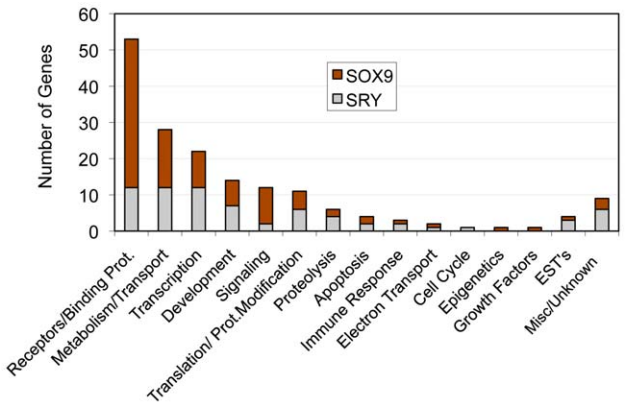

Figure 6. Functional gene categories for SRY and SOX9 direct binding target genes, number of representative genes per functional category listed are indicated.
doi:10.1371/journal.pone.0043380.g006

Tcf21 and *Ntf3* have distinct functions in testicular morphogenesis [28,29,42] and were detected in the SRY ChIP-Chip assay. Therefore, the detection of these known SRY targets in the ChIP-Chip assay helps validate the protocol used.

Another previously identified SRY downstream target gene is Cbln4 [25] and was found to be one of the downstream targets of SRY, but not of SOX9. The sequences of the Cbln4 induced by the SRY-enriched ChIP DNA fragment did not have a putative SRY-binding motif, so we categorized Cbln4 as an atypical binding target of SRY. Previously Cbln4 was reported to be one of the downstream targets of SRY based on cloning of the *in vivo* ChIP DNA [25]. In the current study the ChIP-Chip assay required at least three biological replicates of the ChIP experiments to be positive while the IgG background signals of hybridization are bioinformatically removed. The stringency of our ChIP protocol (absence of protein cross-linking) and bioinformatics analysis will likely eliminate some SRY targets, but we are confident that the direct binding target lists reported are accurate.

Following the analysis of the SRY ChIP data, promoter regulatory regions that were enriched with the *in vitro*-derived DNA binding motif [A/T]AACAA[A/T] were termed as direct downstream binding targets. Similar analysis for the SOX9-associated regions identified the same binding motif as shown above and in addition a consensus of Sox9-specific *in vitro*-derived binding motif [17]. Since a large number of downstream direct binding targets were identified for SRY and SOX9, we performed a sequence motif analysis of all the sites and developed a refined DNA sequence binding motif for both SRY and SOX9. These initial motifs overlapped well with the new motifs, but the new motifs have expanded the variability and significance of specific nucleotides. These new SRY and SOX9 binding motifs were utilized by all the direct downstream binding targets identified. The regions that overlapped between SRY and SOX9 target sequences contained predominantly SRY-specific HMG motif indicating that SOX9 interacts with DNA with a higher degree of variability and differently from SRY binding to its consensus motif. Future analysis of the SRY and SOX9 consensus motif identified will require mutagenesis and in vivo binding experiments to confirm the functional role of these motifs. The majority of the ChIP enriched regions of the SRY binding targets did not contain an SRY consensus motif, suggesting that SRY can act indirectly in transcriptional complexes not involving direct binding to the DNA target. In contrast, 80% of the SOX9 targets contained a consensus binding motif [9], suggesting a more direct binding role for SOX9 in regulation of downstream targets. The indirect actions of SRY on the atypical binding targets potentially expand its functional role in regulating genome activity and testis development.

Interestingly, observations demonstrate SRY and SOX9 have different downstream binding targets with minimal (<10%) overlap. Previous suggestions were made that SOX9 would singularly replace SRY during development, but the current observations suggest *Sry* and *Sox9* have distinct roles during development. Therefore, SRY induces a cascade of transcriptional events that do not simply have SOX9 to replicate SRY actions. However, the possibility that SRY and SOX9 may act at distinct targets, but influence similar cellular pathways and gene networks was considered. Similar functional categories of genes were observed in both the SRY and SOX9 direct binding targets, Figure 6. Therefore, more detailed analysis of specific signaling pathways and gene networks was performed. The only predominant signaling pathway represented by both SRY and SOX9 was the olfactory transduction pathway, Table 3. However, all the genes in this pathway were olfactory receptors, Supplemental Figure S3, and the functional impact of such a pathway is difficult to assess during testis development. No other major specific pathways were in common between SRY and SOX9. A final consideration used a gene network analysis to determine if direct connection (interaction) genes were common between SRY and SOX9. No significant direct connection gene networks were affected by SRY or SOX9. Therefore, the genes in the downstream direct binding targets did not have significant functional links or connections. Subsequent gene network analysis with SRY and SOX9 direct downstream binding target genes for indirect associations with functional cellular processes revealed SRY and SOX9 did have common connections to several processes, such as cell differentiation, cell proliferation, chromatin remodeling, cell death, and apoptosis. In contrast to the limited number of direct connections (interactions) within SRY or SOX9 target genes, a large number of associations were observed with cellular processes. Similar indirect associations have been reported for DMRT1 regulated genes in postnatal testis where DMRT1 recognizes a SOX9 motif like element for binding [43]. Combined observations identify the primary cellular processes and functional categories affected by SRY, but limited overlap was observed with

Table 3. Cellular Pathways Enrichment for Sox9 and Sry.

	Number of Affected Genes	
Pathway Name	**Sox9**	**Sry**
Olfactory transduction	16	7
Ribosome	5	1
Tryptophan metabolism	4	
Inositol phosphate metabolism	3	1
HTLV-I infection	3	
Neurotrophin signaling pathway	3	
Steroid hormone biosynthesis	3	
Protein processing in endoplasmic	2	3
Huntington's disease	2	3
Alzheimer's disease	2	3
Oxidative phosphorylation	1	3
Parkinson's disease	1	3

doi:10.1371/journal.pone.0043380.t003

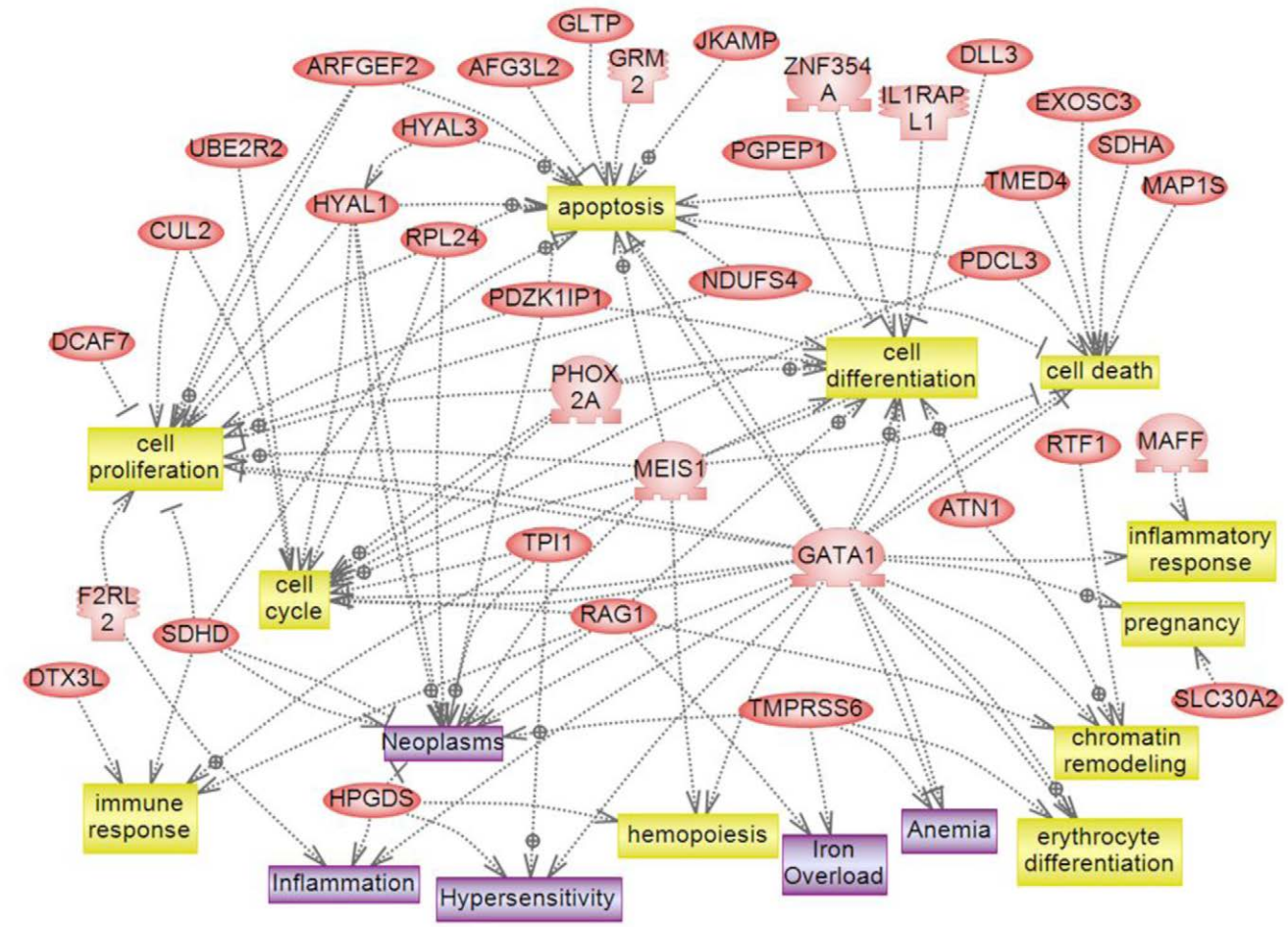

Figure 7. Gene network of shortest connections to cellular processes for 71 direct downstream gene targets of SRY, as obtained by global literature analysis using Pathway Studio 7.0 (Ariadne Genomics, Inc., Rockville, MD).
doi:10.1371/journal.pone.0043380.g007

SOX9 binding targets. Therefore, the downstream targets of SRY suggest a large number of different genes effect a wide variety of processes with no underlying gene network involved.

Analysis of the gene expression of the SRY and SOX9 direct downstream targets used our previously published rat testis development microarray database at embryonic day E3, E14 and E16 [33,34]. The majority of SRY and SOX9 direct target genes did not have altered gene expression during the fetal developmental period investigated. A limitation of these gene expression observations is that whole embryonic gonads were used in the analysis which contain multiple cell types. Therefore, Sertoli cell gene expression was not assessed directly and the expression data is due to a combination of cells. This could mask gene expression changes or suggest an alteration when changes in cell populations develop (e.g. Leydig). Observations suggest there are no major gene expression changes of the SRY or SOX9 target genes during this developmental period, but future studies will need to examine purified populations of Sertoli cells and downstream expression cascade affects. Expression results suggest that SRY target genes *Cpa2* and *Timm2b* were suppressed during early periods, but increased dramatically later. In contrast, SRY targets *Loc869226*, *Tmed4*, *Znf507*, *Rtf1* and *Id2* showed decreasing patterns during the three day window of rat testicular differentiation. A number of genes (*3beta-HSD*, *Cyp11a1*, *Insl3*) that could contribute to prepubertal Sertoli cell steroidogenesis were found as direct downstream targets of SOX9.

Although the current study was designed to identify the binding targets for SRY and SOX9, no information is provided on the transcriptional regulation of the binding targets identified. Future studies involving the transcriptional regulatory actions of SRY and SOX9 on these targets are needed. As a preliminary experiment a previous report that used E13 rat gonadal cell culture and transient transfection of an SRY-expression construct to over-express SRY was used to examine regulated gene expression with a microarray analysis [27]. Comparing the regulated gene set from this analysis with the current SRY binding targets demonstrated 13 genes appear to be directly regulated by SRY. Since SRY and SOX9 are known to also have a gene repression role, chromatin remodeling role, and RNA processing role, not all the SRY or SOX9 binding targets are anticipated to be regulated in a SRY

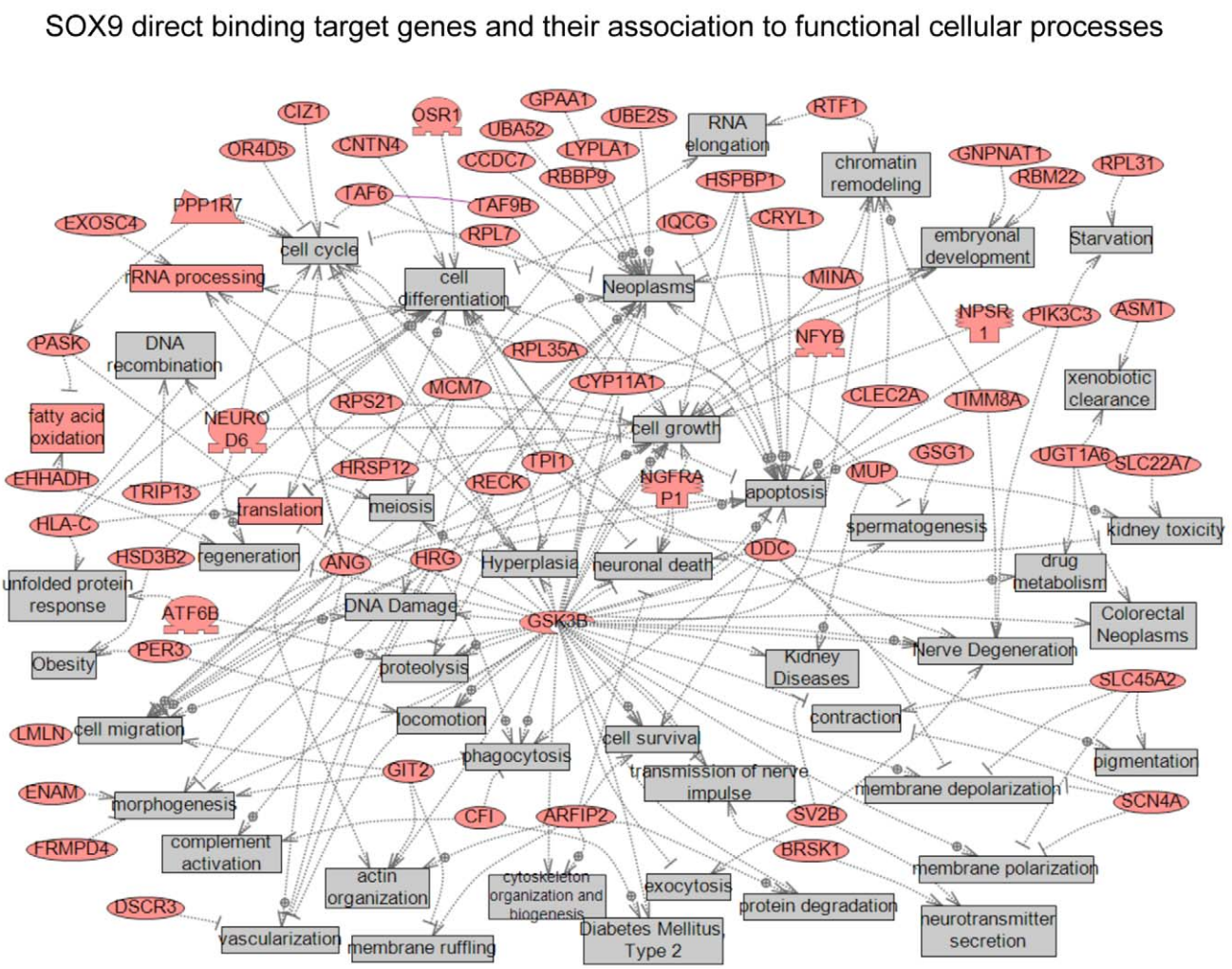

Figure 8. Gene network of shortest connections to cellular processes for 109 direct downstream gene targets of SOX9, as obtained by global literature analysis using Pathway Studio 7.0 (Ariadne Genomics, Inc., Rockville, MD).
doi:10.1371/journal.pone.0043380.g008

over-expression study. However, this preliminary analysis supports the transcriptional regulatory role of SRY on a number of the binding targets identified.

The tilling array used for this experiment represents only 5 kb of the proximal regions of the promoter sequences which represent less than 5% of the rat genome. In the current study, SRY-bound regions from the non-promoter areas were not assessed. In the future it is important to perform whole genome ChIP-Chip or ChIP-Seq (i.e. next generation sequencing) experiments to determine how many additional regions in the genome are bound by SRY and SOX9. These regions might represent tissue specific enhancers for the target gene expression, similar to the TESCO sequence located 7 kb upstream of the Sox9 promoter and involved in regulation of *Sox9* expression by SRY [24]. Therefore, the SRY and SOX9 downstream direct targets identified represent a subpopulation of a potential larger gene set that remains to be elucidated.

The combined observations identify genome wide *in vivo* targets of SRY and SOX9 as an initial attempt to define the mechanisms of male sex determination at the systems level. A large number of direct downstream binding targets were identified for both SRY and SOX9, which were distinct with minimal overlap. Therefore, SRY and SOX9 have distinct functions during testis development involving different downstream targets. The downstream targets influenced a variety of cellular pathways and processes, but did not involve unique gene networks, so acted independently to influence more global processes involving induction of Sertoli cell differentiation. Refined DNA sequence binding motifs were identified for SRY and SOX9 that help explain the distinct actions of SRY versus SOX9. Observations provide insights into the molecular control of testis determination initiated by SRY and induction of Sertoli cell differentiation. Current findings widen the arena for further systems biology investigations of the role of the SRY.

Materials and Methods

Tissue preparation

Harlan Sprague-Dawley rats were used for the study. All the rats were kept in a temperature controlled environment and given food and water *ad libitum*. Estrous cycles of female rats were monitored by cellular morphology from vaginal smears. Rats in early estrus were paired with males overnight and mating confirmed by sperm positive smears, denoted day 0 of pregnancy. Pregnant rats were euthanized at embryonic day 13 (E13) of pregnancy, and embryonic gonads were collected for chromatin immunoprecipitation. Sex was determined by PCR using primers

specific for *Sry* on genomic DNA isolated from embryo tails as previously described [44]. All procedures were approved by the Washington State University Animal Care and Use Committee (IACUC approval # 02568-026).

In vivo Chromatin Immunoprecipitation (ChIP) Assay

A modified ChIP (cChIP) assay was adopted from O'Neill et al., (2006) [45] and performed according to Bhandari et al (2011) [27]. The conditions for the native-ChIP (not including cross linking) were optimized for immunoprecipitating with SRY and SOX9 antibodies. The native-ChIP was used to identify high affinity binding sites and reduce low affinity sites, and was validated with PCR for *Sox9, Tcf21* and *Ntf3*. To run a replicate of the ChIP assay, at least twenty male gonads from thirty 13 dpc (12–18 tail somite stage) rat embryos were used per array. All three ChIP experiments were with different biological samples. *Drosophila* SL2 cells (American Type Culture Collection (ATCC) Catalog no. CRL-1963) were used as a carrier. Densely-grown cells (approximately 5×10^7 cells) were pelleted and washed three times in ice-cold phosphate buffered salve (PBS), 5 mM sodium butyrate and resuspended in 0.5 ml NB buffer (15 mM Tris-HCL, pH 7.4, 60 mM KCl, 15 mM NaCl, 5 mM $MgCl_2$, 0.1 mM EGTA, 0.5 mM 2-mercaptoethanol, 0.1 mM PMSF). Testis samples were mixed with SL2 cells and homogenized to make single cell suspension. Nuclei were pelleted, resuspended in 10 ml NB buffer, 5% (vol/vol) sucrose, pelleted and resuspended again in 1.5 ml digestion buffer (50 mM Tris-HCl pH 7.4, 0.32 M sucrose, 4 mM $MgCl_2$, 1 mM $CaCl_2$, 0.1 mM PMSF). Following micrococcal nuclease digestion (NEB, USA) for 5 minutes at 28°C, the digested samples were gently spun (800× g) for 15 minutes and supernatant set aside on ice. The pellet was resuspended in 250 ul digestion buffer and again centrifuged gently at 800× g for 15 minutes at 4 degrees. Both the supernatants were pooled and a fraction (50 ul) out of it was kept aside to use as input. The remaining supernatant was incubated with either non-immune IgG or anti-SRY (Santa Cruz, CA, USA) or anti-SOX9 (ABcam, CA, USA) antibodies at 4°C overnight. The specificity of these antibodies on western blots have been previously described and validated [27].

After incubation with 100 µl of pre-swollen protein A-Sepharose beads (SL2 DNA blocked) for 2 h at 4°C, the bead-bound immunoprecipitates were centrifuged gently and washed five times with wash buffer (50 mM TrisHCl pH 7.5, 10 mM EDTA, 5 mM Na butyrate and 50–150 mM NaCl). The protein-DNA complexes were incubated at room temperature with elution buffer (1% SDS in TE) and centrifuged at 11500× g for 10 minutes. Elution was repeated two times and eluted DNA was pooled. Co-immunoprecipitated DNA was purified by phenol/chloroform extraction, and ethanol precipitation. Final concentration of immunoprecipitated DNA varied from 200 to 500 ng per assay. Three different experiments and ChIP assays were performed. Exactly 30 ng of immunoprecipitated DNA from each assay was amplified by whole genome amplification kit developed by Sigma (Sigma #WGA2 50 RXN). At least five separate whole genome amplifications were performed and DNA was pooled. Pooled whole genome amplified DNA was purified by using Promega's Wizard SV40 PCR cleanup kit (Promega). Purified DNA was checked on the gel and sent to Nimblegen for ChIP-chip hybridization (Nimblegen, Iceland). A three plex array (3×720 RefSeq Promoter Array) was used for hybridization comparisons. Confirmation of ChIP immunoprecipitation was done in a PCR by using primers against Tcf21 promoter [27] and SOX9 TESCO as previously described [26,27]. Confirmation of the selected candidate genes were done by semi-quantitative PCR method with primers listed in Supplemental Table S4.

Bioinformatics Analysis of ChIP-Chip Data

The ChIP-Chip hybridization used a Roche Nimblegen's Rat ChIP-chip 3×720K RefSeq Promoter Array. The enrichment for each probe on the array was calculated as the log ratio of the intensities of hybridization for SRY or SOX9 ChIP DNA (Cy5) to control DNA from IgG control (Cy3). Array contained on average 4,000 bp of promoter for each of 15,287 promoters in the rat genome corresponding to 15,600 RefSeq transcripts (approximately 3880 bp upstream and 970 bp downstream from transcription start site). The analysis of ChIP-chip data was performed as previously described [32]. For each hybridization experiment raw data from both the Cy3 can Cy5 channels were imported into R (R Development Core Team (2010), R: A language for statistical computing, R Foundation for Statistical Computing, Vienna, Austria. ISBN 3-900051-07-0, URL http://www.R-project.org), and data checked for quality and converted to MA values (M = Cy5-Cy3; A = (Cy5+Cy3)/2). The R codes that were used for analysis and annotation are available in the following website: http//www.skinner.wsu.edu. All the tiling array Chip data was deposited in the NCBI GEO site (GEO# pending).

Within each array, probes were separated into groups by GC content and each group was separately normalized using the LOESS normalization procedure [46]. This allowed for groups with optimal GC content, which exhibited a reduced quality issue, to receive a normalization curve specific to that group. After each array was normalized within array, the arrays were then normalized across arrays using the A-quantile normalization procedure [47]. Following normalization the probe's normalized M values (and then A) were replaced with the median value of all probe M values (and then A) within a sliding window of 600 bp [48,49,50], due to the size of DNA fragments used. Following normalization each probe's M value represents the median intensity difference between Cy5 and Cy3 of a 600 bp window. Significance was assigned to probe differences between experimental (SRY or SOX9) and IgG control by calculating the median value of the intensity differences as compared to a normal distribution scaled to the experimental mean and standard deviation of M. Regions of interest were then determined by combining consecutive probes with significance p-values less than 10^{-3}. Significance was assigned to probe differences between experimental and control by calculating the median value of the increasing differences as compared to a normal distribution scaled to the experimental mean and standard deviation of the mean. A Z-score and P-value were computed from that distribution with the use of R code analysis. The statistically significant peaks of hybridization were identified and P-value associated with each peak presented. Each peak of interest was then annotated for the gene. Every promoter exceeding the intensity threshold was considered positive for SRY or SOX9 binding. The final list of SRY or SOX9 targets includes the promoter-proximal regions that made the threshold in an average of the three replicates. Hybridization signals for all the candidate promoters that were within the cutoff line ($p\leq1\times10^{-7}$) were plotted (average of the three replicates), Supplemental Figure S1. The genes that were not in the list but seemed to be masked by IgG negative signals were designated as questionable positives. These questionable positive promoters were manually chosen and confirmed by PCR, Supplemental Figure S2.

Gene Network and Pathway Analysis

Gene network analysis identified groups functionally interconnected genes whose expression is linked to cellular processes. In the current study gene networks for both SRY and SOX9 downstream binding target genes were constructed separately

using previously published criteria for developmental network analysis [51]. Global literature analysis of various gene lists was performed with Pathway Studio software using BiblioSphere Pathway Edition (Genomatix Software GmbH, Munchen, Federal Republic of Germany) which performs direct gene interaction (connection) analysis and relationship with cellular processes (indirect interactions).

The cellular signaling pathway analysis of direct downstream target genes was performed according to the protocol previously described [51]. The downstream binding targets of SRY and SOX9 and their associations with pathways were analyzed for KEGG (Kyoto Encyclopedia for Genes and Genome, Kyoto University, Japan) pathway enrichment using Pathway-Express, a web-based tool freely available as part of the Onto-Tools (http://vortex.cs.wayne.edu). A program based on literature analysis Pathway Studio (Ariadne, Genomics Inc. Rockville MD) was used to evaluate cellular processes connected to binding targets associated genes. The analysis of statistical over-representation of genes within a pathway used a Fisher's Exact test using 2×2 contingency table. The pathway analysis is distinct from the gene network analysis described above.

Developmental Expression Profiles and SRY Over-expression Analysis of Select Binding Target Genes

The direct downstream binding targets of SRY and SOX9 were separately compared with lists of genes in our previous microarrays from rat developmental studies [34]. The expression profiles of each gene from the ChIP-chip list of downstream targets that had a significant ($p<0.05$) change in expression were presented.

The influence of SRY over-expression on the downstream binding target genes was evaluated from a previously published microarray analysis on E13 gonadal cell cultures [27]. The E13 rat gonadal cells were cultured and transiently transfected with an Sry expression plasmid to then examine effects on gene expression six days after transfection with a microarray analysis. The SRY binding targets with a statistically significant ($p<0.05$) change in gene expression after SRY over-expression were identified and presented.

PCR Confirmation of Select Binding Target Genes

Primers were designed for at least 10 statistically significant binding targets from the region of probe hybridization peaks and tested using WGA-amplified ChIP DNA in a PCR (ChIP-PCR). Primers are listed in Supplemental Table S5. We used non-immune IgG as a negative control in all our ChIP-PCR assay replicates. Data were analyzed by subtracting negative and background signals. Experiments were designed to contain input as a positive control, IgG as a negative control and ChIP enrichment by specific antibody as an experimental. PCR results with positive bands from at least two biological replicates of the ChIP were considered positive and presented.

Supporting Information

Figure S1 SRY downstream direct binding target gene promoters. The positive hybridization is specific to SRY ChIP-DNA signal and negative hybridization to the non-immune IgG ChIP-DNA signal. Hybridization signals are the average of three biological replicates of ChIP assays. Hybridization signals below the statistical significance of $p<1\times10^{-7}$ was not considered. Data represent assays from three different experiments and biological replicates.
(PDF)

Figure S2 Hybridization signals masked by adjacent larger peaks of IgG binding. (A) *Hes2* hybridization profile with horizontal bar with arrows identifying SRY binding site and PCR confirmation of SRY with anti SRY (aSRY), IgG and input DNA. (B) *Scn4a* hybridization profile with horizontal bar for SOX9 binding and ChIP-PCR confirmation of *Sox9* (aSOX9). ChIP DNA from IgG represented negative control (IgG) in PCR. PCR was conducted on 200 ng DNA amplified by whole genome amplification kit (Sigma). Data represent ChIP-PCR assay from three different experiments and biological replicates.
(PDF)

Figure S3 Olfactory transduction signaling pathway from KEGG pathway. The SRY and SOX9 direct binding targets are listed in the olfactory receptor insert box.
(PDF)

Table S1 Atypical downstream binding targets of SRY during male sex determination in the rat. Atypical targets were pulled down by SRY antibody, but the hybridization occurred through indirect binding as the peak of hybridization signal did not contain the SRY consensus motif.
(PDF)

Table S2 Questionable downstream binding target genes of SRY. Their hybridization signals were masked by negative binding by IgG, so appeared to be negative in the bioinformatic analysis. These promoters were manually extracted from the database. Confirmation of positive binding in the promoter was done by PCR as shown in the supplemental figure S2.
(PDF)

Table S3 Atypical downstream binding targets of SOX9 during male sex determination in the rat. Atypical targets were pulled down by SOX9 antibody, but the hybridization occurred though indirect binding as the peak of hybridization signal did not contain HMG or in vitro derived SOX9 consensus motif.
(PDF)

Table S4 Questionable downstream targets of SOX9 during male sex determination in the rat. Their hybridization signals were masked by negative binding by IgG, so appeared to be negative in the bioinformatic analysis. These promoters were manually extracted from the database.
(PDF)

Table S5 PCR Primers Utilized.
(PDF)

Acknowledgments

We thank Ms. Tiffany Hylkema for assistance in PCR confirmation of downstream targets, Dr. Marina Savenkova for gene family and network data analysis, Dr. Mohan Manikkam and Ms. Rebecca Tracey for time-pregnant animals, Ms. Ellyn Schinke for assistance in dissection of embryos, and Dr. Ingrid Sadler-Riggleman for cell culture assistance. We thank Drs Mohan Manikkam, Eric Nilsson, and Carlos Guerrero-Bosagna for critically reviewing the manuscript. The current address for Dr. Ramji Bhandari is Department of Physiological Sciences, College of Veterinary Medicine, University of Florida, Gainesville FL.

Author Contributions

Conceived and designed the experiments: MKS. Performed the experiments: RKB MMH. Analyzed the data: MKS RKB MMH. Wrote the paper: MKS RKB. Edited the manuscript: MKS RKB MMH.

References

1. Jost A, Price D, Edwards G (1970) Philosophical Transactions of the Royal Society of London, Series B. Biological Sciences 259: 119–131.
2. Jost A (1947) Recherches sur la différentiation sexuelle de lembryonde de lapin. Arch Anat Microsc Morph Exp 36: 271–315.
3. Jost A (1953) Problems of fetal endocrinology: the gonadal and hypophyseal hormones. Recent Prog Horm Res 8: 379–418.
4. Wachtel SS, Ono S, Koo GC, Boyse EA (1975) Possible role for H–Y antigen in the primary determination of sex. Nature 257: 235–236.
5. Ohno S, Nagai Y, Ciccarese S, Iwata H (1979) Testis-organizing H-Y antigen and the primary sex-determining mechanism of mammals. Recent Prog Horm Res 35: 449–476.
6. Page DC, Brown LG, de la Chapelle A (1987) Exchange of terminal portions of X- and Y-chromosomal short arms in human XX males. Nature 328: 437–440.
7. Page DC, Mosher R, Simpson EM, Fisher EM, Mardon G, et al. (1987) The sex-determining region of the human Y chromosome encodes a finger protein. Cell 51: 1091–1104.
8. Gubbay J, Collignon J, Koopman P, Capel B, Economou A, et al. (1990) A gene mapping to the sex-determining region of the mouse Y chromosome is a member of a novel family of embryonically expressed genes. Nature 346: 245–250.
9. Sinclair AH, Berta P, Palmer MS, Hawkins JR, Griffiths BL, et al. (1990) A gene from the human sex-determining region encodes a protein with homology to a conserved DNA-binding motif. Nature 346: 240–244.
10. Koopman P, Gubbay J, Vivian N, Goodfellow P, Lovell-Badge R (1991) Male development of chromosomally female mice transgenic for Sry. Nature 351: 117–121.
11. Sekido R, Bar I, Narvaez V, Penny G, Lovell-Badge R (2004) SOX9 is up-regulated by the transient expression of SRY specifically in Sertoli cell precursors. Dev Biol 274: 271–279.
12. Morais da Silva S, Hacker A, Harley V, Goodfellow P, Swain A, et al. (1996) Sox9 expression during gonadal development implies a conserved role for the gene in testis differentiation in mammals and birds. Nat Genet 14: 62–68.
13. Arango NA, Lovell-Badge R, Behringer RR (1999) Targeted mutagenesis of the endogenous mouse Mis gene promoter: in vivo definition of genetic pathways of vertebrate sexual development. Cell 99: 409–419.
14. De Santa Barbara P, Bonneaud N, Boizet B, Desclozeaux M, Moniot B, et al. (1998) Direct interaction of SRY-related protein SOX9 and steroidogenic factor 1 regulates transcription of the human anti-Mullerian hormone gene. Mol Cell Biol 18: 6653–6665.
15. Kim Y, Bingham N, Sekido R, Parker KL, Lovell-Badge R, et al. (2007) Fibroblast growth factor receptor 2 regulates proliferation and Sertoli differentiation during male sex determination. Proc Natl Acad Sci U S A 104: 16558–16563.
16. Kim Y, Capel B (2006) Balancing the bipotential gonad between alternative organ fates: a new perspective on an old problem. Dev Dyn 235: 2292–2300.
17. Wilhelm D, Hiramatsu R, Mizusaki H, Widjaja L, Combes AN, et al. (2007) SOX9 regulates prostaglandin D synthase gene transcription in vivo to ensure testis development. J Biol Chem 282: 10553–10560.
18. Schmahl J, Kim Y, Colvin JS, Ornitz DM, Capel B (2004) Fgf9 induces proliferation and nuclear localization of FGFR2 in Sertoli precursors during male sex determination. Development 131: 3627–3636.
19. Kashimada K, Koopman P (2010) Sry: the master switch in mammalian sex determination. Development 137: 3921–3930.
20. Nef S, Vassalli JD (2009) Complementary pathways in mammalian female sex determination. J Biol 8: 74.
21. Sekido R, Lovell-Badge R (2009) Sex determination and SRY: down to a wink and a nudge? Trends Genet 25: 19–29.
22. Wilhelm D, Palmer S, Koopman P (2007) Sex determination and gonadal development in mammals. Physiol Rev 87: 1–28.
23. DiNapoli L, Capel B (2008) SRY and the standoff in sex determination. Mol Endocrinol 22: 1–9.
24. Sekido R, Lovell-Badge R (2008) Sex determination involves synergistic action of SRY and SF1 on a specific Sox9 enhancer. Nature 453: 930–934.
25. Bradford ST, Hiramatsu R, Maddugoda MP, Bernard P, Chaboissier MC, et al. (2009) The cerebellin 4 precursor gene is a direct target of SRY and SOX9 in mice. Biol Reprod 80: 1178–1188.
26. Clement TM, Bhandari RK, Sadler-Riggleman I, Skinner MK (2011) Sry Directly Regulates the Neurotrophin-3 Promoter During Male Sex Determination and Testis Development in Rats. Biology of Reproduction 85: 227–284.
27. Bhandari RK, Sadler-Riggleman I, Clement TM, MK S (2011) Basic Helix-Loop-Helix Transcription Factor TCF21 is a Downstream Target of the Male Sex Determining Gene SRY. PLoS ONE 6: e19935.
28. Cui S, Ross A, Stallings N, Parker KL, Capel B, et al. (2004) Disrupted gonadogenesis and male-to-female sex reversal in Pod1 knockout mice. Development 131: 4095–4105.
29. Cupp AS, Uzumcu M, Skinner MK (2003) Chemotactic role of neurotropin 3 in the embryonic testis that facilitates male sex determination. Biol Reprod 68: 2033–2037.
30. Barrionuevo F, Bagheri-Fam S, Klattig J, Kist R, Taketo MM, et al. (2006) Homozygous inactivation of Sox9 causes complete XY sex reversal in mice. Biol Reprod 74: 195–201.
31. Harley VR, Lovell-Badge R, Goodfellow PN (1994) Definition of a consensus DNA binding site for SRY. Nucleic Acids Res 22: 1500–1501.
32. Guerrero-Bosagna C, Settles M, Lucker BJ, Skinner MK (2010) Epigenetic transgenerational actions of vinclozolin on promoter regions of the sperm epigenome. PLoS ONE 5: e13100.
33. Small CL, Shima JE, Uzumcu M, Skinner MK, Griswold MD (2005) Profiling gene expression during the differentiation and development of the murine embryonic gonad. Biol Reprod 72: 492–501.
34. Clement TM, Anway MD, Uzumcu M, Skinner MK (2007) Regulation of the gonadal transcriptome during sex determination and testis morphogenesis: comparative candidate genes. Reproduction 134: 455–472.
35. McElreavey K, Vilain E, Abbas N, Herskowitz I, Fellous M (1993) A regulatory cascade hypothesis for mammalian sex determination: SRY represses a negative regulator of male development. Proc Natl Acad Sci U S A 90: 3368–3372.
36. Pontiggia A, Rimini R, Harley VR, Goodfellow PN, Lovell-Badge R, et al. (1994) Sex-reversing mutations affect the architecture of SRY-DNA complexes. Embo J 13: 6115–6124.
37. Ohe K, Lalli E, Sassone-Corsi P (2002) A direct role of SRY and SOX proteins in pre-mRNA splicing. Proc Natl Acad Sci U S A 99: 1146–1151.
38. Thevenet L, Albrecht KH, Malki S, Berta P, Boizet-Bonhoure B, et al. (2005) NHERF2/SIP-1 interacts with mouse SRY via a different mechanism than human SRY. J Biol Chem 280: 38625–38630.
39. Kashimada K, Svingen T, Feng CW, Pelosi E, Bagheri-Fam S, et al. (2011) Antagonistic regulation of Cyp26b1 by transcription factors SOX9/SF1 and FOXL2 during gonadal development in mice. FASEB J 25: 3561–3569.
40. Bowles J, Feng CW, Spiller C, Davidson TL, Jackson A, et al. (2010) FGF9 suppresses meiosis and promotes male germ cell fate in mice. Dev Cell 19: 440–449.
41. Koubova J, Menke DB, Zhou Q, Capel B, Griswold MD, et al. (2006) Retinoic acid regulates sex-specific timing of meiotic initiation in mice. Proc Natl Acad Sci U S A 103: 2474–2479.
42. Levine E, Cupp AS, Skinner MK (2000) Role of neurotropins in rat embryonic testis morphogenesis (cord formation). Biol Reprod 62: 132–142.
43. Murphy MW, Sarver AL, Rice D, Hatzi K, Ye K, et al. (2010) Genome-wide analysis of DNA binding and transcriptional regulation by the mammalian Doublesex homolog DMRT1 in the juvenile testis. Proc Natl Acad Sci U S A 107: 13360–13365.
44. Levine E, Cupp AS, Miyashiro L, Skinner MK (2000) Role of transforming growth factor-alpha and the epidermal growth factor receptor in embryonic rat testis development. Biol Reprod 62: 477–490.
45. O'Neill LP, VerMilyea MD, Turner BM (2006) Epigenetic characterization of the early embryo with a chromatin immunoprecipitation protocol applicable to small cell populations. Nat Genet 38: 835–841.
46. Smyth GK, Speed T (2003) Normalization of cDNA microarray data. Methods 31: 265–273.
47. Bolstad BM, Irizarry RA, Astrand M, Speed TP (2003) A comparison of normalization methods for high density oligonucleotide array data based on variance and bias. Bioinformatics 19: 185–193.
48. Tukey J (1977) Exploratory data analysis. Reading, MA: Addison-Wesley.
49. Hardle W, Steiger W (1977) Algorithm AS 296: Optimal median smoothing. Appl Stat: 258–264.
50. Toedling J, Skylar O, Krueger T, Fischer JJ, Sperling S, et al. (2007) Ringo–an R/Bioconductor package for analyzing ChIP-chip readouts. BMC Bioinformatics 8: 221.
51. Nilsson EE, Savenkova MI, Schindler R, Zhang B, Schadt EE, et al. (2010) Gene bionetwork analysis of ovarian primordial follicle development. PLoS ONE 5: e11637.

SCIENTIFIC REPORTS
nature research

OPEN

TET2 catalyzes active DNA demethylation of the *Sry* promoter and enhances its expression

Received: 20 May 2019
Accepted: 5 September 2019
Published online: 17 September 2019

Naoki Okashita[1,2], Shunsuke Kuroki[1,2], Ryo Maeda[1,2] & Makoto Tachibana[1,2]

SRY is the master regulator of male sex determination in eutherian mammals. In mice, *Sry* expression is transcriptionally and epigenetically controlled in a developmental stage-specific manner. The *Sry* promoter undergoes demethylation in embryonic gonadal somatic cells at the sex-determining period. However, its molecular mechanism and *in vivo* significance remain unclear. Here, we report that the *Sry* promoter is actively demethylated during gonadal development, and TET2 plays a fundamental role in *Sry* demethylation. *Tet2*-deficient mice showed absence of 5-hydroxymethylcytosine in the *Sry* promoter. Furthermore, *Tet2* deficiency diminished *Sry* expression, indicating that TET2-mediated DNA demethylation regulates *Sry* expression positively. We previously showed that the deficiency of the H3K9 demethylase *Jmjd1a* compromises *Sry* expression and induces male-to-female sex reversal. *Tet2* deficiency enhanced the sex reversal phenotype of *Jmjd1a*-deficient mice. Thus, TET2-mediated active DNA demethylation and JMJD1A-mediated H3K9 demethylation contribute synergistically to sex determination.

Expression of developmental genes is tuned through crosstalk between transcription factors and epigenetic regulation. The mammalian sex determining gene, *Sry*, is expressed in a certain population of somatic cells, termed as pre-Sertoli cells, in sexually undifferentiated embryonic gonads, thereby triggering the male development pathway[1–3]. *Sry* is expressed in a highly time-specific manner, *i.e.*, its expression starts around embryonic day 10.5 (E10.5), peaks at around E11.5, and almost disappears by E12.5[4–8]. *Sry* expression is positively regulated by several transcription factors[9]. However, research on epigenetic mechanisms that contribute to *Sry* regulation is in its infancy. We previously reported that the H3K9 demethylase JMJD1A (also known as TSGA/JHDM2A/KDM3A) plays a pivotal role in mouse sex determination through *Sry* activation[10]. Recently, it was reported that histone acetyltransferases are also involved in *Sry* activation[11].

In addition to histone modifi ation, DNA methylation plays a pivotal role in developmental gene regulation[12,13]. DNA methylation is found to occur predominantly on cytosine followed by guanine residues (CpG)[14–16]. DNA methylation is induced by the *de novo* DNA methyltransferases DNMT3A/DNMT3B, and is maintained by a maintenance DNA methyltransferase DNMT1 during DNA replication. CpG methylation marks can be removed by replication-dependent and independent mechanisms[17]. The former is regulated by inhibition of DNA methyltransferase activity during *de novo* DNA synthesis, whereas the latter (also known as active demethylation) is induced by the oxidation of 5-methylcytosine (5mC) by ten-eleven translocation proteins (TET1/TET2/TET3) to produce 5-hydroxymethylcytosine (5hmC)[18]. 5hmC is further oxidized to 5-formylcytosine (5fC) and 5-carboxycytosine (5caC) by TET enzymes, both of which can be repaired by the base excision repair (BER) pathway to produce unmodifi d cytosine[19]. Previous studies have reported that the CpG sequences of the *Sry* promoter are demethylated in gonadal somatic cells at the sex-determining period[20,21]. These observations indicated that DNA demethylation in *Sry* promoter preceded *Sry* expression onset and that DNA demethylation was more pronounced in the *Sry* promoter region than in other *Sry* loci[20]. Furthermore, promoter activity assay showed that *in vitro* methylation of the 5′-flanking region of *Sry* suppressed reporter activity[21]. Although these results suggest a possible link between DNA demethylation and *Sry* expression, the regulatory mechanism of DNA demethylation in *Sry* promoter and its functional signifi ance for sex determination remain elusive.

[1]Division of Epigenome Dynamics, Institute of Advanced Medical Sciences, Tokushima University, 3-18-15 Kuramoto-Cho, Tokushima, 770-8503, Japan. [2]Laboratory of Epigenome Dynamics, Graduate School of Frontier Biosciences, Osaka University, 1-3 Yamadaoka, Suita, Osaka, 565-0871, Japan. Correspondence and requests for materials should be addressed to M.T. (email: tachiban@fbs.osaka-u.ac.jp)

Here, we show that the active DNA demethylation pathway is involved in *Sry* regulation. 5hmC levels on *Sry* promoter were increased with increasing *Sry* expression in the somatic cells of developing gonads. Deficiency of *Tet2*, but not *Tet1*/*Tet*3, induced an increase in DNA methylation and disappearance of 5hmC in *Sry* promoter, indicating the pivotal role of TET2 in the dynamic regulation of DNA methylation in *Sry* promoter. Importantly, *Sry* expression was diminished in *Tet2*-deficient gonadal somatic cells at the sex-determining period. Furthermore, *Tet2* deficiency had a synergistic effect on the sex reversal phenotype, observed in a *Jmjd1a*-deficient background. These results identify TET2 as a responsible enzyme for DNA demethylation in *Sry* promoter and reveal that active DNA demethylation acts synergistically with histone modifications for epigenetic regulation of *Sry* and male sex determination.

Results

5-hydroxymethylcytosine is preferentially enriched in NR5A1-positive gonadal somatic cells. Active DNA demethylation plays important roles in the processes of development and differentiation in mammals[22]. 5hmC, an intermediate in the active DNA demethylation pathway, is generated by oxidation of 5mC. To elucidate whether active DNA demethylation occurs during embryonic gonadal development, we performed double immunostaining analyses on XY embryonic gonad sections at the sex-determining period (E11.5) with antibodies against 5hmC and NR5A1 (also known as AD4BP/SF-1), which is transcription factor expressed in gonadal somatic cells but not in germ cells and mesonephric cells. We observed strong 5hmC signals in NR5A1-positive gonadal somatic cells, whereas these were weak in mesonephric cells (Fig. 1a, left). Quantitative analysis indicated that the average intensity of 5hmC was about two-fold higher in NR5A1-positive gonadal somatic cells compared to that in mesonephric cells (Fig. 1a, right). These data suggest that active DNA demethylation might arise in developing gonads around the sex-determining period.

To confirm the previous result, we measured global 5hmC levels in gonadal somatic cells and mesonephric cells by dot-blot analysis. We previously established *Nr5a1-hCD271*-transgenic (tg) mice in which NR5A1-positive gonadal somatic cells were tagged with a cell surface antigen, hCD271[10,23]. Using this tg line, we isolated NR5A1-positive cells (hereafter referred as gonadal somatic cells) from gonad-mesonephros pairs of E11.5 XY embryos, and then used them for 5hmC quantification. 5hmC levels in gonadal somatic cells were higher than those in mesonephric cells (Fig. 1b, left). Quantification analysis showed that 5hmC content was about 1.5-fold higher in gonadal somatic cells than that in mesonephric cells (Fig. 1b, right). These findings support the fact that active demethylation occurs preferentially in the gonadal somatic cell population at the sex-determining period.

***Sry* promoter undergoes active DNA demethylation during gonadal development.** To examine the kinetic relationship between *Sry* expression and DNA methylation/demethylation of *Sry*, we collected gonadal somatic cells from XY embryos at the tail somite (ts) stages 9 to 23 (E10.6-E12.0). In accordance with the known expression profile of *Sry*, its transcripts were highly enriched in the gonadal somatic cell fraction with a peak at the ts stage 16–17 (E11.4) (Fig. 2a). As shown in Fig. 2b, the *Sry* promoter contains 6 CpG sites. Genomic DNA isolated from gonadal somatic cells was used for Tet-assisted bisulfite (TAB) sequencing analysis, by which 5hmC can be quantitatively detected at single-base resolution[24] (Fig. 2c). We found that 5hmC was detected in the *Sry* promoter in gonadal somatic cells, whereas it was barely detectable in E8.5 embryos and mesonephric cells (Fig. 2c). Notably, 5hmC levels in the *Sry* promoter in gonadal somatic cells fluctuated with kinetics similar to those of *Sry* expression during gonadal development (compare Fig. 2a with Fig. 2c). To confirm the correlation between 5hmC enrichment and DNA demethylation dynamics, we next examined DNA methylation (5mC + 5hmC) levels in the *Sry* promoter in gonadal somatic cells by bisulfite sequencing (Fig. 2d). With the development of gonads, DNA methylation levels of the *Sry* promoter were reduced progressively in gonadal somatic cells, whereas those of in E8.5 embryos and mesonephric cells were constantly close to 100% (Fig. 2d). These results collectively suggest that active DNA demethylation through 5mC oxidation might account for the reduction of DNA methylation in *Sry* promoter in the developing gonads, at least in part.

To confirm the involvement of the active DNA demethylation pathway in *Sry* regulation, we utilized 3-aminobenzamide (3-AB), a pharmacological inhibitor of the BER components PARP1. Several studies showed that 3-AB preserves 5mC levels by blocking the BER-dependent DNA demethylation pathway in primordial germ cells and embryonic stem cells[25–27]. 3-AB was intraperitoneally injected into pregnant females carrying E10.5 XY *Nr5a1-hCD271*-tg embryos (Fig. 2e). Gonadal somatic cells were isolated from the corresponding embryos 24 hours after injection and used for bisulfite sequence analysis (Fig. 2e). The averages of DNA methylation at the *Sry* promoter were 56.5% and 73.1% in the control and 3-AB treated gonadal somatic cells, respectively (Fig. 2e). The higher level of DNA methylation in 3-AB-treated cells supports the involvement of the active DNA demethylation pathway in the *Sry* regulation of gonadal somatic cells.

TET2 plays a pivotal role in active DNA demethylation of the *Sry* promoter. Active DNA demethylation is triggered by hydroxylation of 5mC to 5hmC, which is catalyzed by TET proteins[18]. Because all Tet subfamily proteins, TET1, TET2, and TET3, have an enzymatic activity toward 5hmC production, we aimed to identify the enzyme responsible for *Sry* demethylation. mRNAs for *Tet1*, *Tet2*, and *Tet3* were detected in the gonadal somatic cells at the 16–17ts stage when *Sry* expression reached a peak (Fig. 3a and Supplementary Table S1). As shown in Fig. 3b, we found that mRNAs of *Tet2* were gradually increased, whereas those of *Tet1* and *Tet3* were unchanged in the somatic cells of developing gonads. To address the loss of function phenotype of TET enzymes, we generated mice carrying each mutant allele for *Tet1*, *Tet2*, and *Tet3* (hereafter described as *Tet1*Δ, *Tet2*Δ, and *Tet3*Δ) using the CRISPR/cas9 system (Supplementary Fig. S1). Each of the *Tet*-mutant lines was crossed with the *Nr5a1-hCD271*-tg line for further analysis. Gonadal somatic cells were immuno-magnetically collected from corresponding mutant embryos at the 16–17ts stage and used for TAB and bisulfite sequencing

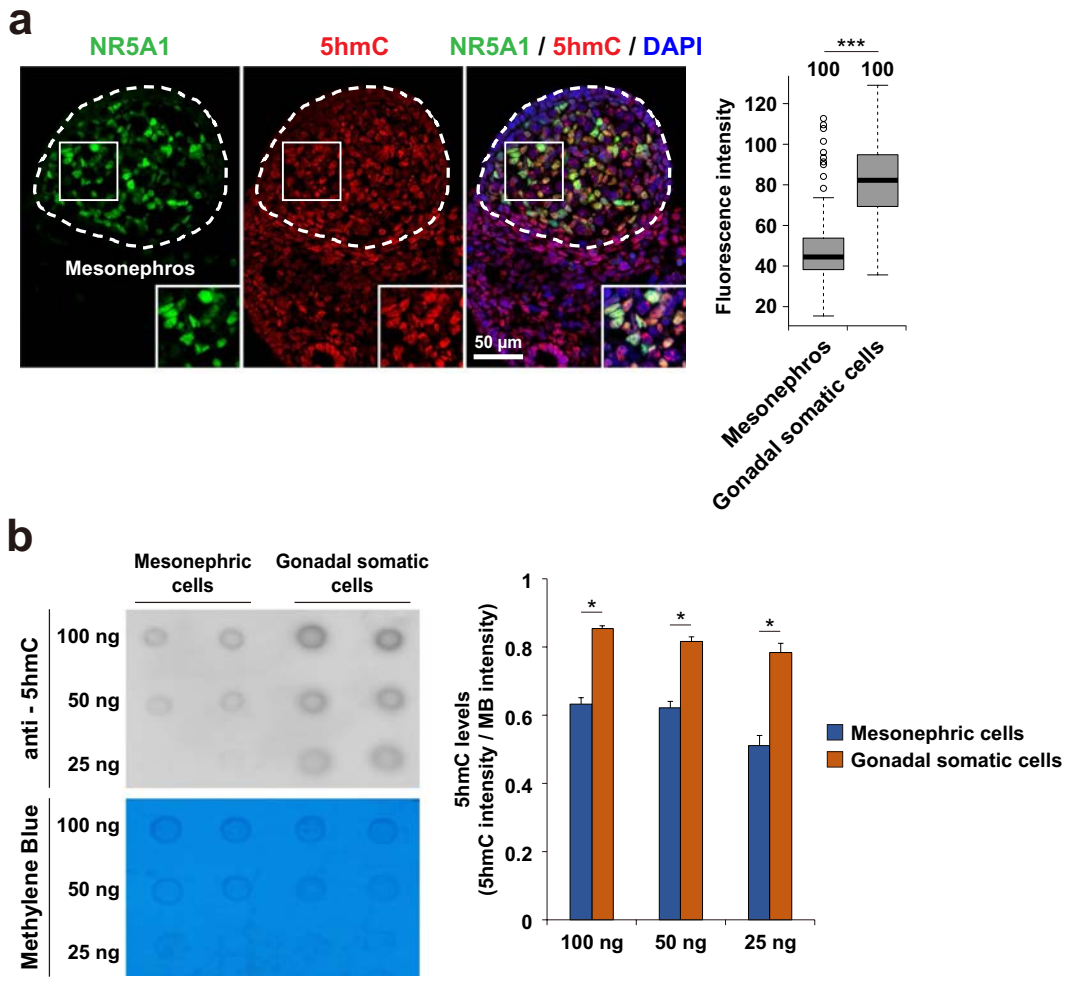

Figure 1. 5-hydroxymethylcytosine is preferentially enriched in NR5A1-positive gonadal somatic cells. (**a**) Co-immunostaining profiles of NR5A1 and 5hmC in the central regions of XY E11.5 gonads. Enlarged boxes indicate co-localization of NR5A1 and 5hmC in gonadal somatic cells. Fluorescence intensity values of 5hmC in every 100 gonadal somatic cells and mesonephric cells were examined and summarized in a box plot (right). Signal intensity was quantifi d using ImageJ software. ***$P < 0.001$. n = 100. (**b**) Comparison of 5hmC amounts between mesonephric cells and gonadal somatic cells. Mesonephric cells and gonadal somatic cells were separated from XY embryos at E11.5 that carried *Nr5a1-hCD271*-transgene (see Materials and Method section) and were introduced into Dot-blot analysis. The relative amounts of 5hmC were calculated by dividing the signal intensity of 5hmC by that of methylene blue (right). Signal intensity was quantifi d using ImageJ software. Error bars indicate the SEM values of duplicates of the dot signal intensity. *$P < 0.05$.

analysis (Fig. 3c,d, respectively). Strikingly, TAB sequence analysis demonstrated that 5hmC at the *Sry* promoter was completely abolished in *Tet2*Δ/Δ gonadal somatic cells, whereas it was unchanged in *Tet1*Δ/Δ or *Tet3*Δ/Δ cells (Fig. 3c). As shown in Fig. 3d, bisulfite sequencing analysis indicated that homozygous mutation of *Tet2* induced a signifi ant increase in DNA methylation in the *Sry* promoter of gonadal somatic cells, whereas mutation of *Tet1* and *Tet3* did not (Fig. 3d). We next examined the kinetics of DNA methylation in *Sry* promoter during gonadal development from ts stages 9 to 23. As summarized in Fig. 3e, DNA methylation levels were progressively decreased in control cells but were almost unchanged in *Tet2*Δ/Δ gonadal somatic cells. From these results, we conclude that TET2 is the bona fide enzyme responsible for active demethylation at *Sry* promoter during gonadal development.

***Tet2* mutation diminishes *Sry* expression in gonadal somatic cells and enhances sex-reversal in XY *Jmjd1a*Δ/Δ mice.** We next aimed to address the role of TET2-mediated DNA demethylation in mouse sexual development. We first examined whether *Sry* expression was affected in *Tet2*Δ/Δ gonadal somatic cells at the sex-determining period. As shown in Fig. 4a, quantitative mRNA expression analysis indicated that *Sry* expression was signifi antly reduced in *Tet2*Δ/Δ gonadal somatic cells, indicating involvement of TET2-mediated DNA demethylation in regulating *Sry* expression. Our previous study demonstrated that JMJD1A-mediated H3K9 demethylation contributes to the regulation of *Sry* expression in developing gonads[26]. Comparative and quantitative analysis of *Sry* mRNA demonstrated that the decreased level of *Sry* expression by

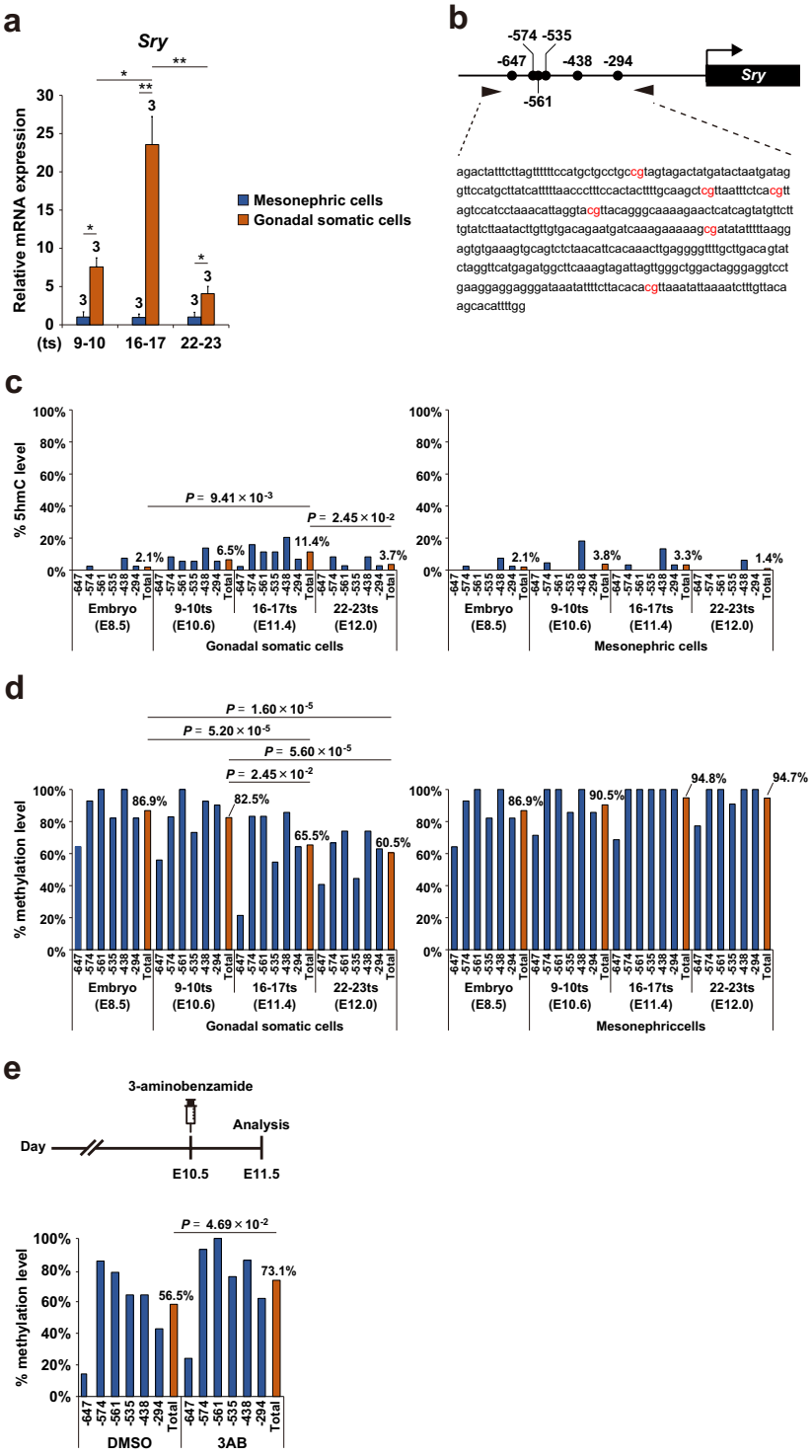

Figure 2. *Sry* promoter undergoes active DNA demethylation during gonadal development. (**a**) qRT-PCR analysis of *Sry* in XY mesonephric cells and gonadal somatic cells at the indicated ts stages. mRNA expression levels in mesonephric cells at the 9–10 ts stage (E10.6) were defi ed as 1. Data are presented as mean ± SD. $^{*}P < 0.05$, $^{**}P < 0.01$. n = 3. (**b**) Schematic representation of *Sry* promoter. *Sry* promoter contains 6 CpG sites. The positions of CpG sites are indicated relative to the start codon. (**c** and **d**) DNA methylation kinetics on *Sry* promoter in XY E8.5 embryos and XY mesonephric/gonadal somatic cells at the indicated developmental stages by Tet-assisted bisulfite sequencing analysis (**c**) and bisulfite sequencing analysis (**d**). Blue bars show the average percentage of methylation at individual CpG sites respectively and the red bar indicates that on total CpG sites. *P* values for bisulfite sequencing were obtained using the non-parametric two-tailed Mann-Whitney *U* test. (**e**) Administration of BER inhibitor inhibits DNA demethylation in the *Sry* promoter in developing gonads. The experimental scheme is shown in the upper panel. A BER inhibitor 3-aminobenzamide (3-AB) was intraperitoneally injected into pregnant females carrying E10.5 embryos. At 24 hours after injection, gonadal

somatic cells were purifi d from XY embryos and used for bisulfite sequencing analysis. The lower panel shows DNA methylation levels of *Sry* promoter in 3-AB-treated and DMSO-treated (as vehicle control) XY gonadal somatic cells. The blue bar shows the average percentage of methylation at individual CpG sites and the red bar shows that of total CpG sites. *P* values for bisulfite sequencing were obtained using the non-parametric two-tailed Mann-Whitney *U* test.

*Tet2*Δ/Δ mutation was moderate compared to that by *Jmjd1a* mutation (Fig. 4a). We next examined whether *Tet2* deficie cy influences sexual development in embryonic gonads. For this, we performed co-immunostaining analysis on E13.5 gonad sections using antibodies against the testicular Sertoli cell marker SOX9 and the ovarian somatic cell marker FOXL2. As shown in Fig. 4b, *Tet2*Δ/Δ gonads possessed typical features of embryonic testis, in which SOX9-positive cells were abundant and testicular tubule formation proceeded, indicating that *Tet2* mutation alone does not induce sex reversal in embryonic gonads. It is possible that *Tet2* deficie cy might affect DNA methylation levels of *Sox9* and *Foxl2*, and thereby influence this expression. To address this issue, we examined DNA methylation levels at the *Sox9* and *Foxl2* promoters in E11.5 gonadal somatic cells. As shown in Supplementary Fig. 2, *Tet2* deficie cy did not alter the DNA methylation levels of *Sox9* and *Foxl2* promoters in gonadal somatic cells.

Our previous study demonstrated that *Jmjd1a* deficie cy does not induce a signifi ant increase in the DNA methylation of *Sry* promoter in gonadal somatic cells, suggesting that active DNA demethylation in *Sry* promoter occurs independently of JMJD1A-mediated H3K9 demethylation[28]. To address the synergistic effect between TET2-mediated DNA demethylation and JMJD1A-mediated H3K9 demethylation on gonadal sex development, we generated *Tet2*/*Jmjd1a*-double deficie t mice and examined their gonadal sex development. *Sry* expression levels of *Tet2*/*Jmjd1a*-double deficie t gonads were signifi antly lower than those of *Jmjd1a*-deficie t gonads at the sex-determining period (Fig. 4c). *Jmjd1a*-deficient gonads at E13.5 were ovotestes composed of testicular cells and ovarian cells (Fig. 4d). Importantly, the ratio of FOXL2-positive cells to SOX9-positive cells was increased in *Tet2*/*Jmjd1a*-double deficie t gonads as compared to *Jmjd1a*-deficie t gonads (Fig. 4d). These results indicate that TET2-mediated DNA demethylation controls testicular development positively and synergistically with JMJD1A-mediated H3K9 demethylation.

Discussion

The CpG sites of *Sry* promoter are demethylated in gonadal somatic cells at the sex-determining period[20,21]. However, its molecular mechanism and *in vivo* significance remain elusive. Here, we discovered that 5hmC was highly enriched in XY gonadal somatic cells at the sex-determining period and that the 5hmC level was increased in *Sry* promoter concomitantly with *Sry* expression in these cells. We also identifi d TET2 as the enzyme responsible for active DNA demethylation in *Sry* promoter. Finally, we revealed that TET2-mediated active DNA demethylation is involved in regulating *Sry* expression and sex development. Here we discuss the role of DNA demethylation in the epigenetic regulation of *Sry*.

Our previous results have shown that *Sry* mRNA is not completely abolished in XY *Jmjd1a*-deficie t embryos. We therefore speculated that along with H3K9 demethylation, other epigenetic regulatory mechanism might also control *Sry* expression[10]. Our present study revealed that *Sry* activation is ensured by active DNA demethylation as well as by H3K9 demethylation (Fig. 5). In this model, JMJD1A-mediated H3K9 demethylation substantially contributes to *Sry* activation whereas TET2-mediated DNA demethylation acts supportively. *Tet2* deficie cy leads to reduced *Sry* expression levels, whereas subsequent gonadal sex development proceeds normally. These facts strongly suggest that *Sry* expression levels in *Tet2*-deficie t gonadal somatic cells are still higher than the threshold required for triggering the testis formation pathway[3]. In contrast, we found that *Tet2* deficie cy synergistically enhances the sex reversal phenotype of *Jmjd1a*-deficie t mice, indicating that TET2-mediated DNA demethylation practically contributes to mouse sex development.

Although *Tet1* and *Tet3* were expressed in gonadal somatic cells at the sex-determining period, DNA methylation at the *Sry* promoter was not affected by *Tet1* or *Tet3* deficie cy (Fig. 3a,b). These results suggest that there might be an unrevealed mechanism by which *Sry* is demethylated specifi ally by TET2. Interestingly, the protein structure of TET2 differs from those of TET1 and TET3, as TET1/TET3, but not TET2, contain the CxxC domain that is essential for CpG site recognition. Therefore, it is plausible that recruitment of TET2 to its target loci depends on its interacting factor[29]. A zinc fi ger-type transcription factor WT1 plays an essential role in male sex-determination[30]. *In vitro* analysis has shown that WT1 (-KTS), one of the WT1 protein isoforms, can bind and activate *Sry* promoter[31–36]. Another study reported that WT1 directly binds to TET2, but not TET1, and recruits TET2 to the target genes[37]. In addition, WT1 displays high affi ty for sequences containing 5mC rather than 5hmC or 5fC[38]. Considering these previous reports, it is possible that a specific DNA binding molecule mediates the recruitment of TET2 to the *Sry* promoter in gonadal somatic cells, and WT1 may be a promising candidate. We found that *Wt1* mRNA was constantly expressed in the developing XY gonads (Supplementary Fig. S4).

Although we showed that TET2 catalyzes active DNA demethylation at *Sry* promoter in gonadal somatic cells at the sex-determining period (Fig. 3c), we could not rule out the possibility that the TET protein-independent pathway also contributes to DNA demethylation at *Sry* promoter. For example, activation-induced deaminase (AID)/APOBEC-family cytosine deaminases are known to be involved in another pathway of active DNA demethylation. AID/APOBEC-family enzymes do not produce 5hmC but produce 5-methyluracil by deaminating the cytidine of 5mC[39], which eventually converts to unmodified cytosine through the BER pathway[40,41]. Several studies have shown that APOBEC3 can discriminate against 5mC[39,42]. In fact, our mRNA expression analysis has demonstrated higher expression of *Apobec3* in gonadal somatic cells than that in mesonephric cells during gonadal development (Supplementary Fig. S3). Therefore, it is worth investigating whether the APOBEC3-mediated DNA demethylation pathway also plays a role in active DNA demethylation at the *Sry* promoter.

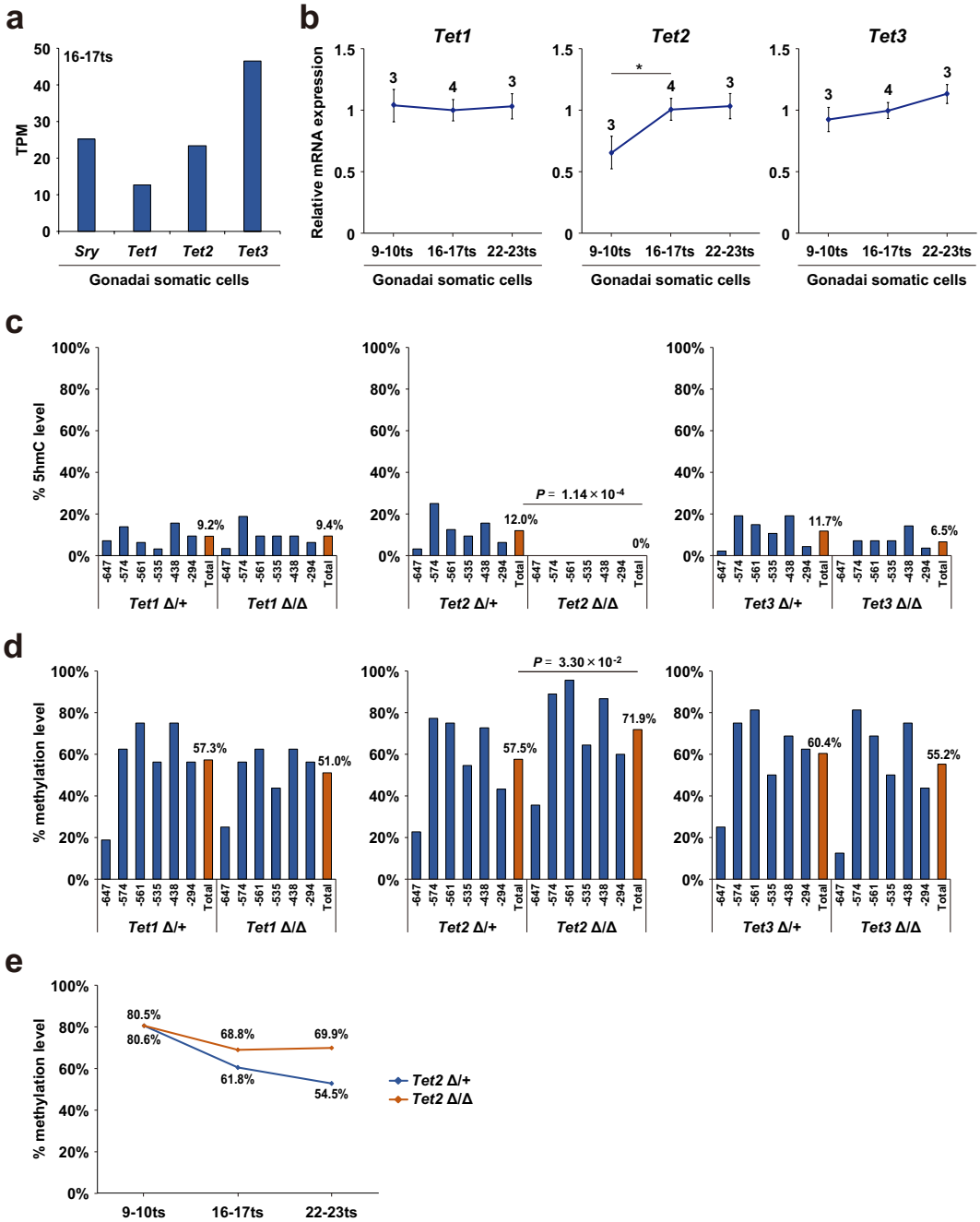

Figure 3. TET2 plays a pivotal role in active DNA demethylation of *Sry* promoter. (**a**) RNA-seq based gene expression values (TPM) of *Sry*, *Tet1*, *Tet2*, and *Tet3* in gonadal somatic cells at the sex-determining period. n = 2. (**b**) Expression kinetics of *Tet1*, *Tet2*, and *Tet3* in gonadal somatic cells. mRNAs were collected from XY gonadal somatic cells at the indicated ts stages and introduced into qRT-PCR analysis. mRNA expression levels in gonadal somatic cells at 16–17 ts stage were defi ed as 1. Data are presented as mean ± SD. * $P < 0.05$. n ≥ 3. (**c** and **d**) DNA methylation levels in the *Sry* promoter in E11.5 XY gonadal somatic cells of the indicated genotypes were measured by TAB sequencing (**c**) and bisulfite sequencing. (**d**) Blue bar shows the average percentage of methylation at individual CpG sites and red bar shows the average percentage of methylation on total CpG sites. *P* values for bisulfite sequencing were obtained using the non-parametric two-tailed Mann-Whitney *U* test. (**e**) Comparison of DNA methylation kinetics in the *Sry* promoter in develoing gonads. Gonadal somatic cells were purifi d from XY *Tet2*Δ/+ and *Tet2*Δ/Δ embryos at the indicated ts stages and were then used for bisulfite sequencing analysis.

Sry demethylation is the earliest event in male embryonic gonad development[20]. Our data showed that the *Sry* promoter is demethylated during *Sry* induction through TET2-mediated active demethylation. Interestingly, we found that methylation of *Sry* promoter was maintained at low levels even at E12.0 (Fig. 2d), whereas *Sry*

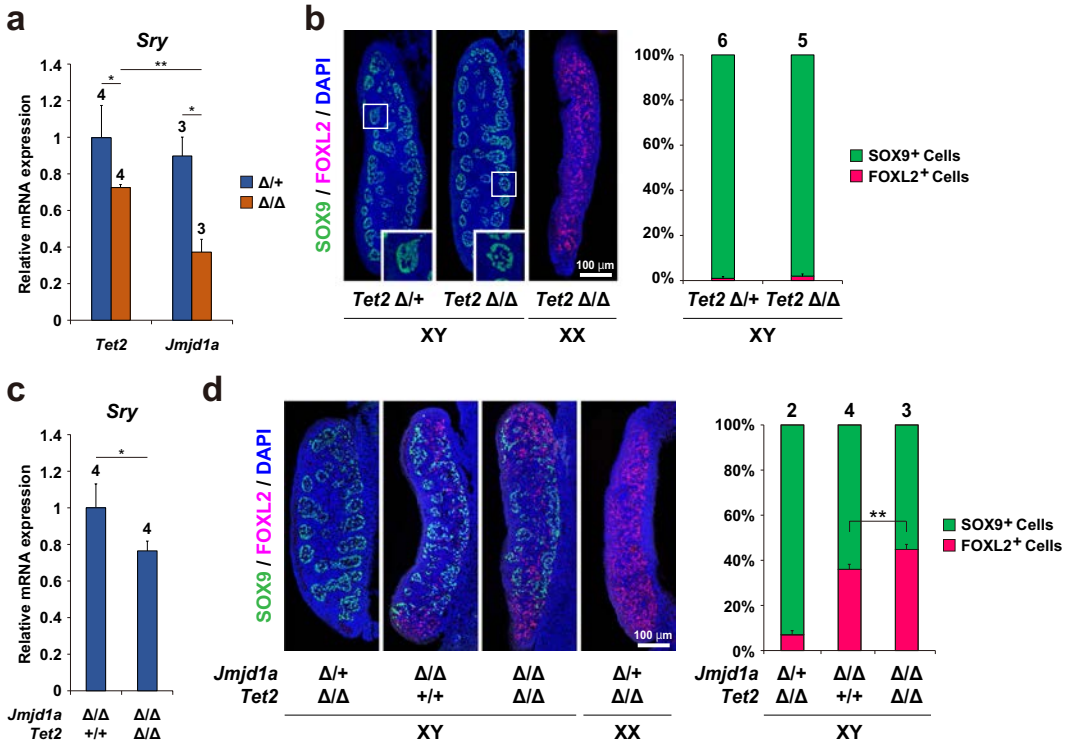

Figure 4. *Tet2* mutation diminishes *Sry* expression in gonadal somatic cells and enhances sex-reversal in XY *Jmjd1a*Δ/Δ mice. (**a**) Comparison of *Sry* mRNA levels between genotypes at the sex-determining period. Gonadal somatic cells were purifi d from E11.5 embryos of the indicated genotypes and were then used for qRT-PCR analysis. mRNA expression levels in *Tet2*Δ/+ gonadal somatic cells were defi ed as 1. Data are presented as mean ± SD. $*P < 0.05$, $**P < 0.01$. n ≥ 3. (**b**) Evaluation of sex development of *Tet2*-deficie t E13.5 gonads by immunofluorescence analysis using antibodies against SOX9 and FOXL2. SOX9 and FOXL2 are markers for testicular Sertoli cells and ovarian somatic cells, respectively. The enlarged box demonstrates testicular tubule-like structures (left). The ratio of SOX9-positive cells to FOXL2-positive cells is summarized in the right. Numbers of embryos examined are shown above the bars. Data are presented as mean ± SD. (**c**) qRT-PCR analysis of *Sry* in XY *Jmjd1a*-deficie t gonads and *Jmjd1a*/*Tet2*-deficie t gonads at E11.5. Each of the samples included one pair of gonads/mesonephros. mRNA expression levels in *Jmjd1a*-deficie t gonads were defi ed as 1. Data are presented as mean ± SD. $*P < 0.05$. n = 4. (**d**) Sex development of E13.5 embryonic gonads of the indicated genotypes was evaluated as in Fig. 4b. The ratio of SOX9-positive cells to FOXL2-positive cells is summarized in the right. Numbers of embryos examined are shown above the bars. Data are presented as mean ± SD. $*P < 0.05$.

expression became diminished until this stage. These results were consistent with a previous report[20]. mRNA expression analysis demonstrated constant expression of *Dnmt3b* and increased expression of *Dnmt1* and *Dnmt3a* in the developing XY gonads from E10.6 to E12.0 (Supplementary Fig. S4). Taking these results together, we postulate that DNA methylation/demethylation are required for *Sry* induction but not for its repression. Instead, *Sry* repression might be achieved independently of epigenetic regulation. Transient expression of SRY initiates *Sox9* expression[43]. Once SOX9 reaches a critical threshold, *Sry* is repressed by a SOX9-dependent negative-feedback loop[43,44]. It is conceivable that *Sry* repression might be achieved by such feedback loop of transcription factors.

Other than JMJD1A and TET2, we previously demonstrated that an H3K9 methyltransferase complex, GLP/G9a is involved in *Sry* regulation with an antagonistic function against JMJD1A[28]. Moreover, recent studies have revealed that histone acetyltransferases p300/CBP play a crucial role in *Sry* activation[11] and that polycomb-group protein CBX2 is involved in testis development by repressing Wnt signal[45]. These fi dings indicate that multiple epigenetic modifie s contribute to the complicated process of gonadal sex differentiation in mammals. However, it is still unclear and further study is required to determine how these enzymes are recruited to specific target loci including *Sry*, during gonadal sex development.

Methods

Animals. All animal experiments and methods were approved and performed in accordance with the relevant guidelines and regulations of the Animal Care Committee of Tokushima University (T29-62) and Osaka University (FBS-18-014). Mice (C57BL/6J and ICR) were supplied by SLC (Shimizu Laboratory Supplier, Kyoto) in Japan. Mouse lines of *Jmjd1a*-deficie t mice and *Nr5a1-hCD271*-transgenic mice[10] were sequentially backcrossed with C57BL/6J, and the F5 or later generation was used. Embryos were staged by counting tail somites

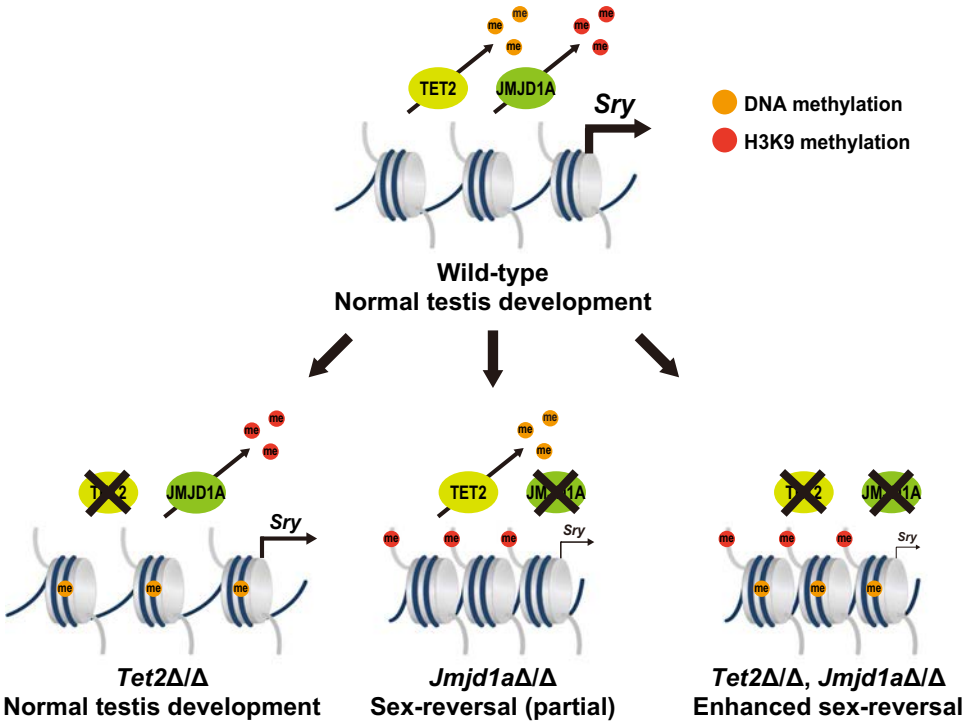

Figure 5. A schematic diagram for the regulation of *Sry* expression by TET2 and JMJD1A. Epigenetic regulation of *Sry* expression through H3K9 demethylation and DNA demethylation in male gonad development. TET2 catalyzes DNA demethylation in the *Sry* promoter. It is conceivable that *Sry* expression levels in *Tet2*-deficie t gonads might be higher than the threshold required for testis development. JMJD1A-mediated H3K9 demethylation plays a dominant role in *Sry* activation. *Jmjd1a* deficie cy lead to substantial reduction of *Sry* expression, thereby inducing sex-reversal. We found that *Tet2* deficie cy synergistically enhanced the sex reversal phenotype of *Jmjd1a*Δ/Δ embryos.

as described, where approximately E10.6, E11.4, and E12.0 correspond to 9–10 ts, 16–17 ts, and 22–23 ts, respectively.

Generation of *Tet* mutant mice using a CRISPR/Cas9 system. Mutant mice for each *Tet* (*Tet1/2/3*) were produced by electroporating *Cas9* mRNA and gRNA into mouse zygotes according to the protocol published recently[46]. Briefly, 400 ng/μl *Cas9* mRNA and 100 ng/μl each gRNAs targeting *Tets* (shown in Supplementary Fig. S2) were introduced into zygotes (C57BL/6 J × C57BL/6 J) by electroporation using Genome Editor GEB15 (BEX, Tokyo, Japan). The electroporation conditions were 30 V (3 msec ON + 97 msec OFF) × 4 times. The surviving 2-cell-stage embryos were transferred to the oviducts of pseudopregnant females (ICR). Mutant mice were backcrossed for more than three generations into the C57BL6/J background.

Magnetic-activated cell sorting (MACS). MACS was performed as described previously[18]. Briefly, a single cell suspension was prepared by trypsinizing the gonads and mesonephros isolated from embryos carrying the *Nr5a1/CD271*-transgene. Immunomagnetic isolation of CD271-expressing cells was performed according to the standard protocol (Miltenyi Biotech).

RNA expression analysis. Total RNA from hCD271-positive/-negative cells and a pair of gonads/mesonephros was extracted using Trizol (Invitrogen). ReverTra Ace qPCR RT Kit (TOYOBO) was used for cDNA synthesis, following the manufacturer's instructions. Subsequently, cDNA was used as the template for RT-qPCR using a StepOnePlus Real-Time PCR System (Applied Biosystems) and SYBR Premix Ex Taq II (TaKaRa) with gene-specific primers. The primer sets used in this analysis were as follows:

Sry forward 5′-TACCTACTTACTAACAGCTGACATCAC-3′
Sry reverse 5′-TGTCATGAGACTGCCAACCACAGGG-3′
Tet1 forward 5′-CCATTCTCACAAGGACATTCACA-3′
Tet1 reverse 5′-GCAGGACGTGGAGTTGTTCA-3′
Tet2 forward 5′-GCCATTCTCAGGAGTCACTGC-3′
Tet2 reverse 5′-CTTCTCGATTGTCTTCTCTATTGAGG-3′
Tet3 forward 5′-TCAGGGATGCTTTCTGTAGGG-3′
Tet3 reverse 5′-ATTTGGGATGTCCAGATGAGC-3′
Apobec3 forward 5′-AGCATGCAGAAATCCTCTTCC-3′

Apobec3 reverse 5′-AGATCTGGACGATCCCTTTTG-3′
Dnmt1 forward 5′-ATCAGGTGTCAGAGCCCAAAG-3′
Dnmt1 reverse 5′-TGGTGGAATCCTTCCGATAAC-3′
Dnmt3a forward 5′- CAGACGGGCAGCTATTTACAG-3′
Dnmt3a reverse 5′- TGGTTCTCTTCCACAGCATTC-3′
Dnmt3b forward 5′-TCGCAAGGTGTGGGCTTTTGT-3′
Dnmt3b reverse 5′-CTGGGCATCTGTCATCTTTGCA-3′
Wt1 forward 5′-ATGGCCACACGCCCTCGCATCACGC-3′
Wt1 reverse 5′-AGCGAGCCCTGCTGGCCCATGGGGT-3′
Gapdh forward 5′-ATGAATACGGCTACAGCAACAGG-3′
Gapdh reverse 5′-CTCTTGCTCAGTGTCCTTGCTG-3′

Bisulfite sequencing analysis. Total genomic DNA was isolated from hCD271-positive/-negative gonad-mesonephros pairs of 3 embryos or from 3 whole embryos (E8.5). Genomic DNA was extracted using the Wizard SV Genomic DNA Purifi ation System (Promega). Genomic DNA was treated with sodium bisulfite using the MethylEasy Xceed Rapid DNA Bisulfite Modifi ation Kit (Human Genetic Signatures) following the manufacturer's instructions. The bisulfite-treated DNA was PCR-amplifi d using respective primer sets. PCR products were subcloned into the pGEM-T Easy vector (Promega) and sequenced. Methylation levels of *Sry* promoter analyzed by every >30 sequencing. The primer sets used in this analysis were as follows:

Sry 1st forward 5′-TTTATATTGGGTTATAGAGTTAGAATAGAT-3′
Sry 2nd forward 5′-AGATTATTTTTTAGTTTTTTTTTATGT-3′
Sry 1st and 2nd reverse 5′-CCAAAATATACTTATAACAAAAATTTTAAT-3′
Sox9 1st forward 5′-GTAGTAGAAGTTTTAGTTATTAT-3′
Sox9 2nd forward 5′-GATTATTTTTAAGTATTTTTTTT-3′
Sox9 1st and 2nd reverse 5′-ATATAAATTTACTCTCTACTCTC-3′
Foxl2 1st forward 5′-GGTTTTGTTTTTTTTTATTTGAA-3′
Foxl2 2nd forward 5′-GAGGTTTGGATTATTTTTTTTT-3′
Foxl2 1st and 2nd reverse 5′-ATTTTCTTAACTAAACTCTCCC-3′

Tet-assisted bisulfite sequencing analysis. The 5hmC TAB-seq kit (WiseGene) was used for converting 5mC to 5caC, according to the manufacturer's instructions. Briefly, 5hmC in genomic DNA was first protected with glycosylation by β-glycosyltransferase for 6 h at 37 °C. Genomic DNA was then treated with Tet protein overnight at 37 °C. Tet oxidized DNA was treated with sodium bisulfite using the same method as in bisulfite sequencing analysis. For verifi ation, 5mC control DNA and 5hmC control DNA were mixed at 0.5% and 0.3% volume of total gDNA, respectively.

Immunohistochemical staining. Th s method was performed as described previously[26]. Briefly, tissues were fi ed in 4% paraformaldehyde, embedded in Tissue-Tek OTC compound (Sakura Finetek Japan) and cut into 10-μm sections. The sections were incubated with primary antibodies (rat anti-Nr5a1 (Trans Genic Lnc, KO610), rabbit anti-5hmC (Active Motif, #39791), anti-Sox9 (Millipore, AB5535), goat anti-Foxl2 (Abcam, ab-5096)), overnight at 4 °C. For fluorescence staining, the sections were incubated with Alexa-conjugated secondary antibodies (Life Technologies) at room temperature for 1 h and counterstained with DAPI. The sections were mounted in Vectashield (Vector) and observed with a confocal laser scanning microscope (LSM700, Carl Zeiss). Co-immunostaining for Nr5a1 and 5hmC was performed in the order: antibody reaction for Nr5a1 (1st: 4 °C, O/N and 2nd: RT, 1 h) → 2 N HCl treatment (RT, 20 min) → antibody reaction for 5hmC (1st: RT, 1 h and 2nd: RT, 1 h).

***In vivo* inhibitor analysis.** 3-AB (Sigma) was prepared as a 2.5 g/ml stock solution with DMSO; 4 ml of the 3-AB stock solution was diluted with 500 ml of PBS[47]. Pregnant females at E10.5 were intraperitoneally administered 500 ml of the inhibitor solution.

Dot-blot analysis. Total genomic DNA was isolated from hCD271-positive/-negative cells of the gonad-mesonephros pairs of 3 embryos. Sonicated genomic DNA was prepared as 25, 50, 100 ng/μl. 1 μl of sample was spotted onto the nitrocellulose membrane. After baking at 80 °C for 1 h and blocking with 5% non-fat milk PBS-T for 1 h at room temperature, the membrane was incubated overnight with anti-5hmC antibody (Active Motif, #39791, 1:10,000) at 4 °C. Following the primary antibody reaction, the membrane was incubated with secondary horseradish peroxidase-coupled antibody. Detection was performed using the Western Lighting Plus-ECL (PerkinElmer). To ensure equal loading, the membrane was stained with methylene blue post-immunoblotting.

RNA-seq analysis. Total RNA from hCD271-positive cells of 3 embryos was extracted using the Direct-zol RNA MicroPrep kit (ZYMO RESEACH). Quality control check for length distribution and concentration of RNA fragments in the prepared libraries was performed using the Agilent 2100 Bioanalyzer (Agilent Technologies). The cDNA library was constructed using standard methods (Illumina TruSeq mRNA stranded kit) with index adapters (Illumina TruSeq indexes). DNA was sequenced as single-end, 50 base-length reads on the Illumina HiSeq. 1500 instrument (Illumina Inc.) with 10 million reads. Raw sequence reads were mapped to mm10 by STAR (v2.6.0a) with mostly default parameters except the following:–outFilterMultimapNmax 1. TPM (Transcripts Per Kilobase Million) for *Sry*, *Tet1*, *Tet2*, and *Tet3* was estimated using the rsem-calculate-expression command of RSEM (v1.3.1). The TPM values for all genes are listed in Supplementary Table 1. RNA sequencing data have been uploaded to NCBI Sequence Read Archive (SRA) with the accession number PRJNA557299.

References

1. Nikolova, G. & Vilain, E. Mechanisms of disease: transcription factors in sex determination-relevance to human disorders of sex development. *Nat Clin. Pract. Endocrinol. Metab.* **2**, 231–238 (2006).
2. Sekido, R. & Lovell-Badge, R. Sex determination and SRY: down to a wink and a nudge? *Trends Genet.* **25**, 19–29 (2009).
3. Kashimada, K. & Koopman, P. Sry: the master switch in mammalian sex determination. *Development* **137**, 3921–3930 (2010).
4. Koopman, P., Münsterberg, A., Capel, B., Vivian, N. & Lovell-Badge, R. Expression of a candidate sex-determining gene during mouse testis differentiation. *Nature* **348**, 450–452 (1990).
5. Hacker, A., Capel, B., Goodfellow, P. & Lovell-Badge, R. Expression of Sry, the mouse sex determining gene. *Development* **121**, 1603–1614 (1995).
6. Jeske, Y. W., Bowles, J., Greenfi ld, A. & Koopman, P. Expression of a linear Sry transcript in the mouse genital ridge. *Nat. Genet.* **10**, 480–482 (1995).
7. Bullejos, M. & Koopman, P. Spatially dynamic expression of Sry in mouse genital ridges. *Dev. Dyn.* **221**, 201–205 (2001).
8. Wilhelm, D. *et al*. Sertoli cell differentiation is induced both cell-autonomously and through prostaglandin signaling during mammalian sex determination. *Dev. Biol.* **287**, 111–124 (2005).
9. Larney, C., Bailey, T. L. & Koopman, P. Switching on sex: transcriptional regulation of the testis-determining gene Sry. *Development* **141**, 2195–2205 (2014).
10. Kuroki, S. *et al*. Epigenetic regulation of mouse sex determination by the histone demethylase Jmjd1a. *Science* **341**, 1106–1109 (2013).
11. Carré, G. A. *et al*. Loss of p300 and CBP disrupts histone acetylation at the mouse Sry promoter and causes XY gonadal sex reversal. *Hum. Mol. Genet.* **27**, 190–198 (2018).
12. De Smet, C., Lurquin, C., Lethé, B., Martelange, V. & Boon, T. DNA methylation is the primary silencing mechanism for a set of germ line- and tumor-specific genes with a CpG-rich promoter. *Mol. Cell Biol.* **19**, 7327–7335 (1999).
13. Weber, M. *et al*. Distribution, silencing potential and evolutionary impact of promoter DNA methylation in the human genome. *Nat. Genet.* **39**, 457–466 (2007).
14. Gruenbaum, Y., Stein, R., Cedar, H. & Razin, A. Methylation of CpG sequences in eukaryotic DNA. *FEBS Lett.* **124**, 67–71 (1981).
15. Razin, A. *et al*. Variations in DNA methylation during mouse cell differentiation *in vivo* and *in vitro*. *Proc. Natl. Acad. Sci. USA* **81**, 2275–2279 (1984).
16. Boyes, J. & Bird, A. Repression of genes by DNA methylation depends on CpG density and promoter strength: evidence for involvement of a methyl-CpG binding protein. *EMBO J.* **11**, 327–333 (1992).
17. Wu, S. C. & Zhang, Y. Active DNA demethylation: many roads lead to Rome. *Nat. Rev. Mol. Cell Biol.* **11**, 607–620 (2010).
18. Ito, S. *et al*. Tet proteins can convert 5-methylcytosine to 5-formylcytosine and 5-carboxylcytosine. *Science* **333**, 1300–1303 (2011).
19. He, Y. F. *et al*. Tet-mediated formation of 5-carboxylcytosine and its excision by TDG in mammalian DNA. *Science* **333**, 1303–1307 (2011).
20. Gierl, M. S., Gruhn, W. H., von Seggern, A., Maltry, N. & Niehrs, C. GADD45G functions in male sex determination by promoting p38 signaling and Sry expression. *Dev. Cell* **23**, 1032–1042 (2012).
21. Nishino, K., Hattori, N., Tanaka, S. & Shiota, K. DNA methylation mediated control of Sry gene expression in mouse gonadal development. *J. Biol. Chem.* **279**, 22306–22313 (2004).
22. Rasmussen, K. D. & Helin, K. Role of TET enzymes in DNA methylation, development, and cancer. *Genes Dev.* **30**, 733–750 (2016).
23. Kuroki, S. *et al*. Development of a general-purpose method for cell purifi ation using Cre/loxP-mediated recombination. *Genesis.* **53**, 387–393 (2015).
24. Yu, M. *et al*. Base-resolution analysis of 5-hydroxymethylcytosine in the mammalian genome. *Cell* **149**, 1368–1380 (2012).
25. Hajkova, P. *et al*. Genome-wide reprogramming in the mouse germ line entails the base excision repair pathway. *Science* **329**, 78–82 (2010).
26. Ciccarone, F. *et al*. Poly(ADP-ribosyl)ation acts in the DNA demethylation of mouse primordial germ cells also with DNA damage-independent roles. *PLoS One* **7**, e46927 (2012).
27. Okashita, N. *et al*. PRDM14 promotes active DNA demethylation through the ten-eleven translocation (TET)-mediated base excision repair pathway in embryonic stem cells. *Development* **141**, 269–280 (2014).
28. Kuroki, S. *et al*. Rescuing the aberrant sex development of H3K9 demethylase Jmjd1a-deficient mice by modulating H3K9 methylation balance. *PLoS Genet.* **13**, e1007034 (2017).
29. Ko, M. *et al*. Modulation of TET2 expression and 5-methylcytosine oxidation by the CXXC domain protein IDAX. *Nature* **497**, 122–126 (2013).
30. Hammes, A. *et al*. Two splice variants of the Wilms' tumor 1 gene have distinct functions during sex determination and nephron formation. *Cell* **106**, 319–329 (2001).
31. Ladomery, M. Multifunctional proteins suggest connections between transcriptional and post-transcriptional processes. *BioEssays* **19**, 903–909 (1997).
32. Ladomery, M. & Dellaire, G. Multifunctional zinc fi ger proteins in development and disease. *Ann. Hum. Genet.* **66**, 331–342 (2002).
33. Hossain, A. & Saunders, G. F. The human sex-determining gene SRY is a direct target of WT1. *J. Biol. Chem.* **276**, 16817–16823 (2001).
34. Hossain, A. & Saunders, G. F. Role of Wilms' tumor 1 (WT1) in the transcriptional regulation of the Mullerian-inhibiting substance promoter. *Biol. Reprod.* **69**, 1808–1814 (2003).
35. Matsuzawa-Watanabe, Y., Inoue, J. & Semba, K. Transcriptional activity of testis-determining factor SRY is modulated by the Wilms' tumor 1 gene product, WT1. *Oncogene* **22**, 7900–7904 (2003).
36. Miyamoto, Y., Taniguchi, H., Hamel, F., Silversides, D. W. & Viger, R. S. A GATA4/WT1 cooperation regulates transcription of genes required for mammalian sex determination and differentiation. *BMC Mol. Biol.* **44** (2008).
37. Wang, Y. *et al*. WT1 recruits TET2 to regulate its target gene expression and suppress leukemia cell proliferation. *Mol. Cell.* **57**, 662–673 (2015).
38. Hashimoto, H. *et al*. Wilms tumor protein recognizes 5-carboxylcytosine within a specific DNA sequence. *Genes Dev.* **28**, 2304–2313 (2014).
39. Nabel, C. S. *et al*. AID/APOBEC deaminases disfavor modifi d cytosines implicated in DNA demethylation. *Nat. Chem. Biol.* **8**, 751–758 (2012).
40. Zhu, J. K. Active DNA demethylation mediated by DNA glycosylases. *Annu. Rev. Genet.* **43**, 143–166 (2009).
41. Teperek-Tkacz, M., Pasque, V., Gentsch, G. & Ferguson-Smith, A. C. Epigenetic reprogramming: is deamination key to active DNA demethylation? *Reproduction* **142**, 621–632 (2011).
42. Wijesinghe, P. & Bhagwat, A. S. Efficient deamination of 5-methylcytosines in DNA by human APOBEC3A, but not by AID or APOBEC3G. *Nucleic Acids Res.* **40**, 9206–9217 (2012).
43. Sekido, R., Bar, I., Narváez, V., Penny, G. & Lovell-Badge, R. SOX9 is up-regulated by the transient expression of SRY specifi ally in Sertoli cell precursors. *Dev Biol.* **274**, 271–279 (2004).
44. Chaboissier, M. C. *et al*. Functional analysis of Sox8 and Sox9 during sex determination in the mouse. *Development.* **131**, 1891–1901 (2004).
45. Garcia-Moreno, S. A. *et al*. CBX2 is required to stabilize the testis pathway by repressing Wnt signaling. *PLoS Genet.* **15**, e1007895 (2019).

46. Hashimoto, M. & Takemoto, T. Electroporation enables the effici t mRNA delivery into the mouse zygotes and facilitates CRISPR/Cas9-based genome editing. *Sci. Rep.* **5**, 11315 (2015).
47. Kawasaki, Y. *et al*. Active DNA demethylation is required for complete imprint erasure in primordial germ cells. *Sci. Rep.* **4**, 3658 (2014).

Acknowledgements

We are grateful to Hitoshi Miyachi and Satsuki Kitano for providing technical assistance with embryo manipulation. We are especially grateful to the members of the Tachibana laboratory for technical support and stimulating discussions. Th s study was supported by JSPS KAKENHI grant number 16K18429 (NO), 17H06423 (MT), 17H06424 (MT), 18H02419 (MT), and the Senri Life Science Foundation (NO).

Author Contributions

S.K. performed immunohistochemical staining. R.M. and S.K. contributed RNA-seq analysis. N.O. performed most analyses. N.O. and M.T. designed the experiments and wrote the manuscript.

Additional Information

Supplementary information accompanies this paper at https://doi.org/10.1038/s41598-019-50058-7.

Competing Interests: The authors declare no competing interests.

Publisher's note Springer Nature remains neutral with regard to jurisdictional claims in published maps and institutional affiliations.

Endocrinology, 2022, Vol. 163, No. 1, 1–9
https://doi.org/10.1210/endocr/bqab217
Research Article

Research Article

Human *SRY* Expression at the Sex-determining Period is Insufficient to Drive Testis Development in Mice

Atsumi Tsuji-Hosokawa,[1,2] Yuya Ogawa,[1,3] Iku Tsuchiya,[1,3] Miho Terao,[1] and Shuji Takada[1,3]

[1]Department of Systems BioMedicine, National Research Institute for Child Health and Development, Tokyo 157-8535, Japan; [2]Department of Pediatrics and Developmental Biology, Graduate School of Medical and Dental Sciences, Tokyo Medical and Dental University (TMDU), Tokyo 113-8510, Japan; and [3]Department of NCCHD, Graduate School of Medical and Dental Sciences, Tokyo Medical and Dental University (TMDU), Tokyo 113-8510, Japan

ORCiD numbers: 0000-0001-8226-2618 (A. Tsuji-Hosokawa); 0000-0002-9406-4683 (S. Takada).

Abbreviations: dpc, days postcoitum; HMG, high mobility group; ORF, open reading frame; sgRNA, single-guide RNA; UTR, untranslated region

Received: 21 July 2021; Editorial Decision: 12 October 2021; First Published Online: 18 October 2021; Corrected and Typeset: 12 November 2021.

Abstract

The sex-determining region of the Y chromosome, *Sry/SRY,* is an initiation factor for testis development in both humans and mice. Although the functional compatibility between murine SRY and human SRY was previously examined in transgenic mice, their equivalency remains inconclusive. Because molecular interaction and timeline of mammalian sex determination were mostly described in murine experiments, we generated a mouse model in which *Sry* was substituted with human *SRY* to verify the compatibility. The mouse model had the human *SRY* open reading frame at the locus of murine *Sry* exon 1—$Sry^{(SRY)}$ mice—and was generated using the CRISPR/Cas9 system. The reproductive system of the mice was analyzed. The expression of human *SRY* in the fetal gonadal ridge of $Sry^{(SRY)}$ mice was detected. The external and internal genitalia of adult $Sry^{(SRY)}$ mice were similar to those of wild-type females, without any significant difference in anogenital distance. $Sry^{(SRY)}$ mice obtained gonads, which were morphologically considered as ovaries. Histological analysis revealed that the cortical regions of gonads from adult $Sry^{(SRY)}$ mice contained few follicles. We successfully replaced genes on the Y chromosome with targeted genome editing using the CRISPR/Cas9 system. Because the $Sry^{(SRY)}$ XY mice did not develop testis, we concluded that human SRY was insufficient to drive testis development in mouse embryos. The difference in response elements and lack of glutamine-rich domains may have invalidated human SRY function in mice. Signal transduction between *Sry*/*SRY* expression and *Sox9*/*SOX9* activation is possibly organized in a species-specific manner.

ISSN Online 1945-7170

Key Words: SRY, testis, sex development, human, mouse

The sex-determining region of the Y chromosome, *Sry/SRY*, is a member of the SOX (SRY-related high mobility group [HMG]) family and is regarded as an initiation factor of testis development in both humans and mice (1, 2). Because the Y chromosome does not completely recombine with the X chromosome during meiosis, it evolved rapidly and specifically in each species (3-5). The amino acid sequence of the HMG domain in murine SRY is almost 70% homologous to that of human SRY, but other domains are poorly homologous. In addition, murine SRY has a glutamine-rich domain and a newly discovered exon2 (6, 7). Homologous sequences were not detected in the human Y chromosome. Despite this lack of similarity, Lovell-Badge et al. reported that human *SRY* could function as an initiator of testis development in mice under the control of the murine *Sry* promoter (8) (Fig. 1). However, this report did not describe the copy number of the transgene, meaning that there is a possibility that a high copy number of the transgene amplified its function. Thus, the functional equivalence of murine SRY and human SRY in murine testis development remains unknown.

Because the detailed mechanisms and timeline of mammalian sex determination have been mostly described using murine experiments, it is important to distinguish common mammalian pathways and those that are species-specific within the signal transduction of sex differentiation. To compare the function of human *SRY* and murine *Sry*, we generated a mouse model in which *Sry* was substituted with human *SRY*, of which only 1 copy was expressed by the murine *Sry* promoter and their compatibility was verified by analyzing the reproductive system of these mice.

Materials and Methods

Animal experiments

C57BL/6J and hybrid F_1 C57BL/6J × DBA/2 (BDF1) mice were purchased from the Sankyo Lab (Tokyo, Japan). Jcl:ICR female mice were purchased from CLEA Japan (Tokyo, Japan). The generation of $Sry^{(SRY)}$ mice is explained in the next section. All animal protocols were approved by the Animal Care and Use Committee of the National Research Institute for Child Health and Development, Tokyo, Japan. All experiments were conducted in accordance with the approved animal protocols (protocol #2016-002 and #2020-007).

Generation of $Sry^{(SRY)}$ mice using the CRIPSR/Cas9 system

To substitute the murine *Sry* open reading frame (ORF) with the human *SRY* ORF, 2 single-guide RNAs (sgRNAs) that targeted the 5′ and 3′ ends of the ORF in murine *Sry* exon 1 were designed using an online tool (https://crispr.dbcls.jp/) (9) (Fig. 2A). The selected sequences are listed in Table 1. The sgRNAs were prepared using the CUGA7 gRNA Synthesis Kit (Nippon Genetech, Tokyo, Japan). A donor plasmid containing the ORF of human *SRY* (chrY:2 786 989-2 787 603/hg38) and each 500-bp sequence located upstream (C-arm) and downstream (T-arm) of ORF in murine *Sry* exon 1 as homology arms (chrY:2 663 659-2 664 549/mm39 and chrY:2 661 580-2 662 470/mm39) was constructed by IDT (Coralville, IA, USA) (Fig. 2A).

The microinjection of sgRNAs, Cas9 protein, and the donor plasmid into the pronuclei and cytoplasm of fertilized eggs at the 1-cell stage and transplantation of embryos to pseudopregnant recipient mice was performed as previously described (10).

Genetic analysis of murine *Sry* exon 1 locus and sexing of $Sry^{(SRY)}$ mice

Genomic DNA was extracted from the amniotic membrane, clipped toe, or tail. All mice were sexed via PCR using X- and Y-specific primers designated the *Xist* and *Zfy* loci, respectively. The GeneAmpFast PCR Master Mix (Applied Biosystems, Waltham, MA, USA) was used for sexing (11-13). Transgenes in the genome were detected using PCR with BioTAQ DNA Polymerase (Meridian Bioscience, Cincinnati, OH, USA) with primers targeting the human *SRY* ORF. XX mice without transgenes were designated as control female mice for subsequent experiments. For knock-in check, the primers were designed to target the upstream region of the C-arm (Sry UF2) and downstream region of the T-arm (Sry DR1) (Fig. 2B), and PCR was performed with PrimeSTAR GXL DNA Polymerase (TaKaRa Bio Inc., Shiga, Japan). The amplicons of all XY mice were processed for direct sequencing to confirm indels around the target sites of sgRNAs and knock-in of human SRY. Moreover, the degree of mosaicism was analyzed by cloning the amplicon in a pCR-Blunt Vector (Thermo Fisher Scientific, Waltham, MA, USA) and sequencing (Fig. S4A) (14). The sequences of all primers used for sexing and genotyping are listed in Table 1.

RNA isolation and semiquantitative PCR

Noon of the day when the recipient mice received 2-cell stage fertilized eggs after microinjection were designated as 0.5 days postcoitum (dpc) and F_0 $Sry^{(SRY)}$ embryos were collected from recipients at 11.5 dpc. Because no embryo

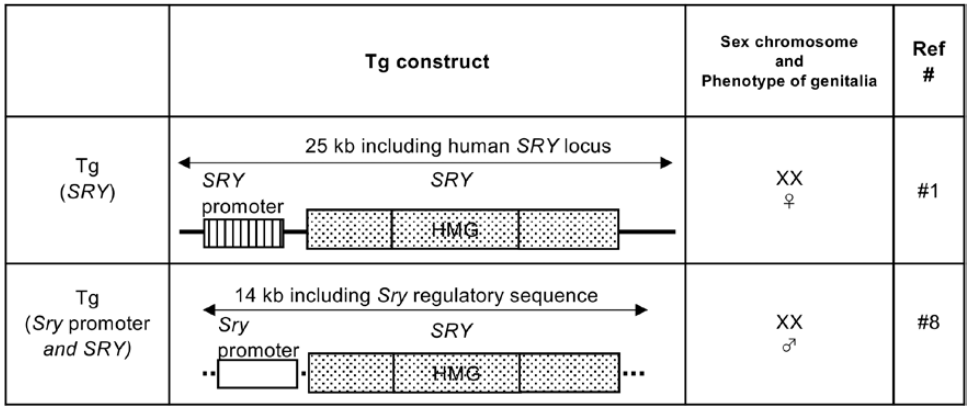

Figure 1. Genotype and phenotype of human *SRY* transgenic mice. The bold solid line in the construct scheme indicates the human genomic sequence, whereas the dotted line indicates the murine genomic sequence. Abbreviation: Tg, transgenic.

with the XY karyotype obtained a complete *Sry* sequence, embryos from pregnant B6D2F1 mice at 11.5 dpc were used as the experimental control. Embryonic gonads and mesonephroi from the embryos were dissected in PBS and immediately frozen in liquid nitrogen. Total RNA from the embryonic gonads was isolated using Isogen (Nippon Genetech) and 750 ng of each RNA sample was processed with TurboDNase (Invitrogen, Carlsbad, CA, USA). The samples were processed for reverse transcription using SuperScript II (Invitrogen), according to the manufacturer's instructions. Semiquantitative PCR reactions were performed using BioTAQ DNA Polymerase (Meridian Bioscience). The primers used for semiquantitative PCR are listed in Table 1 (15).

Anatomical findings

Because the mice used for the $Sry^{(SRY)}$ strain were infertile, F_0 $Sry^{(SRY)}$ mice were analyzed at the age of 8 weeks. Littermate XX mice were used as controls. Littermate XY mice that showed male-type external genitalia were assigned as control XY mice. The genotyping and sequencing results are summarized in Fig. S3 (14). Body length, body weight, and anogenital distance of the mice were measured. Because only 2 live F_0 mice displayed knock-in alleles, statistical analysis was not performed. External and internal genitalia and gonads were observed, and gonads were sampled for subsequent histological analysis. The figure of measured data was created using GraphPad Prism (version 9.1.0 for macOS, GraphPad Software, San Diego, CA, USA; www.graphpad.com).

Histology

Gonads from 8-week-old F_0 $Sry^{(SRY)}$ mice and their littermates were fixed overnight in 4% (w/v) paraformaldehyde in PBS at 4°C, dehydrated with 25% to 100% methanol in PBS 0.1% (v/v)/Triton X-100, and embedded in paraffin. The blocks were sectioned at a thickness of 10 µm and stained with hematoxylin and eosin. The block was serially sectioned, and developing follicles, including secondary and Graafian follicles, were counted in every tenth section of the ovaries according to methods reported previously (16, 17).

Construct for translation studies on the human SRY protein

The conventional murine *Sry* transcript sequence was obtained from a study by Jeske et al. (18). The 5′ untranslated region (UTR) sequence of murine *Sry* (chrY:2 663 935-2 663 659/mm39), human *SRY* ORF (chrY:2 786 989-2 787 603/hg38), and 3′ UTR sequence of murine *Sry* (chrY:2 662 470-2 660 402/mm39) were serially cloned into the XhoI/BamHI site of a pcDNA3.1(-) vector (Invitrogen). As a positive control, the expression vector of human *SRY* (pRP[Exp]-CMV>hSRY) was constructed and packaged using the VectorBuilder platform (VectorBuilder, Inc., Chicago, IL, USA). The vector identification number is VB191222-3304huj.

Transfection and immunocytochemistry

NIH3T3 cells were plated at 7.5×10^5 cells/well in 6-well plates at 6 hours before transfection, and 2.5 µg of the expression vector was added to each well. The total quantity of DNA was standardized using the control vector, pcDNA3.1(-). The cells were collected 30 hours posttransfection. The collected cells were then suspended in PBS. The suspension was diluted to 1.5×10^5 cells/mL, and 500 µL of the suspension was applied to a cell collector (catalog #SC-2, TOMY SEIKO Co., Ltd, Tokyo, Japan). After centrifugation, the cells were spread onto the slides, air-dried, fixed in 4% (w/v) paraformaldehyde in PBS at room temperature for 15 minutes, and permeabilized in 0.2% (w/v) Triton X-100 in PBS at

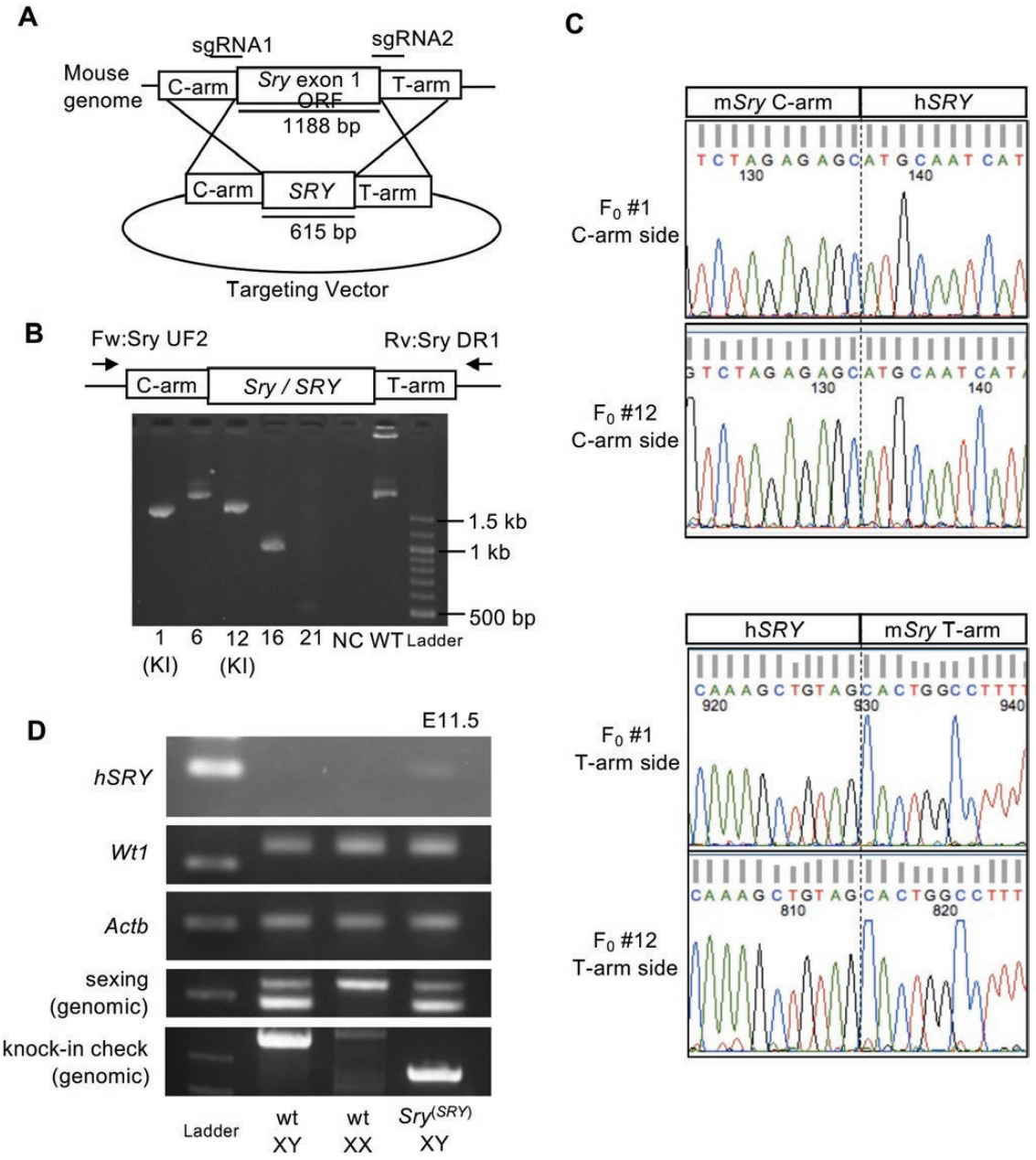

Figure 2. Genetic and expression analyses of the *Sry*$^{(SRY)}$ strain. (A) Scheme of genome editing for generating *Sry*$^{(SRY)}$ mice. (B) Results of the genetic analysis of *Sry*$^{(SRY)}$ mice. PCR was performed using the primer set comprising Sry UF2 and Sry DR1, which were designed based on the outer loci of the donor vector sequence. The amplicon size of the wild-type genome was 2385 bp, whereas that of the genome with human SRY substitution was 1812 bp. Arrow: primer locus; the number beneath the gel photo: mouse ID. (C) Genome sequence of *Sry*$^{(SRY)}$ mice around sgRNA target site. The sequence confirmed human SRY was knocked-in at the locus of murine *Sry* ORF. (D) Expression analysis of E11.5 fetal gonads from *Sry*$^{(SRY)}$ mice. Expression of human *SRY* was confirmed in gonads of *Sry*$^{(SRY)}$ mice. The image "sexing (genomic)" displays the sexing result with genomic DNA eluted from each embryo used for RNA extraction. An XX embryo shows a single band with the *Xist* amplicon (233 bp), whereas an XY embryo shows 2 bands with the *Xist* and *Zfy* amplicons (183 bp). The image "knock-in check (genomic)" displayed the PCR results with the primer set comprising Sry UF2 and Sry DR1, which were used in the experiment described in Fig. 2B. Abbreviations: C-arm, centromeric side arm; ladder, DNA ladder markers; NC, negative control; T-arm, telomere side arm; WT, wild-type.

room temperature for 5 minutes. After 3 washes in PBS, the cells were incubated in 10% (w/v) of donkey serum in PBS with 0.3% (w/v) Triton X-100 at room temperature for 60 minutes and treated overnight with a diluted primary antibody at 4°C. The anti-human SRY antibody (#OACD07509; Aviva Systems Biology, San Diego, CA, USA; RRID: AB_2893396; http://antibodyregistry.org/AB_2893396) was diluted at a ratio of 1:50. After 3 washes in PBS, the cells were incubated with the secondary antibody conjugated with donkey anti-rabbit Alexa Fluor 488 (A21206, Life Technologies; RRID: AB_2535792; http://antibodyregistry.org/AB_2535792) for 1 hour at room temperature. The cells were rinsed three times in PBS, counterstained with 1:1000 diluted 4,6-diamidino-2-phenylindole (#D212, Fujifilm Wako Chemicals Co., Ltd,

Table 1. Primer sequence list

Primer names	Sequences	Amplicon size	Reference no.
sgRNA			
sgRNA for N-term of Sry exon1 ORF	5′–TGACAATTGTCTAGAGAGCA–3′	119 bp	
sgRNA for C-term of Sry exon1 ORF	5′–GGTTGGCAGTCTCATGACAC–3′	119 bp	
Sexing primers			
Zfy Fw	5′–GACTAGACATGTCTTAACATCTGTCC–3′	183 bp	12
Zfy Rv	5′–CCTATTGCATGGACAGCAGCTTATG–3′		
Xist Fw	5′–AGGATAATCCTTCATTATCGCG–3′	233 bp	13
Xist Rv	5′–AAACGAGCAAACATGGCTGGAG–3′		
Genotyping primers			
hSRY Fw for transgene check	5′–ATGCAATCATATGCTTCTGC–3′	615 bp	
hSRY Rv for transgene check	5′–CTACAGCTTTGTCCAGTGGC–3′		
Sry UF2 for knock-in check	5′–TTTCTCACGTTAGTCCATCC–3′	wt.: 2385 bp	
Sry DR1 for knock-in check	5′–TCTAGTAAGAGTCCTTGACC–3′	KI:1812 bp	
Semiquantitative PCR primers			
hSRY-mSry_RT_F	5′–CCAGCTAGGCCACTTACCG–3′	102 bp	
hSRY-mSry_RT_R	5′–GGTAGGAGAAAAGGCCAGTG–3′		
mWt1_RT_F	5′–CATCTGAAGACCCACACCAG–3′	136 bp	
mWt1_RT_R	5′– TGTTTCTCTGATGCATGTTG–3′		
mActb_RT_F	5′–CGTGAAAAGATGACCCAG–3′	100 bp	15
mActb_RT_R	5′–TGGTACGACCAGAGGCATACAG–3′		

Abbreviations: Fw, forward; Rv, reverse; ORF, open reading frame; sgRNA, single-guide RNA; wt, wild-type.

Osaka, Japan), and mounted using Fluoromount (Diagnostic BioSystems, Pleasanton, CA, USA). Digital images were obtained using an Olympus BX53 inverted microscope (Olympus, Tokyo, Japan) and transferred to Photoshop CC (Adobe, San Jose, CA, USA) for image acquisition.

Endocrinological assay

The mice were euthanized by isoflurane inhalation. After the arrest of breathing was confirmed, blood was collected from the heart. The blood specimens were incubated at room temperature for 1 to 2 hours. Serum was separated by centrifugation at the speed of 1500*g* for 15 minutes at 4°C and stored at -80°C. Specimens from 8-week-old $Sry^{(SRY)}$ mice were collected at random time points in the estrous cycle. The serum of wild-type XX was sampled from 8-week-old female B6D2F1 mice at various stages of the estrous cycle, including proestrous, estrous, and metestrous. The control serum from wild-type XY was sampled from 8-week-old male B6D2F1 mice. The serum levels of estradiol and testosterone were measured using liquid chromatography/tandem mass spectrometry. The measurement was performed by ASKA Pharma Medical Co., Ltd.

Results

Knock-in mice were generated and human SRY expression was confirmed

Twenty-three F_0 mice were born, of which 10 were XY mice. Genotyping revealed that only 2 mice displayed the knock-in allele and were confirmed as $Sry^{(SRY)}$ mice (Fig. 2B and Fig. 2C). The deletion of murine *Sry* exon 1 and knock-in of human *SRY* were confirmed by sequencing (Fig. S4A-E) (14). Small indels at the 5′ or 3′ end of *Sry* exon 1 were observed in the XY littermates (Fig. S3) (14). Because these indels were not expected to disrupt *Sry* function (6) and these mice showed male-type external genitalia, they were designated as control male mice in our study. For the expression study, 97 embryos were obtained, and 5 of 39 XY mice were $Sry^{(SRY)}$ mice. Expression of human *SRY* was confirmed in the $Sry^{(SRY)}$ gonadal ridge (Fig. 2D). To confirm the translation of human SRY protein knocked in at the murine *Sry* locus, an in vitro overexpression study was performed with a construct containing the human *SRY* ORF linked to the 5′ UTR and 3′ UTR sequences of murine *Sry* was performed. Human SRY was detected in the nuclei of transfected cells (Fig. S5A-B) (14).

$Sry^{(SRY)}$ mice displayed female-type genitalia and morphological ovaries with fewer follicles

External and internal genitalia of $Sry^{(SRY)}$ mice were similar to those of wild-type females, and the development of nipples was observed (Fig. 3A). In accordance with this, the anogenital distance was almost the same as that of the wild-type female (Fig. 3B). Although the gonads of $Sry^{(SRY)}$ mice were morphologically considered as ovaries, and developing follicles, including preovulatory follicles, were observed (Fig. 4A–D), some cortical regions of $Sry^{(SRY)}$ mice contained only a few follicles, and the total follicle number

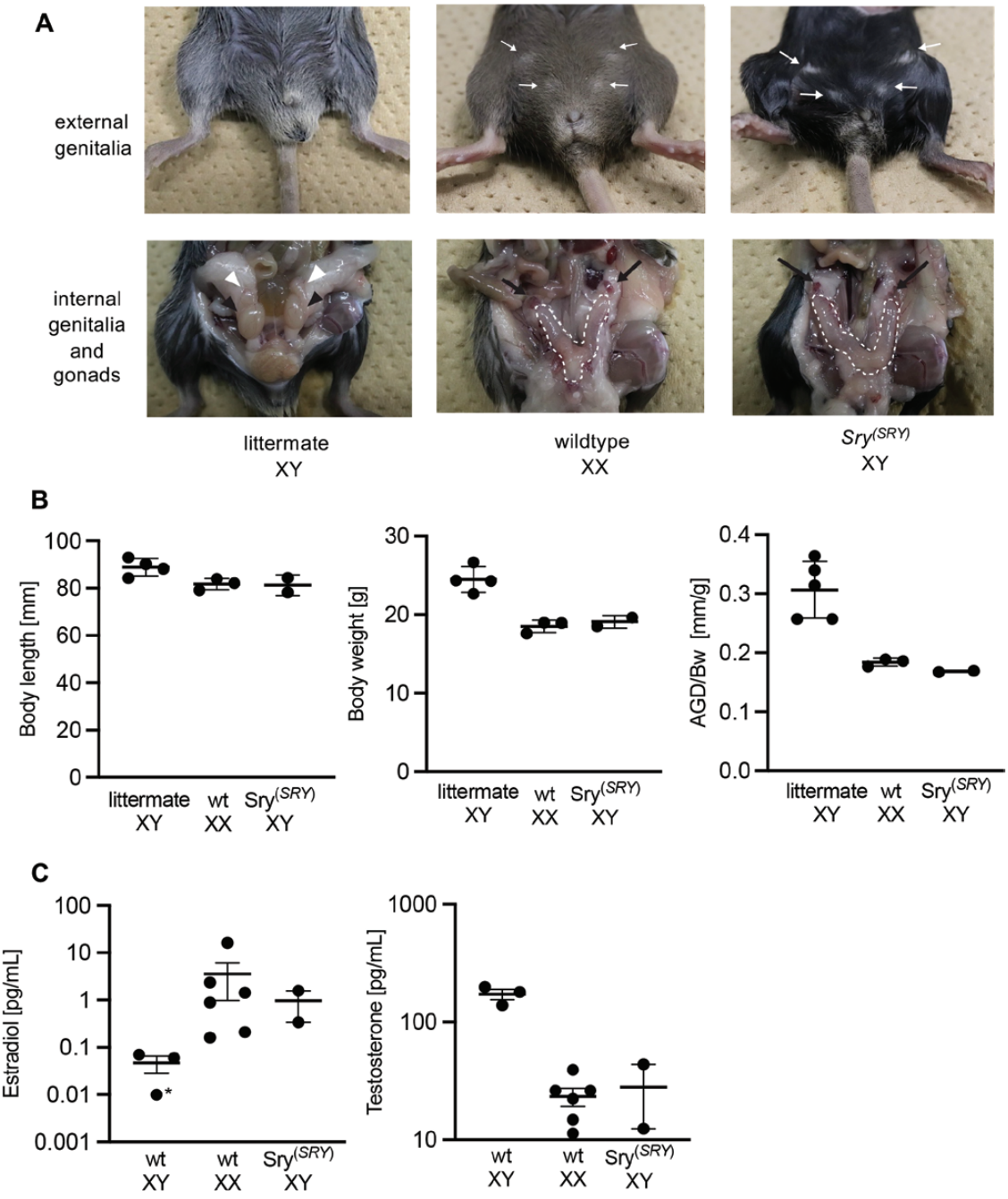

Figure 3. Anatomical phenotype of the reproductive system and endocrinological data of *Sry*$^{(SRY)}$ mice. (A) External genitalia, internal genitalia, and gonads of *Sry*$^{(SRY)}$ mice. The white arrow and black arrow indicate a nipple and an ovary, respectively. The white dashed line outlines the uterus. The white and black arrowhead indicates an epididymis and a testis, respectively. (B) Measurement of auxological data. Mean (± SD) body length, body weight, and anogenital distance. n_{mice} = 4 in littermate XY, 3 in wild-type XX, and 2 in *Sry*$^{(SRY)}$ XY. (C) Mean (± SEM) serum levels of estradiol and testosterone. The specimens from *Sry*$^{(SRY)}$ mice were collected at random stages of the estrous cycle, whereas that from wild-type XX was collected from 8-week-old female B6D2F1 mice at various stages of the estrous cycle, including proestrous, estrous, and metestrous. The control serum from wild-type XY was sampled from 8-week-old male B6D2F1 mice. n_{mice} = 3 in wild-type XY, 6 in wild-type XX, and 2 in *Sry*$^{(SRY)}$ XY. Asterisk indicates that the value was below lower limit (0.01 pg/mL) of the assay. Abbreviations: AGD, anogenital distance; wt, wild-type.

was fewer than that of the wild-type (Fig. 4C, E, F). No seminiferous tubule structure was observed. This histological result was line with that previously reported for *Sry* knockout mice (17). Endocrinological assays revealed estradiol production in *Sry*$^{(SRY)}$ mice. The serum level of estradiol in *Sry*$^{(SRY)}$ mice was within the range obtained for wild-type female mice, and the testosterone level in *Sry*$^{(SRY)}$ mice was as low as that in wild-type female mice.

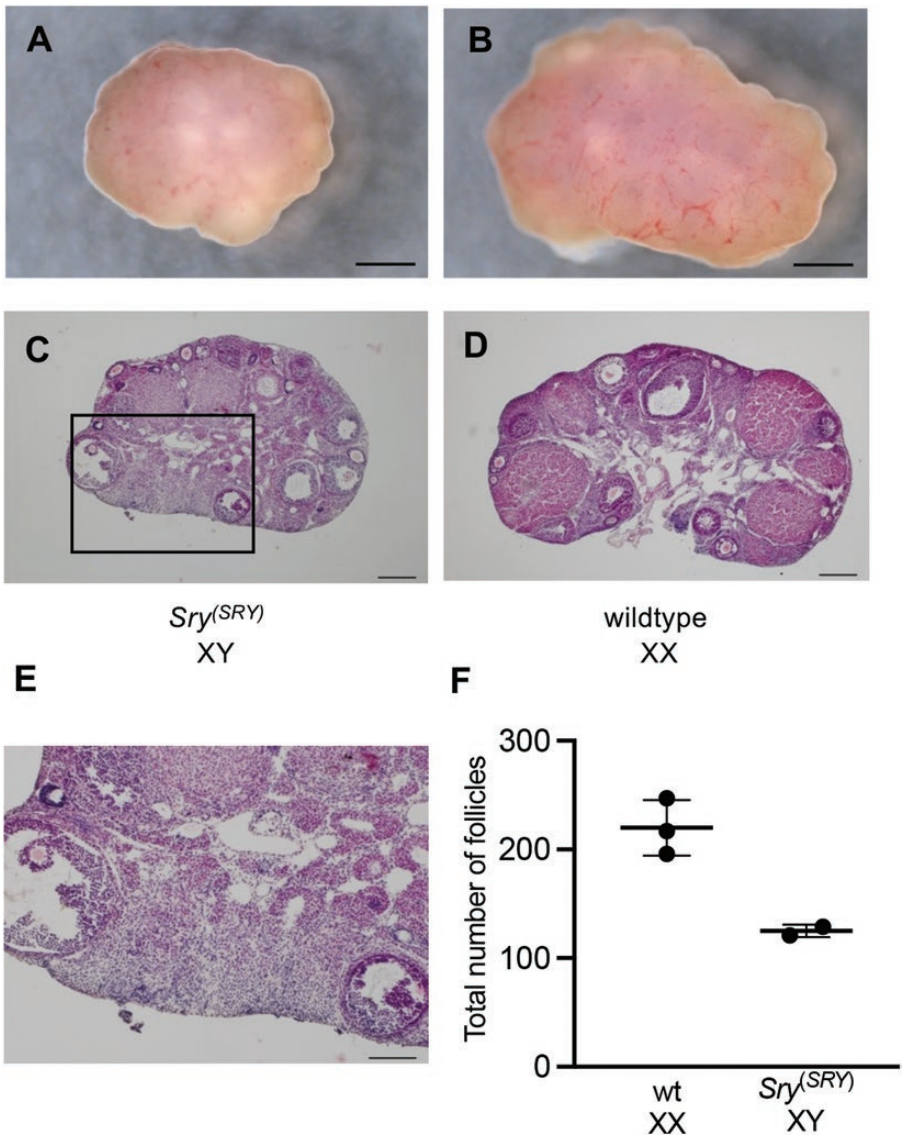

Figure 4. Morphology and histology of adult gonads in *Sry*$^{(SRY)}$ mice. (A, B) Whole-mount image of gonads. (C-E) Ovarian cross-section of the wild-type XX mice and *Sry*$^{(SRY)}$ mice. (E) A higher magnification image of the area within the rectangles in panel C. (F) Mean (± SD) total number of follicles in 8-week-old ovaries. Three in wild-type XX, and 2 in *Sry*$^{(SRY)}$ XY. Scale bars in panels A and B = 500 μm, in panels C and D = 200 μm, and in panel E = 100 μm, respectively.

Discussion

We generated a genetically humanized murine *Sry* model. Targeted genome editing of the locus on the Y chromosome is difficult for the following reasons (19). First, in the case of genome editing in fertilized eggs, one-half of the collected eggs carry the Y chromosome. In addition, there is 1 copy of the Y chromosome in the XY eggs. Thus, the chance of genome editing on the Y chromosome would be one-quarter of that on autosomes. Second, the Y chromosome contains many palindromes, which makes it difficult to select specific sgRNAs with low risk of off-targets (20). Although the efficiency of substitution in our study was not as high as expected, our replacement regimen was confirmed to be applicable to genome editing of the Y chromosome.

Our study revealed that human SRY is insufficient to drive testis development in mouse embryos. The evaluation of adult *Sry*$^{(SRY)}$ mice indicated that their genital morphology and endocrinological profile were similar to that of wild-type female mice. Conversely, adult *Sry*$^{(SRY)}$ mice lacked characteristics of male development, such as the presence of seminiferous tubules in the gonads or the Wolffian duct structure. Developing follicles at various stages were observed in the ovaries of *Sry*$^{(SRY)}$ mice, and the serum levels of estradiol in *Sry*$^{(SRY)}$ mice were within the range observed in control female mice. This finding implied that *Sry*$^{(SRY)}$ mice had an estrous cycle. However, the regularity and frequency of the cycle must be investigated in future, because the ovaries contain fewer follicles than usual.

Previously, it was reported that human *SRY,* with its own regulatory element, did not complement murine SRY function in an analysis of transgenic XX mice (Fig. 1) (1). Although the expression of human *SRY* in fetal gonadal ridges at E11.5 was confirmed in 2 lines, testis development was not observed in the XX transgenic mice. It is possible that the location effect of the transgene may have affected the results. Conversely, the locus and regulation of knocked-in human *SRY* was specified in our study. Thus, we concluded that human SRY did not function as an initiator of murine testis development.

There are 2 possible reasons for this insufficiency. First, the HMG domain in human SRY is almost 70% homologous to that of murine SRY (4). The poor homology was thought to result in an insufficient function of human SRY. Two types of response elements for murine SRY have been reported: "ACAA[T/A]" and "ATTATAAT" (21). Because the latter sequence has not been reported as a motif for human SRY, human SRY may not have bound to a murine SRY response element and could not initiate testis development in mice (22). The other possibility is that the lack of a glutamine-rich domain invalidated the human SRY function. A previous study revealed that transgenic mice of *Sry* without a glutamine-rich domain do not induce sex reversal in XX mice (23). To validate these possibilities, we intend to perform gene editing in $Sry^{(SRY)}$ mice. We believe that investigations in $Sry^{(SRY)}$ mice, which express human SRY with a murine HMG box or human SRY linked to the glutamine-rich domain of murine SRY, may provide insights on this topic.

Additionally, the copy number must be considered. As stated at the beginning of this article, it has been reported that human *SRY* transgenic XX mice show sex reversal when *SRY* is regulated by the murine *Sry* promoter (Fig. 1) (8). We assumed that this discrepancy may have resulted from the difference in the copy number. Because human *SRY* was knocked-in at the location of murine *Sry* exon 1, $Sry^{(SRY)}$ mice are supposed to express 1 copy of human *SRY*; this may not have been sufficient to initiate a male-specific pathway in "bipotential gonad" if its expression was the same level as original murine *Sry* expression. If a high copy number of human *SRY* drives testis development in mice, the potency of murine SRY to initiate murine testis development may be higher than that of human SRY. Murine SRY contains several species-specific structures that increase its stability. One such structure is the second exon of murine *Sry*, which complements the degron structure in the first exon (6). A glutamine-rich domain has also been reported to stabilize the SRY protein (24). These structures may affect the potential of murine SRY to initiate testis development in mice. Studies on human *SRY* transgenic mice with various copy numbers of the transgene are necessary to answer this question.

In embryonic mice, expression of the *Sry* linear transcript is almost totally restricted to the fetal gonadal ridge during the sex-determining period (18, 25, 26). The same surge in *SRY* expression is observed in the human embryonic gonads (27, 28). However, the human SRY protein has also been detected in the late embryonic stage (29). The reason for the rapid downregulation of murine *Sry* around E11.5 remains unknown (30). Further studies on the functional differences between murine SRY and SRY sequences of other mammals may highlight the characteristics of each SRY protein and provide novel insights.

The major limitation of our study is that the expression of human SRY in $Sry^{(SRY)}$ mice was confirmed at the RNA level, but not at the protein level. However, we compensated for the translation of human SRY knocked-in at the murine *Sry* locus by conducting an in vitro study (Fig. S4) (14).

Although the downstream pathway of SRY in testis development has not yet been fully determined, our data and previous data indicate that signal transduction between *Sry/SRY* expression and *Sox9/SOX9* activation was organized in a species-specific manner.

Conclusion

Human SRY is incompatible with murine SRY to drive murine fetal testis development.

Acknowledgments

We thank Editage (www.editage.jp) for English language editing.

Funding: This work was supported by Japan Society for the Promotion of Science KAKENHI grant numbers 20K18208 (to A.T.-H.) and 20K06678 (to S.T.), and the Japanese Society for Pediatric Endocrinology Future Development Grant, 2019, supported by Novo Nordisk Pharma Ltd (to A.T.-H.).

Author Contributions: Conceptualization, S.T.; methodology, A.T. and S.T.; investigation, A.T., Y.O., I.T., and M.T.; resources, A.T., Y.O., I.T., and M.T.; validation, A.T. and S.T.; formal analysis, A.T.; data curation, A.T. and S.T.; writing—original draft preparation, A.T. and S.T.; writing—review and editing, A.T., Y.O., I.T., M.T., and S.T.; visualization, A.T. and S.T.; supervision, S.T.; project administration, S.T.; funding acquisition, A.T. and S.T.; all authors have read and agreed to the published version of the manuscript.

Additional Information

Correspondence: Shuji Takada, Department of Systems BioMedicine, National Research Institute for Child Health and Development, 2-10-1 Okura, Setagaya, Tokyo 157-8535, Japan. Email: takada-s@ncchd.go.jp.

Disclosures: Y.O., I.T., M.T., and S.T. have nothing to declare. A.T. received a research grant from the Japanese Society for Pediatric Endocrinology and Novo Nordisk Pharma Ltd.

Data Availability: Some generated during and/or analyzed during the current study are not publicly available but are available from the corresponding author on reasonable request.

References

1. Koopman P, Gubbay J, Vivian N, Goodfellow P, Lovell-Badge R. Male development of chromosomally female mice transgenic for Sry. *Nature*. 1991;**351**(6322):117-121.
2. Hawkins JR, Taylor A, Berta P, Levilliers J, Van der Auwera B, Goodfellow PN. Mutational analysis of SRY: nonsense and missense mutations in XY sex reversal. *Hum Genet*. 1992;**88**(4):471-474.
3. Kuroki Y, Toyoda A, Noguchi H, et al. Comparative analysis of chimpanzee and human Y chromosomes unveils complex evolutionary pathway. *Nat Genet*. 2006;**38**(2):1-10.
4. Waters PD, Wallis MC, Graves JAM. Mammalian sex-origin and evolution of the Y chromosome and SRY. *Semin Cell Dev Biol*. 2007;**18**(3):389-400.
5. Hughes JF, Skaletsky H, Pyntikova T, et al. Chimpanzee and human Y chromosomes are remarkably divergent in structure and gene content. *Nature*. 2010;**463**(7280):536-539.
6. Miyawaki S, Kuroki S, Maeda R, Okashita N, Koopman P, Tachibana M. The mouse Sry locus harbors a cryptic exon that is essential for male sex determination. *Science*. 2020;**370**(6512):121-124.
7. Kashimada K, Koopman P. Sry: the master switch in mammalian sex determination. *Development*. 2010;**137**(23):3921-3930.
8. Lovell-Badge R, Canning C, Sekido R. Sex-determining genes in mice: building pathways. *Novartis Found Symp*. 2002;**244**:4-18; discussion 18.
9. Naito Y, Hino K, Bono H, Ui-Tei K. CRISPRdirect: software for designing CRISPR/Cas guide RNA with reduced off-target sites. *Bioinformatics*. 2015;**31**(7):1120-1123.
10. Hara S, Terao M, Tsuji-Hosokawa A, Ogawa Y, Takada S. Humanization of a tandem repeat in IG-DMR causes stochastic restoration of paternal imprinting at mouse Dlk1-Dio3 domain. *Hum Mol Genet*. 2021;**30**(7):564-574.
11. Obata Y, Ono Y, Akuzawa H, Kwon OY, Yoshizawa M, Kono T. Post-implantation development of mouse androgenetic embryos produced by in-vitro fertilization of enucleated oocytes. *Hum Reprod*. 2000;**15**(4):874-880.
12. Kay GF, Barton SC, Surani MA, Rastan S. Imprinting and X chromosome counting mechanisms determine Xist expression in early mouse development. *Cell*. 1994;**77**(5):639-650.
13. Zuccotti M, Monk M. Methylation of the mouse Xist gene in sperm and eggs correlates with imprinted Xist expression and paternal X-inactivation. *Nat Genet*. 1995;**9**(3):316-320.
14. Tsuji-Hosokawa A. Data from: the supplemental information of the manuscript "Human SRY expression at the sex determining period is insufficient to drive testis development in mouse." *Mendeley Data, V2*, 2021. Deposited 5 October 2021. doi: 10.17632/9bkjs4j73f.2.
15. Saito T, Hara S, Kato T, et al. A tandem repeat array in IG-DMR is essential for imprinting of paternal allele at the Dlk1-Dio3 domain during embryonic development. *Hum Mol Genet*. 2018;**27**(18):3283-3292.
16. Sato T, Kim H, Kakuta H, Iguchi T. Effects of 2,3-Bis(4-hydroxyphenyl)-propionitrile on induction of polyovular follicles in the mouse ovary. *In Vivo*. 2018;**32**(1):19-24.
17. Kato T, Miyata K, Sonobe M, et al. Production of Sry knockout mouse using TALEN via oocyte injection. *Sci Rep*. 2013;**3**:3136.
18. Jeske YW, Bowles J, Greenfield A, Koopman P. Expression of a linear Sry transcript in the mouse genital ridge. *Nat Genet*. 1995;**10**(4):480-482.
19. Wang H, Hu YC, Markoulaki S, et al. TALEN-mediated editing of the mouse Y chromosome. *Nat Biotechnol*. 2013;**31**(6):530-532.
20. Matsubara Y, Kato T, Kashimada K, et al. TALEN-mediated gene disruption on Y chromosome reveals critical role of EIF2S3Y in mouse spermatogenesis. *Stem Cells Dev*. 2015;**24**(10):1164-1170.
21. Badis G, Berger MF, Philippakis AA, et al. Diversity and complexity in DNA recognition by transcription factors. *Science*. 2009;**324**(5935):1720-1723.
22. Harley VR, Lovell-Badge R, Goodfellow PN. Definition of a consensus DNA binding site for SRY. *Nucleic Acids Res*. 1994;**22**(8):1500-1501.
23. Bowles J, Cooper L, Berkman J, Koopman P. Sry requires a CAG repeat domain for male sex determination in Mus musculus. *Nat Genet*. 1999;**22**(4):405-408.
24. Zhao L, Ng ET, Davidson TL, et al. Structure-function analysis of mouse Sry reveals dual essential roles of the C-terminal polyglutamine tract in sex determination. *Proc Natl Acad Sci U S A*. 2014;**111**(32):11768-11773.
25. Capel B, Swain A, Nicolis S, et al. Circular transcripts of the testis-determining gene Sry in adult mouse testis. *Cell*. 1993;**73**(5):1019-1030.
26. Boyer TR, Erickson RP. Detection of circular and linear transcripts of Sry in pre-implantation mouse embryos: differences in requirement for reverse transcriptase. *Biochem Biophys Res Commun*. 1994;**198**(2):492-496.
27. Hanley NA, Hagan DM, Clement-Jones M, et al. SRY, SOX9, and DAX1 expression patterns during human sex determination and gonadal development. *Mech Dev*. 2000;**91**(1-2):403-407.
28. Clépet C, Schafer AJ, Sinclair AH, Palmer MS, Lovell-Badge R, Goodfellow PN. The human SRY transcript. *Hum Mol Genet*. 1993;**2**(12):2007-2012.
29. Salas-Cortés L, Jaubert F, Bono MR, Fellous M, Rosemblatt M. Expression of the human SRY protein during development in normal male gonadal and sex-reversed tissues. *J Exp Zool*. 2001;**290**(6):607-615.
30. Larney C, Bailey TL, Koopman P. Switching on sex: transcriptional regulation of the testis-determining gene Sry. *Development*. 2014;**141**(11):2195-2205.